PREPARATION OF NATURAL ZEOLITE SUPPORTED TiO_2 COMPOSITES FOR REMOVAL OF TEREPHTHALIC ACID

A Thesis Submitted to
the Graduate School of Engineering and Sciences of
İzmir Institute of Technology
in Partial Fulfillment of the Requirements for the Degree of

MASTER OF SCIENCE

in Chemical Engineering

by
Özgün DELİİSMAİL

August, 2014
İZMİR

We approve the thesis of **Özgün DELİİSMAİL**

Examining Committee Members:

_____
Prof. Dr. Fehime ÇAKICIOĞLU ÖZKAN
Department of Chemical Engineering, İzmir Institute of Technology

_____
Prof. Dr. Şerife Şeref HELVACI
Department of Chemical Engineering, Ege University

_____
Prof. Dr. Mehmet POLAT
Department of Chemical Engineering, İzmir Institute of Technology

_____
Prof. Dr. Muhsin ÇİFTÇİOĞLU
Department of Chemical Engineering, İzmir Institute of Technology

_____
Assist. Prof. Dr. Güler NARİN
Department of Chemical Engineering, Uşak University

20 August 2014

_____	_____
Prof. Dr. Fehime ÇAKICIOĞLU ÖZKAN	**Prof. Dr. Şerife Şeref HELVACI**
Supervisor, Department of Chemical Engineering	Co-Supervisor, Department of Chemical Engineering
İzmir Institute of Technology	Ege University

_____	_____
Prof. Dr. Fehime ÇAKICIOĞLU ÖZKAN	**Prof. Dr. R. Tuğrul SENGER**
Head of the Department of Chemical Engineering	Dean of the Graduate School of Engineering and Sciences

ACKNOWLEDGMENTS

Firstly, I would like to express my deep and sincere gratitude to my supervisor Prof. Dr. Fehime ÇAKIOĞLU ÖZKAN for her supervision, encouragements and guide throughout my M.Sc. study. I also would like to express special thanks to my co-supervisor Prof. Dr. Şerife Şeref HELVACI for her academic support. I am so grateful to my friend Elif GÜNGÖRMÜŞ for her help, motivation, endless care, understanding and infinite friendship. I warmly express my special thanks to my co-worker, Ahmet Uğur ÇİÇEK for his help, support and friendship. I also would like to express special thanks to Banu YENER, Murat YILMAZ, and Özge ÇALIŞKAN for their help and academic supports.

Finally, I would like to express special thanks to my family. I am grateful for their endless love, support and patience of my mother Esin DELİİSMAİL, my uncle Nazım DELİİSMAİL, my aunt Ayla DELİİSMAİL and my cousins İrem DELİİSMAİL and Volkan DELİİSMAİL to whom I dedicate this thesis for their never ending love, support and encouragement.

This thesis was supported by TUBİTAK (110M451), EBILTEM (2012-BIL-027), and BAP (13MUH031), financially.

ABSTRACT

PREPARATION OF NATURAL ZEOLITE SUPPORTED TiO_2 COMPOSITES FOR REMOVAL OF TEREPHTHALIC ACID

This study focuses on the preparation of natural zeolite supported TiO_2 composites for the removal of model pollutant, terepththalic acid (TPA) via sorption. Natural zeolite was purified and used to prepare natural zeolite supported TiO_2 adsorbents. Prior to sorption, the adsorbents were characterized by Scanning Electron Microscopy, Volumetric Adsorption Instrument, X-ray Diffractometer, Fourier Transformer Infrared, Induced Coupled Plasma Atomic Emmision Spectroscopy, and Thermal Gravimetric Analyzer. It was deduced that natural zeolite was clinoptilolite rich low (Ca) silicate.

The sorption studies of TPA on adsorbents were applied in dark conditions at room temperature by altering adsorbent amount (0.2-1.5 g/l) and initial TPA concentration (20-60 ppm). It was observed that the amount of adsorbed TPA per unit mass of adsorbent decreased with increasing adsorbent amount, and sorption percent was unchanged (about 72%). This can be explained by the affinity of adsorbents to water molecules more than TPA molecules. Much more number of TPA molecules was allocated on the clinoptilolite than TiO_2 composites.

Sorption mechanism was identified by fitting the kinetic data to diffusion (Weber-Morris model, intraparticle/external diffusion) and reaction models (First order and pseudo second order model). First order reaction model was well correlated to experimental data for sorption process. Comparing pore size of the adsorbents to molecular size of TPA indicates that main contribution to intraparticle diffusion was the intercrystalline diffusion. Intraparticle diffusion was not the sole rate-limiting step due to the existence of external resistance. Biot and Weber-Morris calculations corroborated these results.

In the future, photocatalytic performance of these adsorbents will also be tested.

ÖZET

TEREFTALİK ASİDİN GİDERİMİ İÇİN DOĞAL ZEOLİT TAŞIYICILI TiO_2 KOMPOZİTLERİNİN HAZIRLANMASI

Bu çalışma kapsamında polimer, boya, ilaç gibi birçok endüstrinin ortak artığı olan tereftalik asidin (TPA) gün ışığında fotokatalitik bozundurulması kapsamında kullanılacak olan zeolit taşıyıcılı TiO_2 kompozitlerinin üretimi ve TPA adsorpsiyonundaki etkinliklerinin incelenmesi öngörülmüştür. Çalışmanın ilk aşamasında doğal zeolit tüfü modifikasyon işlemlerine tabi tutulmuş olup bu modifikasyonla zeolit tüfü yapısında meydana gelen değişiklikler taramalı elektron mikroskobu, kimyasal analiz, x-ışını kırınımı ve yüzey alanı ölçümleri gibi bir takım karakterizasyon yöntemleri ile izlenmiştir. Yapılan karakterizasyon çalışmaları sonucunda doğal zeolit tüfünün klinoptilolitçe zengin düşük kalsiyum silikat olduğuna karar verilmiştir.

Saflaştırılan ve karakterize edilen bu klinoptilolitlerin üzerine, karanlık ortamda TPA adsorpsiyonu gerçekleştirilmiştir. Bu adsorpsiyon işlemi, farklı adsorban ve miktarlarında (0.2-1.5 g/l) TPA konsantrasyonları (20-60 ppm) değiştirilerek gerçekleştirilmiştir. Adsorban miktarının, başlangıç TPA konsantrasyonun, parçacık büyüklüğünün ve TiO_2 kaplamasının TPA adsorpsiyonuna etkileri incelenmiştir. Adsorbanların gözenek büyüklükleri ile TPA molekülleri kıyaslandığında TPA moleküllerinin gözeneklere adsorblanması mümkün değildir. Adsorban miktarı arttıkça toplam adsorblanan miktar etkilenmemiş ve birim adsorban başına adsorblanan TPA miktarında ciddi bir düşüşe sebebiyet vermiştir. Bu düşüşün sebebi, TPA tanecik boyutunun adsorban gözeneklerinden çok daha büyük olması, adsorban-su molekülleri etkileşiminin daha fazla olması ve tereftalik asidin katman olarak adsorblanmış olabileceği olarak yorumlanabilir. Adsorpsiyon çalışmalarında elde edilen veriler teorik difüzyon (Weber-Morris modeli, Difüzyon modelleri: iç/dış direnç) ve reaksiyon modellerine (birinci mertebe reaksiyon modeli ve yalancı ikinci mertebe reaksiyon modeli) uygulanmıştır. Bütün adsorban tipleri için birinci mertebe reaksiyon modeli uygun model olarak görülmüştür. Klinoptilolit ve klinoptilolit taşıyıcılı TiO_2 kompozitlerinde iç direnç tek başına hız sınırlayıcı basamak olmayıp dış direnç de TPA adsorpsiyonunda önemli bir rol almaktadır. Bu durum Biot sayısı ve Weber-Morris hesaplamalarında da görülmüştür.

TABLE OF CONTENTS

LIST OF FIGURES

LIST OF TABLES

CHAPTER 1

INTRODUCTION

Organic pollutants as phenols, aromatics, aldehydes, organic acids and amines are produced as a result of industrial activity directly linked to developing technology. Mixing of these organic pollutants into the springs causes many threatening factors to the human health, environment and as a matter of fact, the other creatures. Hence, the matters to overcome these possible problems come into prominence and several technologies have been developed to remove these organic pollutants.

Terephthalic acid (TPA), the para form of pthalic acid is produced by the wet air oxidation of p-xylene in the presence of acetic acid and is converted to pure terephthalic acid via hydrogenation. Pure TPA is a raw material in the production of polyester, PET bottles, PET films, paints, medicines, synthetic perfumes, pesticides and other chemicals. The wide application fields of pure TPA result in the production of large quantities, thus very large amount of wastewater arising from its production. Wastewater in which TPA exceeds its limit flows into springs and this causes negative impacts on environment and human health from the point of cardiovascular, kidney and respiratory systems. Long time exposure to the chemical causes damages in the targeted organs. In Turkey, pure terephthalic acid is produced roughly 70000 tone/year by PETKIM A.S in Izmir and 3-4 m^3 wastewater per 1 ton is exposed. This means that roughly 210,000-280,000 m^3 wastewater per year come out. Even though, pure TPA achieved by precipitation method from wastewater is used in varied fields, the high amount TPA in supernatant increase chemical oxygen demand (COD) of water in the wastewater treatment plant. This circumstance shows that precipitation is inadequate to overcome that problem and it is necessary to develop new and discrete processes such as adsorption and degradation.

The most common processes to remove the organic pollutants are adsorption, ion-exchange, wet air oxidation, homogeneous/heterogeneous catalytic wet air oxidation, UV/ozonation, photocatalytic oxidation and Fenton reactions. Adsorption and photocatalytic degradation are the most effective and common methods to remove organic pollutants among the other methods. Photocatalysts can be used in the liquid or

gas phase reactions in the form of either powder or coated on the surfaces of glass, silica, zeolite, and etc. There is limitation for nano powder photocatalyst in the liquid phase (slurry) reactions carried out in the industrial applications due to its reusability problem; even though, it promises high reaction yield. Contrary to that case, photocatalysts coated as film do not suffer from the problem concerning reusability; whereas the reaction yield decreases so as not to provide a chance to use all surfaces of the catalyst, efficiently. Thus, it is worthy to developing a new material promising reusability and high activity. Usage of silica, zeolite or active carbon as support material can enhance the reaction yield and reusability of photocatalyst.

Zeolite is the strong candidate to use as support material due to being natural, inert, porous, and cheap. It is necessary to stress that there are 50 billion tone zeolite reservoirs in the Turkey. Also, it is thought that zeolites would gather the organic substance near the TiO_2 particles due to its high adsorption capacity and there would be the generation of electron trapping locals and Ti-O-Al and Ti-O-Si bonds. Natural zeolite tuff in Turkey is generally rich in clinoptilolite mineral.

In this study, it is targeted to prepare zeolite supported TiO_2 composites and remove the terephthalic acid via adsorption which is preliminary study for photocatalytic degradation.

CHAPTER 2

ZEOLITES

Zeolites are microporous crystalline aluminosilicates that are composed of TO_4 tetrahedral (T=Si, Al) units. The combination of SiO_4 units leads to form SiO_2 being an uncharged solid for a completely siliceous structure. The framework becomes negatively charged due to the +3 charge on the Al upon the incorporation of Al into the silica framework. Moreover, it requires extra framework cations (Ca^{2+}, Na^{+}, Mg^{2+}, K^{+}) to keep its overall framework neutral.

This framework contains channels and interconnected voids which are occupied by the cation and water molecules. The extra framework cations are able to ion-exchange and give rise to the ion-exchange chemistry of these materials. These cations act a very significant role in establishement of the adsorption and gas-separation properties of zeolites. These properties are dependent strongly on the size, charge density, and distribution of cations in the porous structure. Also, the novelty of zeolites stems from their microporosity and it is the result of the topology of the framework. Aluminum amount in the framework of the zeolite varies over a wide range with Si/Al=1 to ∞. When the Si/Al=∞, the completely siliceous form is the polymorphs of SiO_2. Lowenstein proposed that the minimum value of Si/Al is 1 due to the phenomenon that placement of adjacent AlO_4^{-} tetrahedra is not favored owing to electrostatic repulsions between negative charges. Moreover, the composition of the framework is dependent on the synthesis conditions. The modification methods after synthesis are developed to insert Si or Al into the framework. Increasing Si/Al ratio makes the hydrothermal stability and hydrophobicity increase as well. Generally, the internal voids of the zeolite are occupied by the water during the water present synthesis. Thermal treatment/oxidation making the intracrystalline space more suitable is used to remove the sorbed phase and organic non-framework cations. The fact that zeolites keep their structural integrity upon loss of water makes them differ from the other hydrates as $CaSO_4$. Figure 2.1 demonstrates the framework projections and the pore sizes for typically used frameworks. The pore openings are uniform throughout the crystal and it makes them able to discriminate against molecules with dimensional

differences less than 1 A^o. This crystalline nature of the framework makes them called as molecular sieves.

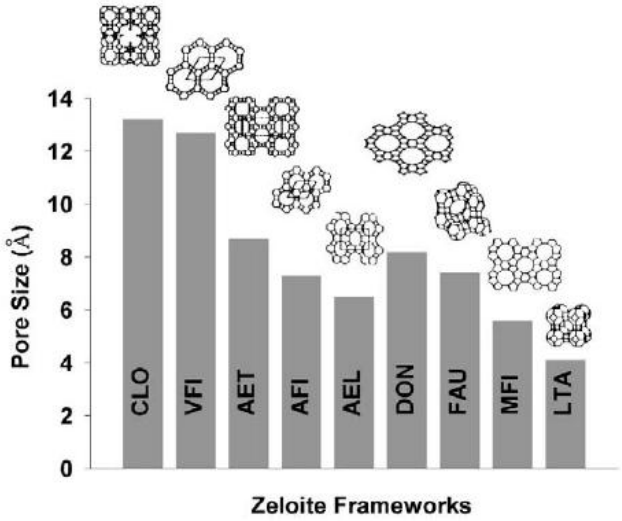

Figure 2.1. Pore size comparison of different framework structures (Source: Auerbach et al. 2003) (CLO: Cloverite, AET: AlPO-8, AFI: AlPO-5, AEL: AlPO-11, FAU: Faujasite, MFI: ZSM-5, LTA: Linde Type-A)

Even if the existence of natural zeolites was noted centuries ago, the zeolite science and technology has been developed until 1950s, following the discovery of methods for large-scale industrial synthesis of zeolites by Union Carbide. As can be seen from Figure 2.1 (a) and (b) that each T atom is coordinated to four oxygen atoms with each oxygen atom bridging two T atoms.

SiO_4 and AlO_4 provided an anionic framework in the aluminosilicate zeolites; whereas this negative charge is balanced by the extra-framework cations. Hence, the empirical formula of aluminosilicate zeolites can be as following;

$A_{x/n}[Si_{1-x}Al_xO_2]\ mH_2O$

where A is the metal cation of valence n. As mentioned previously, the adsorbed water and cations are placed in the channels or cages.

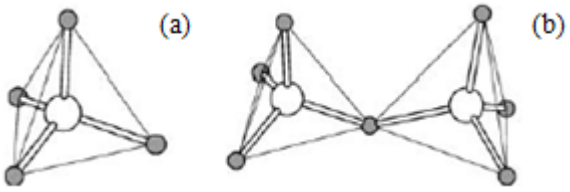

Figure 2.2. Primary building units in zeolite structure (a) TO_4 tetrahedron (b)TO_4 tetrahedra sharing a common oxygen vertex (Source: Xu et al. 2009)

The followings are the significant properties of zeolites making them an important material when compared to other crystalline materials (Breck 1973).

- High degree of hydration,
- Low density and large void volume when dehydrated,
- Stability of the crystal structure of many zeolites when dehydrated,
- Ion-exchange (cation exchange) properties,
- Uniform molecular-sized channels in the dehydrated crystals,
- High adsorption capacity
- Catalytic properties

2.1. Natural Zeolites

Zeolites have been recognized for more than 200 years; whereas during the middle of the 20th century have attracted the attention of scientists and engineers illustrating their technological importance in several fields. The main reason of this interest for natural zeolite is the increasing demand of developing low-cost ion exchange and adsorbent materials in fields such as wastewater treatment, gas separation and heavy metal removal as well as their wide availability on the earth.

Zeolites being group of naturally occurring framework alumina-silicates promise high cation exchange capacities, high adsorption and hydration-dehydration properties. Even if roughly fifty different species of this mineral group have been identified, just eight zeolite minerals make up the major part of volcano sedimentary deposits: analcime, chabazite, clinoptilolite-heulandite, erionite, ferrierite, laumontite, mordenite and phillipsite. The structure of each of these minerals makes them distinguish each other, whereas they have common property that having large open ‘channels’ in the crystal structure providing a large void space for the adsorption and exchange of cations. The internal surface area of these channels can reach as much as several hundred square meters per gram of zeolite, which makes them extremely effective ion exchangers.

Natural zeolites have high cation exchange capacities (CECs) and high ammonium selective properties (Kithome et al. 1998). As mentioned previously, more than 50 different species of this mineral group have been identified (Tsitsishvili et al. 1992). Clinoptilolite (Kithome et al. 1998), ferrierite and mordenite (Townsend, 1986),

erionite (Mondale et al. 1995), and chabazite (Green et al. 1996) are the different kind of zeolites. Table 2.1 illustrates the zeolite classification scheme developed by Breck. The groups changes with respect to framework structure constituted by secondary building units (SBUs). It has been stressed that the characteristics of a zeolite mineral depend on its origin because of variations in natural processes during the genesis (Townsend, 1986; Mondale et al. 1995). Mondale et al. (1995) mentioned that, for instance, structural imperfections, a variety of exchangeable cations, and the presence of clay may lead to pore blockage and slow diffusion rates. Another relevant aspect is that the zeolite mineral concentration of an ore sample depends on the origin of the zeolite.

Table 2.1. Zeolite classification scheme developed by Breck based on SBUs (Source: Dyer 2002)

Group 1 (S4R-single 4-ring)	Group 5 (T_5O_{10})
analcime harmotome phillipsite gismondine paulingite laumontite yugawaralite (P)	natrolite scolecite mesolite thomsonite gonnardite edingtonite
Group 2 (S6R-single 6-ring)	Group 6 (T_8O_{16})
erionite offretite levynite sodalite hydrate (T, omega, losod)	mordenite dichiardite ferrierite epistilbite bikitaite
Group 3 (D4R-double 4-ring)	Group 7 ($T_{10}O_{20}$)
(A, N-A, ZK-4)	heulandite
Group 4(D6R- double 6-ring)	clinoptilolite
Faujasite chabazite gmelinite (X, Y, ZK-5, L)	stilbite brewsterite

The Si/Al ratio can vary considerably within the limits of one structural type, depending upon the composition of original solutions and conditions of crystallization. The Si/Al ratio of natural zeolites changes in the range of 1 to 6 and the upper limit of the Si/Al ratio in the natural zeolites reaches 5 to 6 (clinoptilolite, mordenite and ferrierite). Table 2.2 gives the classification of zeolites depending on Si/Al ratios.

Table 2.2. The classification of zeolites depending on Si/Al ratios
(Source: Auerbach et al. 2003)

Classification	Si/Al
Low silica	≤ 2
Intermediate silica	2 - 5
High silica	≥ 5

2.1.1. Clinoptilolite-Rich Natural Zeolites

Clinoptilolite is the most abundant natural zeolite mineral, but composition and purity vary widely among the deposits found throughout the world. It is a member of the Heulandite group which are isostructural. The empirical formulas of heulandite and clinoptilolite are given as following;

$(Na,K)Ca_4[Al_9Si_{27}O_{72}]\cdot 24H_2O$ (Heulandite)

$(Na,K)_6[Al_6Si_{30}O_{72}]\cdot 20H_2O$ (Clinoptilolite)

Both heulandite, and clinoptilolite has same tetrahedral framework labeled as HEU. As mentioned previously that Si/Al ratio is used to characterize and describe the type of the zeolite. Heulandite is described as a series possessing $2.7< Si/Al < 4$, and $5.25>Si/Al >4.25$ is for clinoptilolite (Breck 1973). Heulandite transforms into two phases at about 230°C and becomes non-crystalline at about 350°C. Clinoptilolite survives its crystal structure up to about 700°C (Tsitsishvili et al. 1992). The crystal structure of heulandite is mostly defined to be monoclinic, space group I2/m, a=17.7, b=17.8, c=7.4 Å, β = 116.4°, Z = 1 (Alberti 1975, Koyama and Takéuchi 1977, Bresciani-Pahor et al. 1980, Alberti and Vezzalini 1983, Hambley and Taylor 1984, Smyth et al. 1990, Armbruster and Gunter 1991, Armbruster 1993, Gunter et al. 1994), and he crystal structure of clinoptilolite is described to be monoclinic, space group C2/m, a=7.41, b=17.89, c=15.85 Å, β = 91.29° (Breck 1973). Even if, lower symmetries (Cm, C1) have been

reported (Alberti 1972, Gunter et al. 1994, Yang and Armbruster 1996, Sani et al. 1999). The characteristic properties of clinoptilolite are summarized by Breck (1973), shown in Table 2.1. Figure 2.3 shows the framework of the the HEU zeolites. Figure 2.3 (a) shows the elliptical ten membered rings generating one set of [001] channels and circular eight membered rings form the smaller B channels while Figure 2.3 (c) demonstrates the C channels being parallel to [100]. These channels are formed by elliptical eight membered rings. Figure 2.3 (c) represents three different sites and water molecules inside. Two different metal sites are available in the A channel (elliptical rings). The cation site occupied by Na is represented by the small black dot while the larger gray-shaded atom shows K ion sites. The small white circles and the larger white circles represent Ca and water molecules in the smaller circular B channel, respectively.

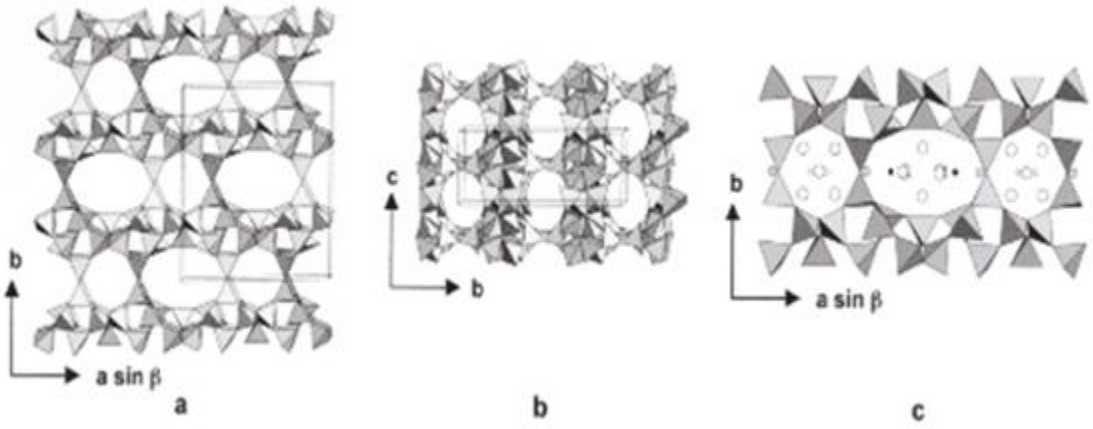

Figure 2.3. The heulandite structure. (a) A (001) projection looking down the c-axis with the b-axis vertical, (b) A (100) projection looking down the a-axis with the c-axis vertical (c) A (001) projection of heulandite looking down the c-axis with the b-axis vertical (Source: Dyer 2002)

As can be seen from the figure that the framework comprise three sets of intersecting channels located in the (010) plane. Also, two channels are parallel to the c axis. A channels are generated by heavily compressed ten-membered rings (aperture 3.0 × 7.6 Å), while B channels are closed by eight-membered rings (aperture 3.3 × 4.6 Å). C channels are generated by eight-membered rings and they are parallel to a-axis ([102]).

Table 2.3. Summary of clinoptilolite characteristic properties
(Source: Breck 1973)

Structure Group:7		
Chemical Compositon		
Typical Oxide Formula:	$(Na_2,K_2)O.Al_2O_3.10SiO_2.8H_2O$	
Typical Unit Cell Contents:	$Na_6[(AlO_2)_6(SiO_2)_{30}].24H_2O$	
Variations:	Ca, K, Mg also present: Na, K>> Ca Si/Al: 4.25 to 5.25	
Cystallographic Data		
Symmetry:	Monoclinic	
Space Group:	l2/m	
Unit Cell Constants:	a=7.41 A b=17.89 A c=15.85 A β=91°29'	Density: 2.16g/cc Unit Cell Volume: 2100 A^3
Structural Properties		
Framework:	Possibly related to heulandite but not determined	
Void Volume:	0.34 cc/cc Framework density:1.71 g/cc	
Effect of Dehydration:	Very stable-in air to 700 °C	
Largest Molecule Adsorbed:	O_2	
Kinetic Diameter,A:	35	

C1, Cm, C2, and C2/m are the possible space groups for heulandite and clinoptilolite. Akizuki et al. (1999) established by using optical methods and X-ray diffraction methods which a macroscopic heulandite crystal is composed of growth sectors showing triclinic and monoclinic symmetry where the triclinic sectors are explained by (Si, Al) ordering on the crystal faces. Yang and Armbruster (1996) and Stolz et al. (2000) explained that symmetry lowering in heulandite can only be resolved from X-ray data when investigated in cation-exchanged samples where the distribution of extra-framework cations also reflects the lower symmetry. Distinct degrees of (Si, Al) ordering have been proposed for heulandite and clinoptilolite. As can be seen from Figure 2.5 (c) that the tetrahedron having highest aluminum content, T2, combines the sheets of $T_{10}O_{20}$ groups by sharing their oxygen. Hambley and Taylor (1984) found that (Si,Al) ordering values were similar to other C2/m corrections.

Cation exchange, catalytic, adsorption properties are predominantly influenced by the type, number and location of the charge balancing in the A, B and C channels. Two main channels have been reported for the cation sites by the researchers. These sites contain Na, Ca, K, and Mg as cations. Na and K are predominantly close the intersection of A and C channels while Ca is placed in the B channel. The regions where Ca is located in the B channel do not contain Na; whereas there is the existence of Ca in

the A channel containing Na. K is centered in the C channel; whereas K and Na occur at nearby sites. All of these cations may be distinguished due to their distinct distances from the framework. Na, K, and Ca ions are located on the (010) mirror plane being present in C2/m or Cm symmetry. There is coordination between these ions and framework oxygens and channel water molecules. Gunter et al. (1994) reported that sodium was nine coordinated to four framework oxygen and it occupied the channel H_2O molecules, partially. Contrary to Na, both Ca and K ions were eight-coordinated to four oxygens and four water molecules of channel. Typically, magnesium is located in the center of A channel.

Dyer (2002) stated that heulandite and clinoptilolite have different amount of water, depending on the extra-framework chemistry and hydration state. Usually, water molecules being in the channel are totally occupied while they are partially occupied in the A channel (Koyama and Takéuchi 1977; Armbruster and Gunter 1991).

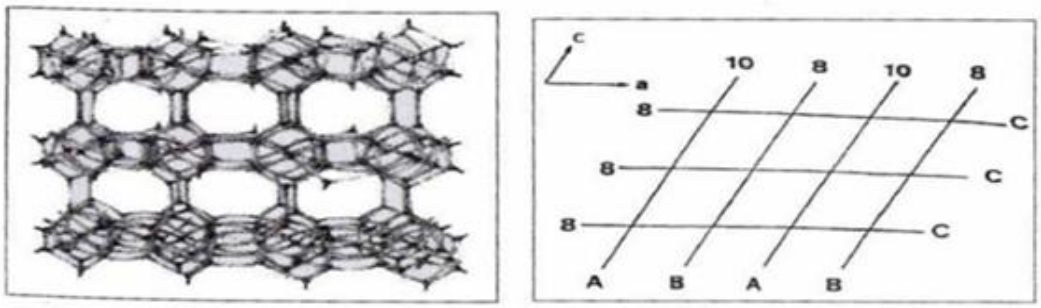

Figure 2.4. (a) Simpler scheme of clinoptilolite framework structure (b) Orientation clinoptilolite structure (Source: Ackley and Yang 1991)

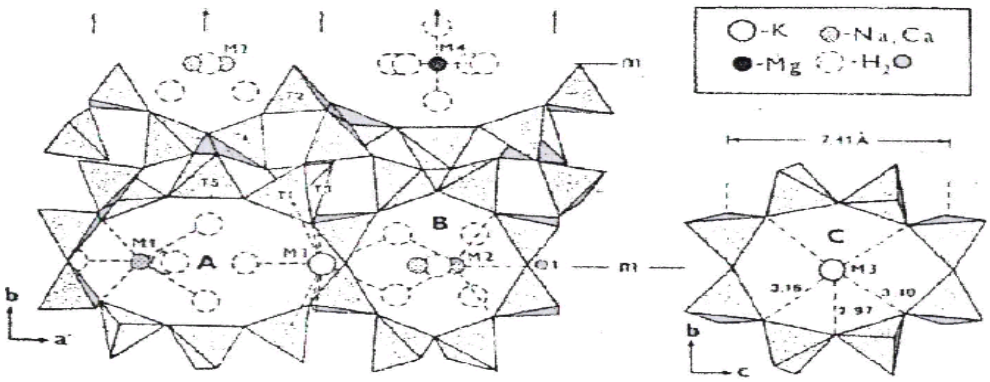

Figure 2.5. The main cation positions in the clinoptilolite structure

Some adsorbents can consist of small microporous crystals generated in a macroporous pellet as shown in Figure 2.6. Such adsorbents such as clinoptilolite rich natural zeolite offers two different diffusional resistances to mass transfer; micropore resistance of the adsorbent crystals or microparticles and the macropore diffusional resistance of the pellet. Also, if component of binary mixture is adsorbed onto adsorbent, there may be another mass transfer resistance associated with transport through the laminar fluid boundary layer surrounding the particle.

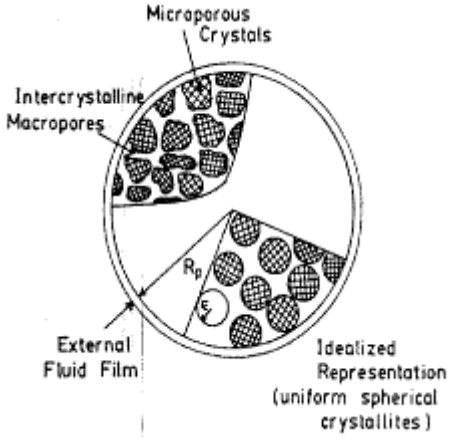

Figure 2.6. Schematic diagram of pellet adsorbent with three mass transfer mechanisms

Micropore and macropore resistances are dependent on the ratio of the diffusional time constants changing with respect to system and conditions. Moreover, diffusional time constant is directly linked to square of the particle radius. Hence, investigation of particle size acts significant role to comprehend the controlling resistance in other words rate-limiting step of the adsorption process. Also, it is simple and straightforward experimental test to understand the nature of the controlling resistance.

2.1.2. Use and Application of Natural Zeolites

Clinoptilolite and the other zeolites promise many advantages to be used in the environmental applications. Adsorption and ion-exchange capacity are the main properties that zeolites provided beside the application of them in catalysis. The widespread applications of clinoptilolite and the other zeolites are given below under

the titles of wastewater, adsorbent, catalyst and gas absorption, ion-exchange, fertilizer, animal feed additive, and other applications.

Wastewater Applications:

The unique cation-exchange feature of zeolites is exploited to use them in water purification. Dissolved cations in water can be removed via exchanging with cations placed in the framework and extra-framework of zeolites.

Erdem et al. (2004) studied the phosphorus removal in a system with bioaugmented activated sludge and zeolite addition. Metabolic activity of activated sludge, phosphorus uptake by phosphate accumulating bacteria which is adsorbed on the natural zeolite, and suspended in solution, and phosphorus adsorption on the natural zeolites were the subject of the study. Moreover, it is reported that zeolites could be used for the removal of arsenate and arsenite from drinking water. As mentioned previously that clinoptilolite is the well-known zeolite for ammonium removal from wastewaters. The capability of clinoptilolite to remove ammonium from wastewater was studied by many researchers. Adsorption rate and ammonium exchange capacity of the zeolites are the most significant parameters for wastewater treatment.

Adsorbent Applications:

Table 2.4 shows the applications of zeolites as adsorbents. The table focuses on the removal of small polar of polarizable molecules by using high aluminum content zeolites and bulk separations via molecular sieving proceses.

Table 2.4. Commercial adsorbent applications of molecular sieve zeolites

A. Purification	B. Bulk Seperation
Drying: • natural gas (including LNG) • cracking gas (ethylene plants) • insulated windows • refrigerant CO_2 removal: • Natural gas, flue gas (CO_2+N_2) • Cryogenic air separation plants Sulfur compound removal Sweetening of natural gas and liquefied petroleum gas Pollution abatement: removal of Hg, SO_x, NO_x Removal of organic and inorganic iodide compounds from commercial acetic acid feed streams	Normal iso/paraffin separation Xylene separation Olefin separation Separation of organic solvents O_2 from air Separation of CO_2, SO_2, NH_3 Sugar separation Separation of amino acids, n-nitrosoamines

Catalyst and Gas Absorption Applications:

Table 2.5 lists the applications of catalysis by zeolites. Transformation of zeolites is applied by strong acidity of zeolites which are prepared via certain pathways involving NH_4^+ and multivalent cation exchange, and via steaming. Another significant property of zeolite relates to a concentration effect of reactants within the channels and cages of the zeolite. This property promotes bimolecular reactions including efficient intermolecular hydrogen transfer. For zeolites having higher Si/Al ratio, the conversion of polar oxygenated hydrocarbons to paraffins and aromatics is promoted by the organophilic nature. In the synthesis of organic intermediates and fine chemicals, zeolites have strong attraction due to providing beneficial advantages which are being exploited include heterogenization of catalysts for easy separation framework, doping with metals for selective oxidation, and ease of regeneration of catalysts.

Moreover, zeolites can hold water up to 60% of their weight owing to high porosity of crystalline structure. These water molecules in the pores can be evaporated or reabsorbed without giving any damage to zeolite structure. Zeolites promise a permanent water reservoir, supplying extended moisture during dry periods. In addition to this, they promote a fast rewetting and improve the lateral spread of water into the root zone during irrigation. As mentioned previously, zeolites have high absorption and adsorption capacity. This feature make them gain the ability to absorb CO, CO_2, SO_2, H_2S, NH_3, HCHO, Ar, O_2, N_2, H_2O, He, H_2, Kr, Xe, CH_3OH and the other gases. Hence, natural zeolites can be used to collect these gases and control odors and they are used in intensive animal husbandry sheds, decreasing the ammonia and H_2S content causing undesirable odors. Moreover, zeolites adsorbing NH_4^+ becomes a natural enriched slow release fertilizer. High capacity ammonia absorption leads very effective natural way to control the levels formed especially in fish farms. In addition to this, food crops can be protected from the high amounts of Pb, Cd, and Cu thanks to absorption ability of zeolites (Polat et al. 2004).

In the literature, there are many articles published regarding the adsorption of petroleum products from gaseous and aqueous media by zeolites. The results indicated that zeolites can be used and studied for the development of adsorbent materials. Moreover, Cr (III) removal from aqueous solution was studied by using Mongolian natural zeolite. The effects of modification, pH of the solution, zeolite samples were investigated to interpret on the adsorption performance (Gerasimova 2003). The results showed that clinoptilolite is strong candidate to adsorb Pb^{2+}, Al^{3+}, Zn^{2+}, and Fe^{2+}.

However, it is not a promising adsorbent for ethanol, acetone and South African clinoptilolite shows the similiar features to the other clinoptilolites originated from the other countries (Takashi et al. 2008).

Table 2.5. Applications of zeolites in catalysis

Inorganic reactions	Hydrocarbon conversion:
H_2S oxidation	Alkylation
NO reduction of NH_3	Cracking
CO oxidation, reduction	Hydrocracking
CO_2 hydrogenation	Isomerization
$H_2O \rightarrow O_2+H_2$	
Organic reactions:	
Aromatization (C_4 hydrocarbons)	Dehydration
Aromatics (disproportionation, hydroalkylation, hydrogenation, hydroxylation, nitration, oxidation, oxyhalogenation, etc.)	Epoxidation (cyclohexene, olefins, α-pinene, propylene, styrene)
Aldol condensation	Friedel-craft reaction of aromatic compounds (alkylation of butylphenol with cinnamyl alcohol)
	Fischer-Tropsh reaction (CO hydrogenation)
Alkylation (aniline, benzene, biphenyl, ethylbenzene, naphthalene, polyaromatics, etc.)	Methanol to gasoline
Beckman rearrangement (cyclohexanone to caprolactam)	Methanation
Chiral hydrogenation	MPV (Meerwin-Ponndorf-Verley) reduction (transfer hydrogenation of unsaturated ketones)
CH4 (activation, photocatalytic oxidation)	Oxyhalogenation of aromatics
Chloroaromatics dechlorination	Heck reaction (acetophenone+acrylate→acrylate ester)
Chlorination of diphenylmethane	Hydrogenation and dehydrogenation
Chlorocarbon oxidation	Hydrodealkylation
Chlorofluorocarbon decomposition	Shape-selective reforming
Cinnamaldehyde hydrogenation	
Cinnamate ester synthesis	
Cyclohexane (aromatization, isomerization, oxidation, ring opening)	

Ion-exchange Applications:

Table 2.6 lists the ion-exchange applications of zeolites. Typically, the zeolites are used in the detergent industry for water softening and they are used for substitution of phosphates. It is known that zeolite A is selective to Ca^{+2} and this feature provides unique advantage. As listed in Table 2.7, the natural zeolites are used for the removal of Cs^{+} and Sr^{2+} radioisotopes by ionexchange from radioactive waste streams.

Zeolites have negatively surface charged and this provides an ideal trap for positive cations as sodium, potassium; and for positively charged groups as water and ammonia. Negative charged ions of zeolites attracted both carbonate and nitrate ions within zeolites. Hence, alkali metallic cations are attracted in the same way and zeolites can absorb water. Absorbed cations are mobilized owing to weak attraction, and there is a chance to be replaced by standard ion exchange methods.

Table 2.6. Ion exchange applications of zeolites

Applications	Advantage
Removal of Cs^{+} and Sr^{2+}	Stable to ionizing radiation
Radioisotopes—LINDE AW-500, Mordenite, clinoptilolite	Low solubility, dimensional stability, High selectivity
Removal of NH_4^{+} from wastewater—LINDE W, clinoptilolite	NH_4^{+}- selective over competing cations
Detergent builder zeolite A, zeolite X (ZB-100, ZB-300)	Remove Ca^{2+} and Mg^{2+} by selective exchange, no environmental problem
Radioactive waste storage	Same as Cs^{+},Sr^{+} removal
Aquaculture (AW-500, clinoptilolite)	NH_4^{+} selective
Regeneration of artificial kidney dialysate solution	NH_4^{+} selective
Feeding NPN to ruminant animals	Reduces NH_4^{+} by selective exchange to nontoxic levels
Metals removal and recovery	High selectivities for various metals
Ion exchange fertilizers	Exchange with plant nutrients such as NH_4^{+} and K^{+} with slow release in soil

Table 2.7. Summary of uses of natural zeolites

Bulk applications:	Molecular sieve applications:
Filler in paper Pozzoolanic cements and concrete Dimension stone Lightweight aggregate Fertilizers and soil conditioners Dietary supplement in animal nutrition	• Separation of oxygen and nitrogen from air • Acid-resistant adsorbents in drying and purification • Ion exchangers in pollution abatement processes

Fertilizer Applications:

Fertilizer efficiency can be improved by using zeolites, especially clinoptilolite. Hence, the usage of clinoptilolite in agriculture provides better plant growth, and thus enriches the yield. For example, Torii et al. (1978) noted that the apple yield increased 13-38% thanks to the application of zeolite at the rate of 4-8 tons/acre. The usage of zeolite mineral in the amount of 2-8 kg/tree may provide a better new orchard establishment. As mentioned previously that zeolites can be applied in the cultivation of food crops which are cereals, vegetables, grapes, and other fruits (Burriesci et al. 1984).

Prolonged soil quality can be enhanced by the addition of zeolites to fertilizers due to its aid to retain nutrients (nitrogen, potassium, calcium, magnesium, micro-elements) which soil needs. Thus, this provides the more efficient use of nitrogen and potassium fertilizers by decreasing their rates for the same yield. In the cases of sandy soils, large loses of fertilizers moving out of the leaching often occur (Mumpton 1981). Consequently, the application of zeolite would enrich the plant growth and development via decreasing the loss of valuable nutrients needed for plants.

Animal Feed Additive Applications:

It is known from the literature that clinoptilolite addition to the diet of pig, poultry, and cattle improves their weight gain and feed conversion ratios also are increased. Clinoptilolite acting as a mycotoxin binder absorbs toxins being dangerous to animals. Moreover, it can be used as aid to control aflotoxins in animal feed. Hence, it lowers the mortality from digestive stress and decreases the need for antibiotics. In

addition to these, zeolites absorb other toxins which are produced in the feed by moulds and microscopic parasites.

Other Applications:

Table 2.8 lists the applications of zeolites in health science. Separations coupled into one unit and organic transformations can be applied by using zeolitic membranes. As can be seen from Table 2.5, redox molecular sieves are used in the synthesis of fine chemicals, taking the advantage of both the considerable flexibility in designing frameworks and insertion of reactive elements and compounds into the framework. The other applications field of zeolites involves the sensors, biosensors, photocatalytic oxidation, photochemical organic transformations, preparation of support materials, and conversion of solar energy.

Table 2.8. Health science and zeolites

Detoxification of mycotoxins by selective binding with zeolites Insects control: semiochemicals adsorbed in zeolites and by controlling diffusion-deisorption rate controls concentration of the pheromones in the air Reaction of clinoptilolite and human bile Protein (cytochrome c) adsorption. Encapsulation and immobilization of proteinaceous materials in zeolite Poultry industry: feed additive, toxin binder for environmental protection Milk yield, consumption, carcass characteristics in lactating cows Diets of farm animals: gain, feed conversion, dressing percentage, carcass characteristics of lambs	Biomedical applications: External application Detoxicants Decontaminants Vaccine adjuvants Antibacterial agents Enzyme mimetics Drug delivery Diabetes mellitus Antitumor adjuvants Antidiarrheal agents Hemodialysis Contrast in magnetic resonance Bone formation Biosensors

CHAPTER 3

ADSORPTION

"Sorption" term is the definition of every type of capture of a substance from the external surface of the liquids, solids and internal surface of porous solids and liquids (Skoulikides 1989). Sorption has different types as follows;

Physical Sorption (Physisorption): There is no electron exchange in the physical sorption. Intermolecular attraction between available energy sites occurs. Hence, it is not dependent on the electronic properties of the molecules. Characterization of physisorption is carried out by the interaction energies being comparable to vaporization heats. Weak van der Waals forces are observed between adsorbate and the surface of the adsorbent and multilayers can be generated with roughly same heat of adsorption being at most a few kcal/mole. Thus, physisorption is not stable at temperatures above 150^{o} C.

Chemical Sorption (Chemisorption): Contrary to physisorption, there is electron exchange between surface sites and solute molecules. Hence, there is formation of chemical bonds. The characterization of chemisorption is applied by the interaction energies between adsorbate and surface of the adsorbent being comparable to the chemical bonds' strength. When comparing with physisorption, the bonds formed between adsorbate and adsorbent are stronger and stable at high temperatures. Contrast to physisorption, one layer has formed as a result of adsorption at which chemisorption takes place.

Ion Exchange (Electrostatic sorption): Coulomb attractive forces between ions and charged functional groups have formed during ion exchange.

Table 3.1 illustrates the significant characteristics of chemisorption and physisorption.

Table 3.1. Comparison of chemisorption and physisorption

Properties	Chemisorption	Physisorption
Temperature range	Almost unlimitied	Near or below the condensation point of the gas

(cont. on next page)

Table 3.1. (cont.)

Properties	Chemisorption	Physisorption
Adsorption enthalpy	Wide range (40-800 kJ/mol)	Related to factors like molecular mass and polarity (5-40 kJ/mol)
Adsorption Nature	Dissociative and irreversible	Nondissociative and reversible
Saturation Uptake	One monolayer	Multilayer
Kinetics	Variable; activated process	Fast; nonactivated process

Adsorption is the capture of gaseous and liquids components of mixtures by the external and/or internal surface of adsorbents. In chemical engineering, McCabe et al. (2005) defines the adsorption as separation process during which the surface of adsorbent transfers the components of one phase of a fluid.

If there is a travel of adsorbate species between the atoms, ions, or the molecules of the adsorbent, the phenomenon of "absorption" occurs, and this is the discrimination of absorption from the adsorption taking place on the surface. Increment in the free surface energy of the solids owing to extensive surface provides the adsorption of various substances from solids. As the second law of thermodynamics, this energy must be decreased, and this is overcame by decreasing the surface tension via uptake of extrinsic substances.

If it is considered that a molecule above the surface with a distance being normal to surface, there will be two types of influences. Firstly, there is repulsion between the cloud of electrons in the atoms forming the surface and molecules and van der Waals attraction forces are formed. A much shorter radius of influence is observed in the nuclear attraction and there is "well" in the potential energy curve at a short distance from the surface as an outcome of the balance of these two forces. Figure 3.1 shows the potential energy change with respect to distance. When reaching to "well", molecules or atoms are adsorbed by this potential energy and they cannot run away until they have adequate kinetic energy to be desorbed.

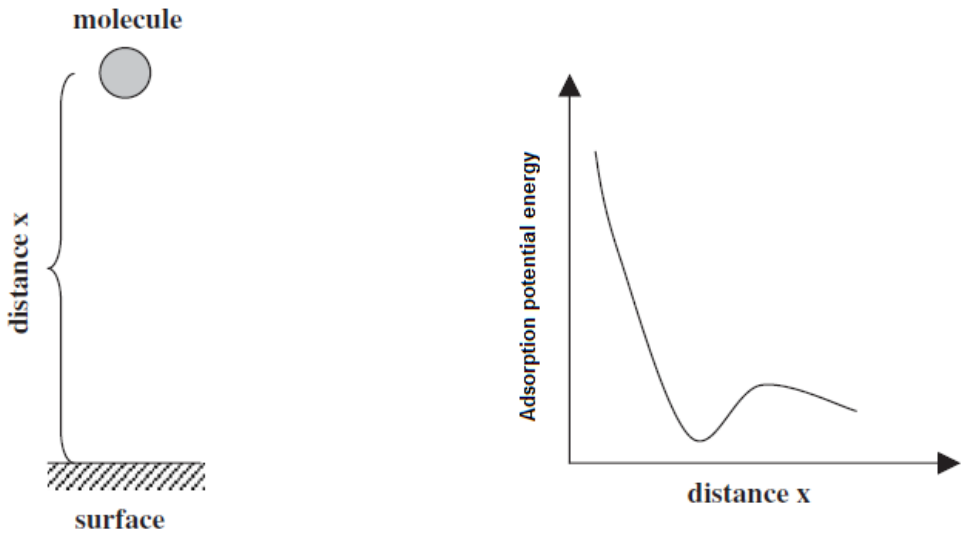

Figure 3.1. Potential energy change with respect to distance
(Source: Inglezakis and Poulopoulos 2006)

As Gregg and Sing (1967) explains that the characterization of surface is applied as external when it has cavities with width being greater than the depth or as internal when it has pores and cavities having depth greater than the width. Also, all surfaces are not straight and show peaks at microscopic level as can be seen via atomic forced microscopy or scanning electron microscopy.

Pore structure is the most significant property for the adsorbents to decide for which reason it should be used. The adsorption capacity of the adsorbent was established by the total number of pores, their shape, and size. Commonly, the pores are classified into three types; macro-, meso-, and micropores. Table 3.2 demonstrates the classification of the pores according to IUPAC.

Table 3.2. Classification of pores

Type	Diameter (nm)
Macropores	$d>50$
Mesopores	$2\leq d\leq 50$
Micropores	$d<2$
Ultramicropores	$d<0.7$
Supermicropores	$0.7<d_0^*<2$

*d_0 is the diameter for cylindrical pores.

Adsorbate initially transfers through macropores to the mesopores and finally transports through the micropores constituting the largest portion of the internal surface. Micropores involve the most to the total pore volume. Due to strong attractive forces and low relative pressure in the microporostiy, the adsorption of especially gaseous particles happens at that region. Hence, adsorption capacity is established by the total pore volume and the pore size distribution.

Adsorption Kinetics:

The equilibrium point of adsorption cannot be determined instantaneously for porous adsorbents. Mass transfer resistances establishing the necessary time to reach equilibrium state prevent the mass transfer from bulk to the adsorption sites within the adsorbent particles. Hence, adsorption kinetics is the time progress of the adsorption process. Usually, the adsorption rate is restricted by diffusion toward the external adsorbent surface and within the porous adsorbent particles. Adsorption kinetics are significant to comprehend the rate-limiting mass transfer mechanisms and to enlighten the characteristic behaviors of mass transfer parameters. Also, equilibrium data, parameters and time to reach equilibrium state are important and essential for establishment of the required contact times in slurry reactors and fixed-bed adsorbers.

Mass Transfer Mechanisms:

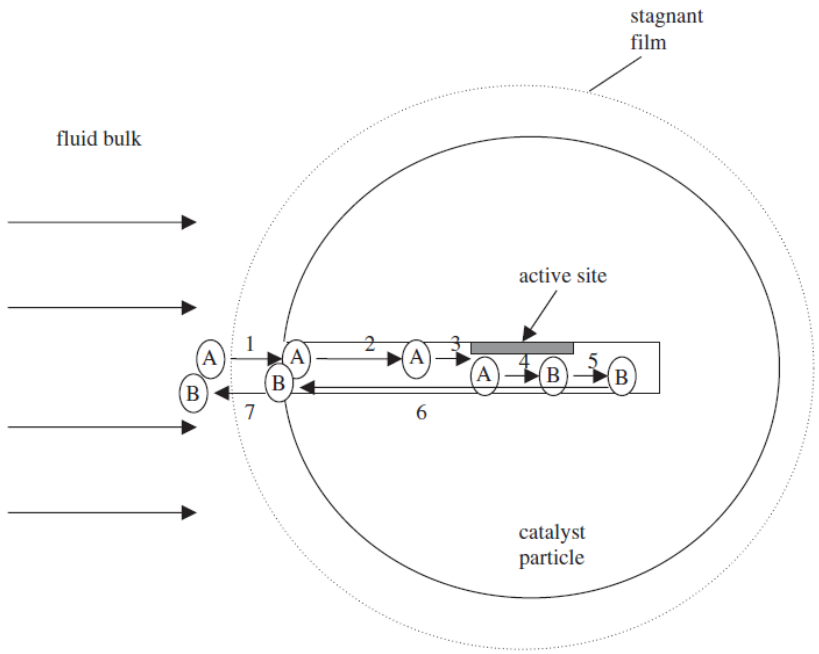

Figure 3.2. Steps involved in mass transfer mechanism of adsorbate
(Source: Inglezakis and Poulopoulos 2006)

Overall progress of the adsorption involves the following steps:

1. Adsorbate transport from the bulk fluid to the hydrodynamic boundary layer localized around the adsorbent particle
2. Adsorbate transport from boundary layer to the exterior surface of the adsorbent (external mass transfer resistance)
3. Transport of adsorbate from the surface to the interior of adsorbents (internal mass transfer resistance) by diffusion through the pores (pore diffusion) or by diffusion in adsorbate state along the internal surface (surface diffusion)
4. Interaction between the molecules of the adsorbate and adsorption sites.
5. If there is a reaction, adsorbed reactants form products and then, products are desorbed. Later, desorbed products transport to the external surface of the adsorbent.

It is assumed that first and fourth steps occur very rapid and overall adsorption rate is established by the external or intraparticle diffusion owing to the fact that external diffusion and intraparticle diffusion act in series and overall adsorption rate is determined by the slower process. Difference between external and intraparticle diffusion is dependent on hydrodynamic conditions especially on stirring rate in slurry reactors. This difference makes able to diversify the transport mechanisms and provides the chance to affect their relative impact on the overall adsorption rate. Increase in the stirring rate increases external (film) diffusion rate owing to decrease in the boundary layer thickness. Contrary to external diffusion, intraparticle diffusion is not dependent on the stirring rate. Particle size influences the both intraparticle diffusion and external diffusion due to alteration of the surface area and diffusion paths. It is known in a normal way that the mass transfer through the adsorbent particle occurs by pore diffusion and surface diffusion in parallel; whereas it is not easy to separate their portions. Thus, intraparticle diffusion is often assumed as predominant in the kinetic model. In the literature, intraparticle diffusion mechanism is typically considered. Also, intraparticle diffusion can be easily defined by a surface diffusion approach.

External Diffusion:

External diffusion (film diffusion) describes the transport of adsorbate from the bulk liquid to the external surface of the adsorbent. The concentration at the external adsorbent surface is always lower than that in the bulk liquid owing to continuing adsorption provided that equilibrium has not reached. That's why, concentration gradient results that extends over a boundary layer of thickness, δ. The driving force of

the external mass transfer is the difference between the concentration in the bulk and the concentration at the external surface. The figure given below illustrates the concentration behavior when the external diffusion is the rate-limiting step and the diffusion through the particle occurs very fast. This means that there is no gradient within the particle and there is no intraparticle diffusion.

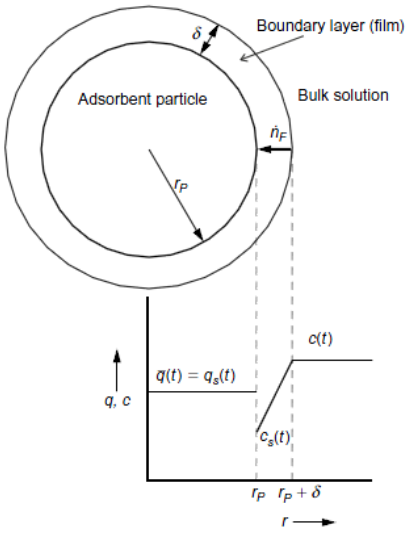

Figure 3.3. The concentration profile in the case of rate-limiting external diffusion (Source: Worch 2012)

The equation describing external diffusion can be yielded by using Fick's law;

$$n_F = D_L \frac{dc}{d\delta} \tag{3.1}$$

where n_F is the flux (for instance; mol/(m^2s) or (g/m^2s), and D_L is the diffusion coefficient in aqueous (m^2/s). Intergration of the Fick's law with the assumption of linear gradient yields that;

$$n_F = k_f (c\text{-}c_s) \tag{3.2}$$

and

$$k_f = \frac{D_L}{\delta} \tag{3.3}$$

where k_f is the external mass transfer coefficient (m/s). The amount of removed adsorbate from the liquid phase and adsorbed onto the adsorbent per unit time, N_F, can be defined by differential material balance.

$$N_F = m_A \frac{dq}{dt} = -V_L \frac{dc}{dt} \tag{3.4}$$

and

$$n_F = \frac{N_F}{As} \tag{3.5}$$

where As it the external surface area of the adsorbent. After substituting the equation into differential material balance;

$$n_F = \frac{m_A}{A_s}\frac{dq}{dt} = -\frac{V_L}{A_s}\frac{dc}{dt} \tag{3.6}$$

After substitution, the following equation is derived;

$$\frac{dq}{dt} = \frac{k_F A_s}{m_A}(c\text{-}c_s) = k_F a_m (c\text{-}c_s) \tag{3.7}$$

where a_m is the surface area of the adsorbent. By using material balance, the concentration decay is calculated as following;

$$-\frac{dc}{dt} = \frac{m_A}{V_L}\frac{dq}{dt} \tag{3.8}$$

The external diffusion equation (Linear Driving Force Rate Law, LDF) is finally derived as;

$$-\frac{dc}{dt} = k_F a_m \frac{m_A}{V_L}(c\text{-}c_s) \tag{3.9}$$

There are some factors influencing the external mass transfer coefficient, k_F. The external mass transfer coefficient is dependent on the same influence factors as the diffusion coefficient in liquid, D_L. Molecule size and temperature are the factors affecting the D_L, directly the k_F. Increasing temperature and decreasing molecule size increase the D_L and k_F. Moreover, k_F is dependent on the film thickness. As mentioned previously, increasing stirring rate decreases the film thickness in slurry reactors. Therefore, k_F increases with increasing stirring rate. Empirical correlations between k_F and the influence factors can be used to estimate film mass transfer coefficients in especially fixed-bed adsorber design. These empirical correlations described in the literature are Reynolds (Re), Sherwood (Sh), and Schmidt (Sc) number in different forms.

As described previously, the adsorbate initially reaches to the exterior surface of the adsorbent. Due to liquid film resistance, the adsorbate concentration at the surface of the adsorbent (Cs) is lower than that in the bulk of the fluid (Cb). This difference is dependent on the followings;

- The mass transfer coefficient from the fluid to the surface of the adsorbent
- If it happens, the reaction rate constant.

Hence, the overall rate is expected to be lower than that based on the concentration of the adsorbent in the main body of the fluid. Moreover, temperature gradient can also be evaluated owing to film resistance. That's why, the temperature of the bulk of the fluid (Tb) would be different than the temperature of the exterior surface of the adsorbent (Ts). This difference is dependent on the followings;

- The heat transfer coefficient between the fluid and catalytic surface
- If it happens, the reaction rate constant.

Moreover, the temperature gradient also depends on the reaction type; exothermic or endothermic. The adsorbent surface is hotter than the bulk fluid for exothermic reactions while contrary case occurs for endothermic reactions.

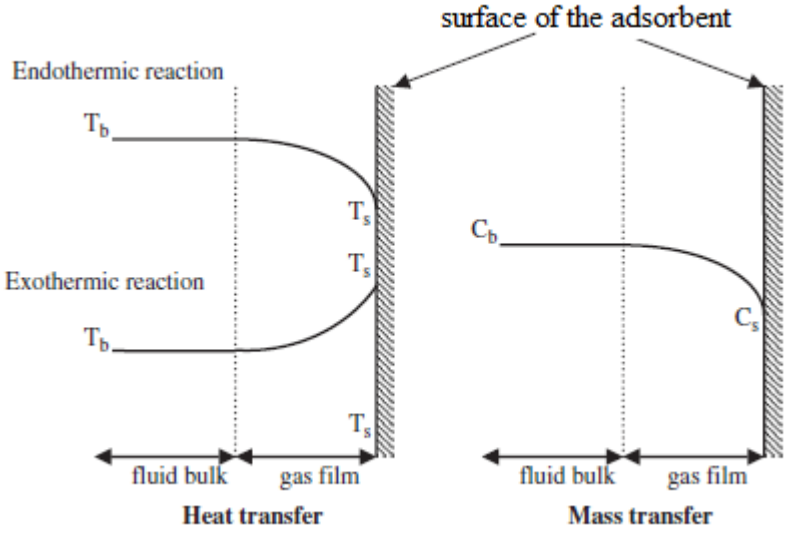

Figure 3.4. Temperature and concentration profiles at the surface of the adsorbent (Source: Inglezakis and Poulopoulos 2006)

As Figure 3.4. illustrates that the overall rate increases with higher temperature on the surface of the adsorbent, whereas it decreases owing to decrease in adsorbate

concentration simultaneously. After the balance between these competitive factors, the conditions of the fluid bulk determines whether overall rate will be higher or lower than the corresponding one. For the endothermic reaction, the overall rate is always lower than the rate corresponding to the conditions of the bulk of the fluid. This phenomenon is named as external not only due to occurring outside the adsorbent but also due to be independent of the chemical reaction. This phenomenon is totally contrary to the internal mass and heat transfer phenomena. Flow conditions, adsorbent properties and fluid determine the mass and heat transfer coefficients. The mass transfer rate of the adsorbate from the fluid bulk to the adsorbent surface is equal to the reaction rate (n^{th} order) under steady state conditions. The equation given below describes the relationship between reaction rate and mass transfer rate;

$$\underset{\text{Mass transfer rate}}{k_F A_s (C_b - C_s)} = \underset{\text{Reaction rate}}{k_m C_s^{\,n}} \qquad (3.10)$$

where;

kf: The external mass transfer coefficient of the reactant (m/s);

km: Reaction rate constant per unit mass of catalyst;

As: External surface area of the adsorbent (m^2/kg)

Cb: Concentration of the reactant at the bulk

Cs: Concentration the reactant at the adsorbent surface

n: Reaction order

The bulk concentration, C_b determined experimentally is used to define the overall rate, r_{ov}. When the reaction order is equal to 1, the overall rate is written as following;

$$r_{ov} = k_{ov} C_b \qquad (3.11)$$

where;

$$\frac{1}{k_{ov}} = \frac{1}{k_m} + \frac{1}{k_F A_s} \qquad (3.12)$$

The overall rate is first order with a constant being the combination of the mass transfer resistance and reaction; whereas there are two cases to determine the rate-limiting step;

The external mass transfer is rate limiting with $k_f << k_m$ and $r_{ov}=k_f A_s C_b$;

The reaction is rate-limiting step with $k_f >> k_m$ and $r_{ov}=k_m C_b$.

Here, it is beneficial to define the external effectiveness factor that is the ratio of the observed overall rate, r_{ov} to the chemical reaction rate r_0 without diffusion (Cs=Cb).

$$\text{The effectiveness factor}=\frac{r_{ov}}{r_0}=\frac{\text{The overall rate}}{\text{Reaction rate without mass transfer}} \tag{3.13}$$

The Damköhler number (Da) is the ratio of the reaction rate to the mass transfer rate and it is used to decide if the external mass transfer is the rate-limiting step or not.

$$Da=\frac{k_m C_b^{n-1}}{k_F A_s} \tag{3.14}$$

A high Damköhler number shows that the global rate is controlled by mass transfer. Thus, Damköhler number can be used to rewritten the process rate and the external effectiveness factor can be deduced. For higher reaction orders, the external mass transfer limitation is seen as more clear. When the Damköhler number is higher than the 0.10, the external mass transfer is controlling the global rate. Also, the external effectivess factor increases with increasing Damköhler number for reaction order of 1 (negative order means that the increasing reactant concentration inhibits the reaction rate.)

Intraparticle Diffusion:

If the diffusion is radial, the diffusion equation can be written as given below for a constant diffusion coefficient;

$$\frac{\partial C}{\partial t}=D\left(\frac{\partial^2 C}{\partial r^2}+\frac{2}{r}\frac{\partial C}{\partial r}\right) \tag{3.15}$$

If u=C*r, the equation can be simplified to;

$$\frac{\partial u}{\partial t}=D\frac{\partial^2 u}{\partial r^2} \tag{3.16}$$

The solutions in radial flow in a sphere can be deduced from the linear problems by the leading of the equation for linear flow in one dimension given above.

Diffusion from a well-stirred solution of limited volume:

When the the volume of the solution (except of the space occupied by the sphere) is *V*, it is supposed that the sphere occupies the space r<a. Also, the solute concentration in the solution is uniform and is C_0. The sphere is free from the solute and

the equation given below shows the relation of the total amount of solute in the sphere after time (t) as the corresponding quantity after infinite time.

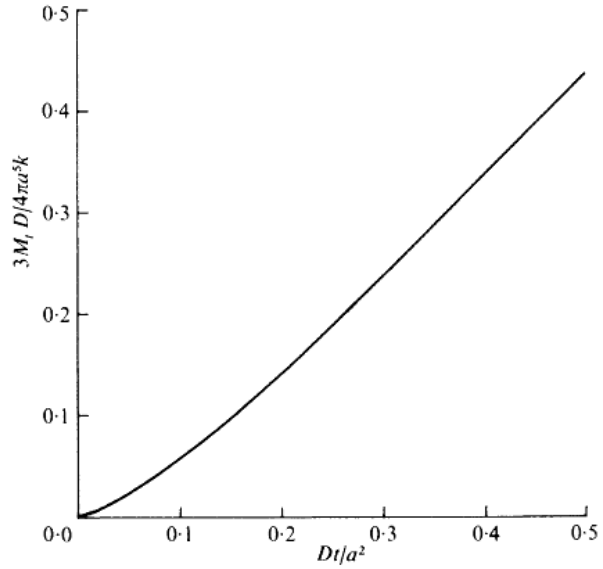

Figure 3.5. Sorption curve for sphere with k_t surface concentration

Following equations were used to describe intraparticle diffusion;

$$\frac{Mt}{M\infty}=1-\sum_{n=1}^{\infty}\frac{6\alpha(\alpha+1)\exp(-\frac{Dqn^2t}{a^2})}{9+9\alpha+qn^2\alpha^2} \tag{3.17}$$

where the qn is the non-zero roots of the equation given below;

$$\tan qn=\frac{3qn}{3+\alpha qn^2} \tag{3.18}$$

and $\alpha=3V/(4\pi a^3)$, the volumes of solution and sphere ratio, or there can be partition factor of K between solute in equilibrium in the sphere and $\alpha=3V/(4\pi a^3K)$. Moreover, the relation given below demonstrates the "α" as the final fractional uptake of solute by the sphere.

$$\frac{M\infty}{VC_0}=\frac{1}{1+\alpha} \tag{3.19}$$

where;

M_t=Total Amount of solute at time t (g)

M_∞=Total Amount of solute at equilibrium (g)

D=Intraparticle Diffusion Coefficient (m^2/s)

q_n=Adsorption Capacity at time t (mg/g)

α=Ratio of volumes of solution and sphere

C_0=Initial solute concentration (mg/l)

V=Volume of solution (l)

α=Spherical catalyst particle radius (m)

Reaction Kinetic Models:

Many of papers have been published in literature to describe adsorption kinetics by simple models based on chemical reaction kinetics, eventhough diffusion models are seen as appropriate models to define the kinetics of adsorption for porous adsorbents. These papers mention with the adsorption of district adsorbates being ot only organic pollutants but also heavy metals onto adsorbents such as biosorbents, natural zeolites and low cost adsorbents. However, these models are applied for several reasons, they should be viewed for the sake of completeness. Also, kinetic models would be very beneficial to comprehend and to establish the rate-limiting step for the certain adsorption system.

The adsorption kinetics can be defines with following equation under the assumption that the adsorbent uptake the adsorbate by the leading of a first-order rate law;

$$\frac{dq}{dt}=k_1(q_{eq}-q) \tag{3.20}$$

where k_1 is the first-order rate constant. Integration the equation within the boundary conditions of q=0 at t=0 yields;

$$\ln\frac{(q_{eq}-q)}{q_{eq}}=-k_1t \tag{3.21}$$

The slope of the plot of ln((qeq-q)/qeq) with respect to time yields the first-order rate constant (k_1). However, first order rate law equation seems as identical with the linear driving force rate law (LDF). The driving forces of LDF and first order rate law are different. In the first order rate law; the driving force is the difference between the final equilibrium loading that is constant for a given initial concentration and adsorbent dosage and the time,t. In the LDF model, the difference between equilibrium adsorbent loading at the surface at time t and the average adsorbent loading at t is the driving force. Hence, the average adsorbent loading is only dependent on the time in the kinetic

model; but both loadings, qs and q alter with time in the LDF model. Thus, there are differences in kinetic curves calculated with reaction kinetic model and linear driving force rate law.

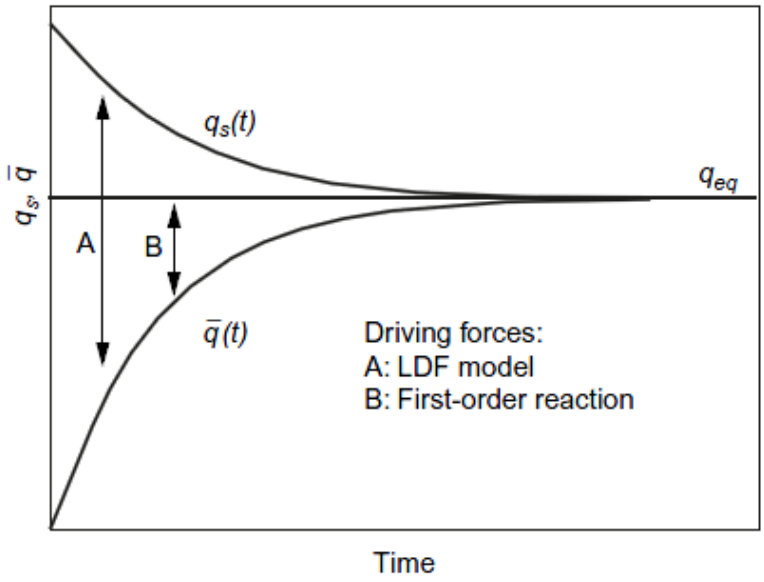

Figure 3.6. Driving forces for LDF model and first-order reaction model (Source: Worch 2012)

The other kinetic approach is based on the pseudo second-order rate law. The equation given below shows the equation based on this law.

$$\frac{dq}{dt}=k_2(q_{eq}-q)^2 \tag{3.22}$$

Where k_2 is the pseudo second-order rate constant. Integration of the equation within the boundary conditions of q=0 at t=0 yields that;

$$\frac{t}{q_t}=\frac{1}{k_2 q_{eq}^2}+\frac{t}{q_{eq}} \tag{3.23}$$

Linear regression should be carried out to calculate the pseudo second-order rate constant. It would be beneficial to apply linear regression with t/q_{eq} as independent variable and with fixed slope of 1 if q_{eq} was calculated from the isotherm. It is clear from the literature that intraparticle diffusion, surface and/or pore diffusion, plays significant role in kinetics and intraparticle diffusion is the rate-limiting step in common cases for the adsorption of pollutants on the porous adsorbents. It is accepted assumption that the final adsorption step is more rapid than the previous adsorbate

transport by diffusion. Additionally, intraparticle diffusion model can be extended by the addition of the film diffusion; whereas there is no report for reaction kinetics regarding such extension. Even if reaction kinetics providing reasonable explanations to adsorption process with porous adsorbents where chemisorption acts significant and major role, make able them to define the batch adsorption experiments with porous adsorbents, the lack of strong theoretical background about adsorption process and transferability of the rate constants to other conditions make kinetic models empirical equations. Thus, this character of kinetic models should be taken into considerations. When compared to diffusion models, kinetic models have taken much more attraction thanks to their simpler structure in order to apply them in the adsorption studies. Moreover, kinetic models are often compared with the linear relationship between q and $t^{0.5}$ (Weber-Morris model) so as to illustrate that certain adsorption system is not relevant to the diffusion, even Weber-Morris model is an approximate solution for the diffusion and initial stage of the adsorption process can only be described by this model. Hence, the plot of q with respect to $t^{0.5}$ over a broader time interval can be used for diffusion-controlled processes and is not used for missing intraparticle diffusion impact on adsorption kinetics.

Surface Chemistry:

Adsorbate-adsorbent interaction was affected by the surface chemistry dependent on the type of the adsorbent. This is true for the adsorption onto oxidic adsorbents.

The characterization of aluminum oxide or ferric hydroxide as oxidic adsorbents are applied by crystalline structures in which positively charged ions and negatively charged oxygen or hydroxide ions are arranged in a way that different charges compensate each other. The charges must be compensated by other ions at the surface. Negative charges of surface oxygen ions are neutralized by the protons; but hydroxide ions neutralize the positive charges of the surface metal ions. Hence, surface OH groups cover the surface of the oxidic adsorbents. Protonation and deprotonation being dependent on the pH value of the solution occurs to these groups.

$$\equiv S\text{-}OH + H^+ \leftrightarrow \equiv S\text{-}OH_2^+$$

$$\equiv S\text{-}OH \leftrightarrow \equiv S\text{-}O^- + H^+$$

where ≡S represents the surface of the solid material. It is known that the surface is positively charged at low pH and negatively charged at high pH values. The net charge at the surface is zero provided that pH value has to be between these regions. This point where the net charge is zero is named as the point of zero charge (zpc). The pH_{zpc} is very significant phenomenon that it helps to comprehend the adsorption of charged species and the influence of pH on the adsorption. It is expected that electrostatic attraction or repulsion forces affects the adsorption of charged species onto charge surfaces.

The surface charge depending on the pH and pH_{zpc} can be established by titration of adsorbent suspension with acids and bases as HCl and NaOH. General mass and charge balance are used to calculate the surface charge, Qs (mmol/g or mol/kg) for each point of the titration curve.

$$Q_s=q(H^+)-q(OH^-)=\frac{V_L}{m_A}(c_a-c_b-c(H^+)+c(OH^-)) \tag{3.24}$$

where $q(H^+)$ is the surface loading with H ion while $q(OH^-)$ is the surface loading with OH^-. The molar concentration of the acid is represented by c_a and c_b is the molar concentration of the base. The proton concentration after equilibrium is measured as pH and it is represented by $c(H^+)$. The OH^- concentration is shown as $c(OH^-)$. Moreover, V_L is the volume of the solution and m_A is the mass of adsorbent.

The surface charge density can be calculated by using surface charge as following;

$$\sigma s=\frac{Q_s\,F}{A_m} \tag{3.25}$$

where F is the Faraday constant and $A_m(m^2/kg)$ is the surface area. The plot of Qs (or σs) vs pH yields the influence of the pH on the surface charge. Also, intersection with the horizontal axis gives the pH_{zpc}.

Bounding of dissolved ions to the surface OH groups occurs via different mechanisms which are specific adsorption in which surface complex formation occurs and nonspecific adsorption. The mechanisms depend on the structure of the electric double layer surrounding the solid particle. There are two different types of reactions in the surface complex formation. These are the formation of inner sphere complexes and outer-sphere complexes. The ions of the adsorbate without water molecules of the

hydration sphere bonds to the surface site by ligand exchange in the term of inner-sphere complexes. The reactions given below show the replacement of the cations and the protons of the surface OH groups.

$\equiv S\text{-}OH + M^{2+}(\text{bivalent cation}) \leftrightarrow \equiv S\text{-}OM^{+} + H^{+}$

$2\equiv S\text{-}OH + M^{2+} \leftrightarrow (\equiv S\text{-}O)_2M + 2H^{+}$

Whereas the reaction given below occurs in the case of anions;

$\equiv S\text{-}OH + A^{2-} \leftrightarrow \equiv S\text{-}OM^{+} + H^{+}$

$2\equiv S\text{-}OH + A^{2-} \leftrightarrow (\equiv S)_2A + 2OH^{-}$

The reactions given above explains that the adsorption of cations increases with increasing pH while the adsorption of anions increases with decreasing pH. Acid-base equilibrium affects the adsorption providing that the adsorbate is a weak acid. Hence, it must be included in the equilibirium calculations. The adsorbed ions are strongly bound and located in a compact layer directly attached to the surface. Also, this part of the electric double layer is called as the surface layer. As the reactions given above implies that neutral or charged surface complexes being dependent on the ion charge and the number of reaction sites is formed by the adsorption of ions.

In the case of outer-sphere complex, it is assumed that ions bond to the surface sites via chemical bonds without losing hydration water. This explains that there is a water molecule between the ion and the adsorption site. Thus, the binding strength is weaker and the distance to the surface is larger for outer-sphere complex when compared to inner-sphere complex formation. The outer-sphere complex formation occurs at the layer called as β layer being the part of the compact layer within the double-layer model. Excess counter ions compensate the left surface charge at the diffuse layer. Until the concentration of the cations equal to the concentration of the anions, the concentration of the counter ions decreases with increasing distance from the surface throughout the diffuse layer. Electrostatic interaction is the reason for the enrichment of counter ions in the diffuse layer. Hence, it is considered as nonspecific adsorption.

A number of various models are developed to describe the charge distribution and the counter ions accumulation. There are three main models used to characterize the adsorption onto oxidic adsorbents. These are the constant capacitance, the diffuse layer, and the triple layer models. These models are used for different assumptions regarding the charge distribution and the location of the adsorbed species. . The Figure 3.7 shows

the surface potential as function of distance from the surface for different complexations.

Table 3.3. The models used to describe surface complex formation and its assumptions

Model	Assumptions
The constant capacitance	• Adsorption of species in the surface plane • No β layer • Charge opposite to that in the surface plane provided by nonspecifically adsorbed ions, all located in the d plane
Diffuse layer	• No β layer • Adsorption of species in the surface plane • Charge opposite to that in the surface plane provided by • nonspecifically adsorbed ions, starting in the d plane and distributed
Triple Layer	• Adsorption of dehydrated species in the surface plane • Adsorption of hydrated species in the β plane • Charge opposite to that in the combined surface and β planes provided by nonspecifically adsorbed ions, starting in the dplane and distributed

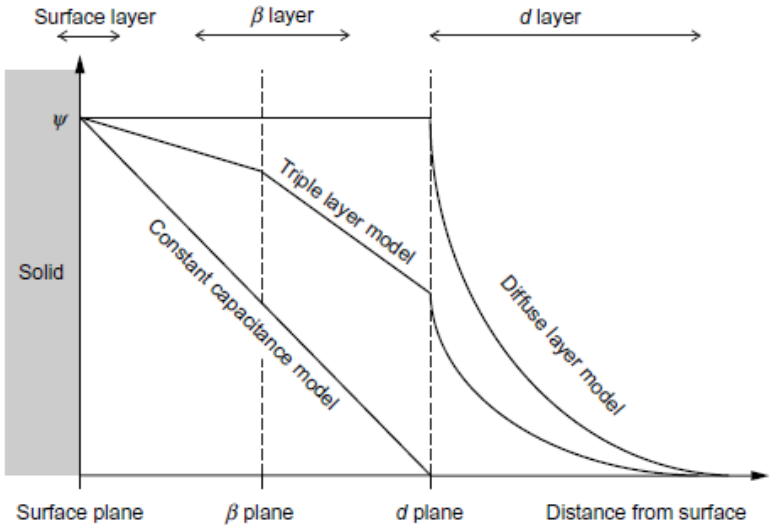

Figure 3.7. The surface potential as function of distance from the surface for different complexations (Source: Worch 2012)

There are many limitations to apply these models into adsorption process as uncertainties regarding model assumptions, the need of simplifications, and the problems in parameter establishment (increasing complexity if a large number ions are exist in the water). Even if, there are problems to apply these models into adsorption isotherms, knowledge concerning the pH dependent charges and the location of the point of zero charge is very beneficial to make interpretation on the adsorption process.

CHAPTER 4

REMOVAL OF POLLUTANTS

4.1. Removal of Pollutants via Zeolite Applications

The industry is faced with tremendous set of environmental problems as remediation of hazardous wastes, contaminated ground waters, and control of toxic air contaminants. Hence, degradation of these hazardous wastes is priority of humanity to avoid their effects. In the United States, 540 million metric tons of solid and liquid wastes has been generated by 14000 installations. Even though some fractions of these wastes are degraded in the land, some of them contaminate the underground or surface water and soil. Ground water seems to be the primary source contacting with people. These wastes involve solvents, volatile organics, chlorinated volatile organics, dioxins, dibenzofurans, pesticides, polychlorinated biphenyls, chlorophenols, asbestos, heavy metals and arsenic compounds.

Fast developments of various industries with the increase of the population bring about many environmental problems. An enormous quantity of wastewater has been produced by industrial processes and applications every day, whereas do very little to treat the wastewater. Many pollutants such as ammonium, inorganic anions, heavy metal ions, oil and organics, which have poisonous and toxic effects on ecosystems are included by wastewater. There are many processes that can be used to remove these contaminants such as adsorption, aerobic treatment system, membrane distillation/bioreactor, activated sludge systems, reverse osmosis, sedimentation, wet oxidation, chemical addition etc. Among them, adsorption is frequently favored due to initial low cost, flexibility, easy of design and operation, and effective technique in order to clean up wastewater (Malkoç 2012)

Zeolite is preferred as a sorbent in wastewater treatments thanks to their low costs, unique ion exchange and sorption properties. Nowadays 40 types of natural zeolites and approximately 200 synthetic zeolites have been reported in literature (Shoumkova 2011). Clinoptilolite, mordenite, phillipsite, chabazite, stilbite, analcime, and laumontite are widespread forms of natural zeolites. On the basis of their ion

exchange property, they can be used for radioactive waste treatment, heavy metal and ammonia removal from wastewater, and also organic compounds removal from wastewater (Breck 1974). The following sections provide a literature review regarding removal of pollutants by using different methods such as adsorption and photocatalytic oxidation processes and application of the zeolites in various wastewater treatment processes.

4.1.1. Adsorption of Pollutants on Zeolites

Most of the industries such as textile, paper, printing, leather, food, cosmetics, etc. use dyes to color their final product. Release of the waste dyes to clean water affects its intended beneficial use, causes light penetration, retards photosynthetic activity, and restrains the growth of biota (McKay et al. 1980).

Wang and Zhou (2006) investigated the adsorption of two dyes, methylene blue and rhodamine B, onto Australian natural zeolites mainly composed of clinoptiloite, quartz and mordenite with a cation exchange capacity of 120 meq/100 g. The results demonstrated that adsorption capacity for methylene blue has higher quantity than that of rhodamine B. The maximal adsorption capacity was reached as 2.8×10^{-5} and 7.9×10^{-5} mol/g at 50^{o}C for rhodamine B and methylene blue, respectively. Kinetic studies showed that adsorption on the Australian zeolite fitted to the pseudo second-order adsorption model with two-step diffusion process. Besides, Langmuir and Freundlich models are used to be fitted the adsorption isotherm.

A natural zeolite (clinoptilolite), which is a clay mineral from Gördes region of Turkey, was tested for three reactive dyes (Everzol black, everzol red, everzol yellow) by a series of batch adsorption experiments. In the study, Armağan et al. (2004) indicated that the uptake of the reactive dyes affects from the degree of hydrophilicity, and also showed the limited adsorption capacity of natural zeolites for the reactive dyes. The capacity was enhanced by modifying its surfaces with quaternary amines. Whilst natural zeolite had slightly positive adsorption density, modified zeolites provided adsorption densities in the range of 2.9 to 7.6 mg/g.

Natural polymers produced by biological decomposition of plants and other organisms are called as humic substances (Abate and Masini 2003). On the basis of their solubility under acidic or alkaline conditions in aqueous solution, humic

substances are usually classified as humin, humic acids and fulvic acids (Leone et al. 2013). Removal of these substances from water is required due to the production of toxic chemicals with the presence of humic substances in water.

Adsorption of humic substances onto natural zeolites is a suggestible method to clean up water. Capasso et al. (2005) conducted a study about adsorption of humic acid onto untreated zeolitic Neapolitan Yellow Tuff (philipsite + chabazite) and Li^{+}-, Na^{+}-, K^{+}-, NH^{4+}-, Ca^{2+}-, Mg^{2+}-, or Ba^{2+}- enriched samples. It was shown that Li^{+}, Na^{+}, K^{+}, and NH_4^{+} (monovalent cations) cause to diminish the adsorption ability of Neapolitan Yellow Tuff, whereas Ca^{2+}, Mg^{2+}, and Ba^{2+} raise the adsorption. Capasso et al. (2007) also investigated Ca^{2+} enriched samples to remove humic acids from water. Adsorption equilibrium tests and dynamic experiments were applied. The results demonstrated that the sorption capacity enhance with the ionic strength and has the highest value at pH 7.4. Besides, Leone et al. (2013) studied Ca^{2+} enriched- clinoptilolite-rich tuff from New Mexico (USA) with batch technique. Kinetic analysis showed that the adsorption process taking quite a few days follows a two-step pattern. In the study, Langmuir and Freundlich models were used to fit the experimental data.

In addition to dyes and humic acids, many pollutants produce from various industrial processes and applications such as phenolic compounds, petroleum, pesticides, and pharmaceuticals etc. Most of them have higher toxicity than dyes and humic acids and need removing from water to prevent adversely ecological effects.

Surfactant modification of zeolite is generally applied to remove the types of organics. Kuleyin (2007) conducted a study about the adsorption of phenol and 4-chlorophenol on hexadecyltrimethylammonium (HDTMA) and benzyldimethyltetradecylammonium (BDTDA) modified natural zeolite. Removal efficiencies were reached to 71% and 73% for phenol, and 81% and 89% for 4-chlorophenol onto HDTMA- and BDTDA- zeolites, respectively. The maximum capacities of surfactant modified zeolite for phenol and 4-chlorophenol were also detected in the range of 0.7647–1.2977 mg/g and 6.4102–12.7065 mg/g, respectively. Like phenol, aniline and nitrobenzene require to remove from water. Ersoy and Çelik, (2004) examined removal of toxic non-ionic organic contaminants (NOCs), aniline and nitrobenzene from wastewater by using natural-zeolite and organo-zeolite in batch and continuous systems. As expected, the adsorption capacity of these contaminants onto natural zeolite surface was limited, whereas modification of zeolite surface by HDTMA causes to increase the adsorption capacity. Besides, the adsorption capacity of NOCs

onto organo-zeolite under the present conditions was determined as 2.36 and 3.25 mg/g for aniline and nitrobenzene, respectively.

Heavy metals are generally considered to be those whose density exceeds 5 g/cm^3. The most hazardous heavy metals can be listed arsenic, cadmium, chromium, copper, nickel, zinc, lead and mercury. Many industries discharge a variety of toxic heavy metals into the environment. Thus, they are compelled to treat waste liquids that contain appreciable quantities of toxic metals. For the removal of heavy metals at trace quantities, zeolite adsorption is considered to be a particularly competitive and effective process.

Oter and Akcay (2007) evaluated the adsorption potential of natural clinoptilolite from Gordes mines (West Anatolia, Turkey) for the uptake of Pb^{2+}, Zn^{2+}, Cu^{2+}, and Ni^{2+} in single and mixed ion solutions with using batch method. Ion sorption parameters as contact time, initial solution pH, solid to liquid ratio, and initial metal cation concentration were determined in the study. The maximum adsorption capacity was found as 0.730, 0.251, 0.227 and 0.173 meq/g for Pb^{2+}, Zn^{2+}, Cu^{2+}, Ni^{2+} in single ion solution, respectively. Though, the adsorption capacity in mixed ion solutions were considerably reduced to 0.299, 0.108, 0.022 and 0.017 meq/g for Pb^{2+}, Zn^{2+}, Cu^{2+}, Ni^{2+}, respectively. Bosso and Enzweiler (2002) investigated removal of Pb^{2+}, Cu^{2+}, Zn^{2+}, Ni^{2+}, and also Co^{2+} and Cd^{2+} from aqueous solutions. The used zeolite was Scolecite associated with to basalts of Parana Continental Igneous Province (PCIP, South America). The maximum adsorption capacities were detected at pH=6, C_i (initial concentration) = 30 mg/L as 0.056, 0.130, 0.064, 0.031, 0.0078, 0.0032 meq/g for Pb^{2+}, Cu^{2+}, Zn^{2+}, Ni^{2+}, Co^{2+}, and Cd^{2+}, respectively. The selectivity potential of zeolite was $Cu^{2+} > Zn^{2+} > Pb^{2+} > Ni^{2+} > Co^{2+} > Cd^{2+}$, which is the opposite order to the report of Oter and Akcay (2007) ($Pb^{2+} > Zn^{2+} > Cu^{2+} > Ni^{2+}$).

High concentrations of ammonia (NH_3) and ammonium ion (NH_4^+) in wastewaters cause eutrophication of rivers, lakes, and epeiric seas. Additionally, NH_3 and NH_4^+ in environmental water cause acute toxicity in fish species even though the concentration is less than 10 mg/L (Ichikawa et al. 2014). Zeolite was also used as adsorbent to separate ammonia (NH_3) and ammonium ion from wastewater.

Chilean natural zeolite mainly composed of clinoptilolite and mordenite was used to remove ammonia from aqueous solution in the study conducted by Englert and Rubio (2005). The removal of ammonia emerged with proceeding through ion-exchange and rapid kinetics (rate constant of 0.3 min^{-1}) at neutral pH value, with removal

capacities up to 0.68 meq NH_4^+/g. The capacity of ammonia adsorption on the zeolite ranged between 11.4 and 14.8 mg/g. The Langmuir isotherm model provided good equilibrium data fitting. Gunay (2007) evaluated NH_4^+ adsorption on natural Bigadic clinoptilolite. The results showed that lower temperature is favorable for ammonium removal by the clinoptilolite and this reaction is exothermic in nature. In the study, the equilibrium data was analyzed with using three two-parameter isotherm models (Langmuir, Freundlich and Temkin) and three three-parameter isotherm models (Redlich–Peterson, Sips and Khan). The best performance among these isotherm models was detected as Khan's model. The capacity of ammonia adsorption on the zeolite were estimated in the range of 14.5 and 15.4 mg/g between 23-70^oC.

4.1.2. Photocatalytic Degradation of Pollutants over Natural Zeolite Supported TiO_2 Composites

With the modification application area of the natural zeolites can be enriched to remove pollutants from aqueous medium. Li et al. (2005) used natural zeolite as support to prepare TiO_2 photocatalyst for degradation of the methyl orange in the existence of 250 W-high Hg lamb. The surface or interface effect between the natural zeolite and TiO_2. Simultaneously, the morphology changes and the bond vibrations were investigated. The kinetic processes of photocatalytic reaction of methyl orange have been measured so as to examine the photoactivity and utility of different photocatalysis. Interaction between TiO_2 and zeolite decreased the structural stability of microporous frame of zeolite during the heat treatment.

In preparation of natural zeolite tuff supported TiO_2 photocatalyst, TiO_2 colloid particles combine with the active sites of clinoptilolite by Ti-O-Al and Ti-O-Si making the load of TiO_2 more durable than simplice physical combination. Another point worth mentioning is that Li et al. (2005) tried to describe the possible mechanism for incorporation of TiO_2 on natural zeolite and they offered three possible methods defining the combination of TiO_2 colloid particles to natural zeolite. In the first scenario, -H coming from the TiO_2 colloid particle reacts with the surface –OH combining with Al being in the zeolite so as to form water. Ti-O-Al bond formation occurred via the formation of ≡Ti-O- and –Al≡. As a second scenario, water is formed

by combination of –OH from TiO_2 colloid particle and H- from zeolite. Thanks to static stress, the bond of Ti-O-Al is generated by the combination of O-Al≡ and ≡Ti-. Thirdly, deposition of Si at the Y crossing provides the combination of Si-O tetrahydron with special Si atom, making the bond between surface O and special Si atom weaker. Si cannot show the similar behavior with Al as mentioned in the second scenario owing to the lower static capability of Si. Thus, -H coming from TiO_2 colloid particles reacts with the surface O of special Si atom to form water and then, Ti-O-Si bond is generated by the combination of –Si ≡ and ≡ Ti-O-.

Nikazar et al. (2008) studied the photocatalytic degradation of azo dye Acid Red 114 by using clinoptilolite supported TiO_2 photocatalyst. Hence, this study would lead to comprehend the effect of natural zeolite on photocatalytic degradation. They chose the solid state dispersion (SSD) method to prepare clinoptilolite supported TiO_2 photocatalyst. Another attractive point of the study was that the effect of the compostion of the supported photocatalyst was investigated. They found that the photocatalyst containing 10%TiO_2 and 90% clinoptilolite showed most effective performance if the SSD was the method to prepare supported photocatalyst. They suggested that surface –OH of the photocatalyst was easily transferred on to the surface of clinoptilolite and adsorbed organic pollutant on clinoptilolite had a chance to be degraded owing to the –OH transferred from photocatalyst surface to clinoptilolite. Hence, photocatalytic performance enhanced when compared to non-supported photocatalyst. Also, they mentioned regarding the synergetic effect between TiO_2 and clinoptilolite owing to the fact that the presence of clinoptilolite maintained the molecules of organic pollutant near the photocatalyst. Shortly, they benefited from the high adsorption capacity of clinoptilolite. They investigated the interaction between the catalyst components by FTIR and XRD. They had seen no diffraction peaks belonging to TiO_2 in the supported photocatalyst. In the FTIR analysis, surface –OH was little weaker after TiO_2 loading and there was new formation of Ti-O-Si and Ti-O-Al stretching vibrations at a range of 945-905 cm^{-1}. Also, the influences of pH, amount of catalyst and initial concentration of dye on photocatalytic degradation of Acid Red 114 were investigated. pH values were adjusted by NaOH and H_2SO_4. The optimum pH was obtained about 4. The photodegradation efficiency increases with an increase in the amount of photocatalyst up to value of 40 ppm and then decreases. Moreover, the photodegradation conversion of AR 114 decreases with increasing in the initial concentration of AR 114 (20, 40, 60,

80 ppm). Another outome of the study is that the kinetics of photocatalytic degradation of AR114 is of the pseudo-first order with K=0, 0127 min^{-1}.

Nikazar et al. (2008) studied the photocatalytic degradation of Azo dye disperse Yellow 23 in water by using clinoptilolite supported TiO_2 photocatalyst. This study showed similarity with their previous study. They found the optimum pH as 11 and the kinetics of photocatalytic degradation of AR114 is of the pseudo-first order with K=0, 0119 min^{-1}.

4.2. Removal of Terephthalic Acid (and its derivatives)

Terephthalic acid, 1, 4-benzenecarboxylic acid (TPA), the para form of phthalic acid is the raw material of polyster fiber, PET bottle, PET film, plastics and feed additives (Figure 4.1).

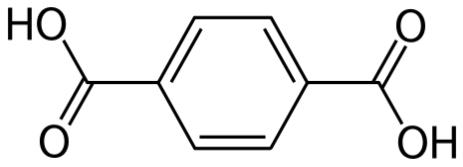

Figure 4.1. Chemical structure of terephthalic acid (TPA)

Specially, it can be found in the sediments, natural or waste waters, soils and aquatic organisms, so that US Environmental Protection Agency placed terephthalic acid in the list of priority pollutants (Thiruvenkatachari et al. 2007). The wastewater in which TPA exceeds its limit, 3.4 µg/l flows into springs and this causes negative impacts on environment and human health from the point of cardiovascular, kidney and respiratory systems. It is quite apparent the requirement for removal of terephthalic acid from the peripheral sources. Several methods such as analytical, biochemical, and physicochemical being able to degrade these hazardous chemicals contaminating soil, air and especially water.

In this study, the aim is to remove terephthalic acid from aqueous medium. Hence, preliminary investigations are very significant to forecast the possible mechanisms, problems, and cases.

Semiconductor photocatalysis comes to forefront among these methods so as to promise the degradation of the organic pollutants with extremely high performance at

ambient conditions. For terephthalic acid the adsorption and advanced oxidation processes as photocatalytic oxidation (UV or visible light-TiO_2), ozonation, fenton oxidation (H_2O_2-Fe). The methods based on the phenomenon that highly oxidizing free radicals oxidizing the organic compound, TPA, are generated and these radicals convert the organic pollutant into harmful compounds or compounds having smaller molecular weight being destructed easily in biological way. The most significant property of the oxidation processes is to have chance to degrade the organic pollutant in ambient conditions (atmospheric pressure and room temperature).

Thiruvenkatachari et al. (2007) studied the oxidation processes so as to destruct the terephthalic acid. Firstly, they studied the photocatalytic oxidation of terephthalic acid by keeping the terephthalic acid and TiO_2 conditions constant and pH of the initial solution alters. In that study, it was found that neutral pH is the most convenient value when compared to highly alkaline condition making a decrement in the efficiency of terephthalic acid. When the initial terephthalic acid concentration was 10, 30, and 50 mg/l and TiO_2 concentration was 1000 mg/L, terephthalic acid was degraded completely at 4, 7 and 10 h, respectively. (pH=8) Should the initial concentration of terephthalic acid was increased to higher values, more time (>10 h) had been needed for the complete degradation of terephthalic acid. At same light intensity, increasing TiO_2 concentration made the photocatalytic efficiency decrease. This means that the increment in TiO_2 concentration affected the light penetration. Hence, the efficiency of the photocatalytic degradation had fallen.

Thiruvenkatachari et al. (2007) performed the photochemical oxidation and photofenton oxidation UV-H_2O_2 and UV-H_2O_2-Fe) experiments. The systems of UV-H_2O_2 generate the OH radicals being very effective for oxidizing. By the addition of Fe (II), OH yield increased due to acting as catalyst. It is found for UV-H_2O_2 that acidic medium was more efficient to remove terephthalic acid from the waste water. Oxygen and water formed by decomposition of H_2O_2 not stepping out of line. Even H_2O_2 was very effective for the destruction of terephthalic acid, more H_2O_2, higher than certain amount did not affect the performance for destruction of TPA. It was found that optimum H_2O_2 amount was 3mM for the destruction of 50 mg/L TPA. It was understood that higher amount of H_2O_2 behaves as the extinguishant for hydroxyl radicals; whereas addition of Fe to UV-H_2O_2 system increased the performance of TPA degradation. That was the proof that pH of the solution was affecting the degradation performance. TPA degradation yield started to decrease at high pH values due to the

lack of free iron in the solution and formation of Fe (II) complexes and precipitation of insoluble iron hydroxides prohibiting the regeneration of ferrous ions. Oxidation of OH radicals shows tendency decrease with an increment of pH. Optimum value generally is around 3, even if terephthalic acid would not favor low pH values in its nature. Increasing Fe solution higher than certain amount made the degradation yield decrease due to competition between Fe ions and organic materials for OH radicals.

Catalytic ozonation (O_3-TiO_2/Fe) seemed as the most effective method compared to others described above. The existence of the catalyst had improved performance instead of using ozone alone in the degradation. It is hardly believable to hear that terephthalic acid almost completely be degraded in 10 min via catalytic ozonation with the aid of 55 mg/L $Fe_2(SO_4)_3$ or 90 mg/L TiO_2. Increasing catalyst amount (TiO_2) did not affect the degradation performance while increasing Fe ion concentration decreased the performance. It can be said easily after revising the articles from literature that the mechanism of degradation is quite discrete in the existence of Fe ion and other transition metal catalysts when drawn a parallel between non-catalyzed ozonation.

It is surely beyond doubt that reuniting the oxidation process would improve the degradation in affirmative way as photofenton combined ozone oxidation (UV-H_2O_2-Fe-O_3) degrading 50 mg/L of TPA just in 6 min. This means that there is a synergy between terephthalic acid and combined systems with the exception of photofenton hetro catalytic ozonation (UV-H_2O_2-Fe-TiO_2-O_3). Hence, adopting the systems each other is acting a significant role due to the necessity to establish optimum amount of oxidizing reagent. The most important factor is to reckon among the overall performance. Figure 4.2 shows the possible mechanism of terephthalic acid degradation.

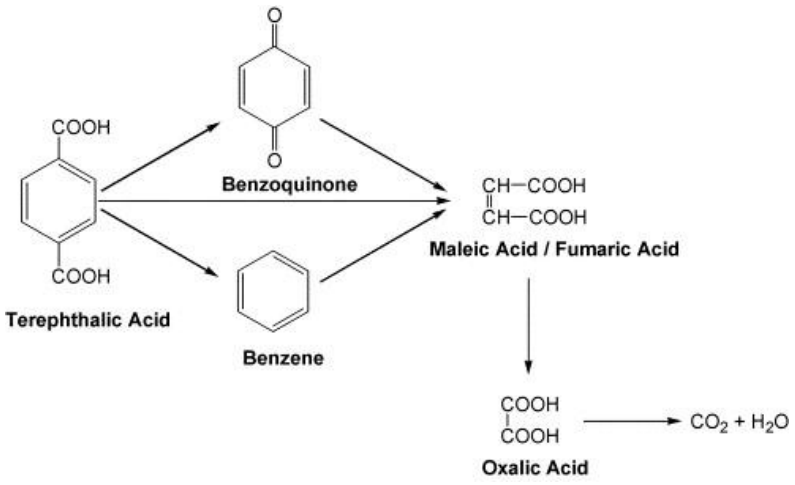

Figure 4.2. Possible degradation mechanism of terephthalic acid (TPA)

Among the advanced oxidation processes mentioned above, the order of efficiency for terepthalic acid degradation can be as follows; Photofenton combined ozone oxidation (UV-H_2O_2-Fe-O_3)> photofenton hetro catalytic ozonation (UV-H_2O_2-Fe-TiO_2-O_3)> catalytic ozonation (O_3-TiO_2)> catalytic ozonation (O_3-Fe(III))> non-catalytic ozonation (O_3) >photofenton oxidation (UV-H_2O_2-Fe)> photochemical oxidation (UV-H_2O_2)> photocatalytic oxidation (UV-TiO_2).

The study of Shafaei et al. (2010) using TiO_2 and ZnO as photocatalysts standed out for removal of terephthalic acid. In the study, degradation of terephthalic acid had performed by immersing powder photocatalysts in slurry in the existence of UV lamb as energy source; whereas there was a problem due to not having a chance to use the photocatalyst again after degradation process. Simultaneously, the effect of influential parameters such as initial pH, catalyst loading, initial TPA concentration and H_2O_2 were investigated. pH was adjusted by NaOH and H_2SO_4. Photodegradation of TPA had increasing tendency up to 6.0 and 9.0 for TiO_2 and ZnO, respectively. Sure enough, increased light intensity increased the decomposition rate of TPA (2,4, and 8 lamps). Moreover, TPA photodegredation enchanced when catalyst amount had increased to 2.5 g/l from 0.2 and 0.3 g/l for TiO_2 and ZnO, respectively. Unsurprisingly, photo degradation rate of TPA increased with certain amount of H_2O_2; whereas there is a decrement in the degradation rate of TPA when the concentration of H_2O_2 was increased from 5.4 to 7.4 mmol/l. As intermediate products; oxalic, formic, maleic, acetic and furmaric acid were determined during the photocataytic degradation of TPA. Additionally, the photocatalyst did not doped with any metal. As a consequence, reuniting of e-/h+ couples and degradation under UV light not visible light had occurred. Hence, there is a necessity to produce more efficient photocatalyst.

The study of Taborda et al. (2001) arouse interest due to dealing with the photocatalytic degradation of phthalic acid in areated sols of TiO_2 nanoparticles. As it is known that terephthalic acid is the para form of phthalic acid and it maintains its importance due to promising to give clue regarding photocatalytic degradation of terephthalic acid. Also, quantum efficiency of catalyst being the most significant phenomenon of photocatalytic reactions is determined. After photocatalytic reaction, they evaluated up to 25 % conversion and the only intermediates detected were the hydroxylate derivatives (3- and 5- hydroxy-phthalate) and salicylate being the product of the photo-Kolbe reaction. At 15 % conversion, near 75 % of phthalate losses is

accounted by salicylate (19%) and the hydroxylated derivatives (57 %). Initial rates for the photocatalytic degradation of the three isomers are almost equal (within 7%).

Even if it seems as the combined oxidation systems are more efficient, it should be careful to optimize the system which used to degrade terephthalic acid. Also, it seems that catalytic oxidation is more economical choice so as to destruct terephthalic acid. It only stands to reason that advanced chemical oxidation methods are not the one and only owing to the fact that adsorption is extremely bodacious opponent to remove terephthalic acid from peripheral sources, especially waste water.

Prior to photocatalytic degradation of hazardous wastes materials such as phthalic acid (Taborda et al. 2001), humic acids (Wiszniowski et al. 2002), the adsorption of waste on composites in the dark conditions are essential. Following decrease waste concentration and proton concentration gives information on adsorption mechanism of waste on the surface. The mechanism of the adsorption can also be prediction step of the kinetics of photocatalytic degradation. In the following of the degradation /adsorption techniques several measurement techniques such as HPLC, pH measurement, COD, TOC and FTIR Drift technique were used together. They had been observed that these carboxylic acids adsorbed on TiO_2 surface by carboxylate groups. Generally adsorption was rapid and equilibrium had been reached in 30 min. It is nonplusing that Langmuir model did not fit the experimental data in this study. It can be interpreted that Langmuir model obeys the physisorption not chemisorption, and surface carboxylate established by DRIFT spectroscopy (strong band at 1580 cm^{-1} and 1390 cm^{-1}, asymmetric and symmetric stretching vibrations) was formed in all studied pH range altering between 1.9-11. Moreover, the samples collected in the adsorption experiments were heterogeneous. Hence, reproducibility of the experiments was restricted. Amount of adsorbed humic acid at equilibrium was influenced by the configuration of adsorbate depending on the concentration of humic acid in solution. All in all, should the maximum adsorption capacity had been the only parameter, the results would have been coherent with the values obtained by Enriquez and Pichat (2001). Robert and Weber (2000) tried to define the adsorption of dicarboxylic acids (oxalic, malonic, succinic, and methylsuccinic acids) on Degussa (P25) in aqueous solution. The demonstration of formation of a dicarboxylate film on the photocatalyst surface was provided via IRFT-DRIFT (the diffuse reflectance infrared spectroscopy). After adsorption experiments, it can be summarized that Langmuir model was well correlated with experimental data. It was found that steric effect has significant role on the adsorption of dicarboxylic acids

as given order: oxalic> malonic> succinic> methylsuccinic acid, maximum adsorption capacity showed decrement with increasing steric effect. This finding is too crucial for the photocatalytic degradation. Electron and hole pairs recombines each other rapidly and interfacial electron transfer is doable if and only if donor or acceptor is preadsorbed before photocatalytic degradation. Hyrdoxyl radicals adsorbed at the photocatalyst surface are formed by OH and H_2O behaving as hole traps. Hence, the direct oxidation of dicarboxylic acids adsorbed by photogenerated holes is possible at the surface of the photocatalyst. Moreover, the adsorption mechanism for the each carboxylic acids were similar due to the comparable n_s^0 being abbreviation of adsorption capacity values. DRIFT mode showed that there is a formation of dicarboxylate film on the photocatalyst surface and it had rapid kinetic of formation.

CHAPTER 5

MATERIAL AND METHODS

In this thesis, natural zeolite supported TiO_2 composites were prepared. After **c**haracterization of these composites, adsorption of terephthalic acid was performed and mass transfer mechanisms were identified.

5.1. Purification of Natural Zeolite Tuff

Natural zeolite tuff from Gördes (Manisa) region was provided by INCAL Corporation. Firstly, natural zeolite tuff at roughly 10 cm in size was grinded by jaw crusher (Fritsch GmbH) to less than 1 cm. Then the size of the natural zeolite tuff decreased to roughly 24 μm via disk crusher (Fritsch GmbH). Thereafter, classification was applied by wet sieving: Natural zeolite tuff was exposed to continuously flow water so as to classify with respect to sieve opening, namely 38 μm and 75 μm. 0.05 g classified tuff was washed with 100 ml sonicated water with homogenizer (Sonics VC 505, CV33). Then, 0.1 g classified tuff was dispersed into 100 ml HCl solution (0.01 M) to remove acid soluble impurities present in the pores and surface of the natural zeolite. Figure 5.1 shows the purification steps of natural zeolite tuff, schematically. Drying at 120 °C for 12 hours (J.P.I, Selecta, s.a.) was carried out to avoid agglomeration before grinding with disk Crusher to maintain its weight before washing steps.

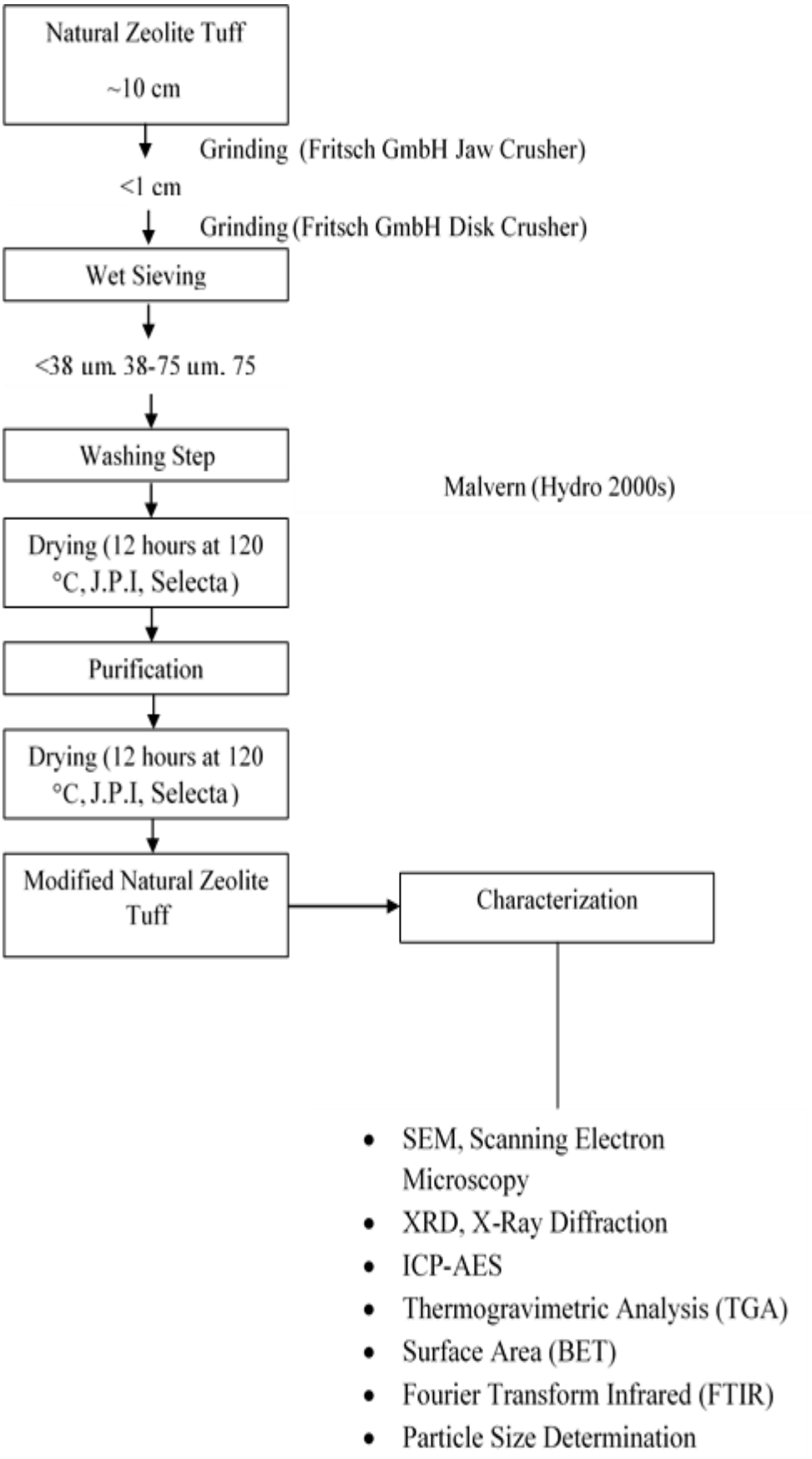

Figure 5.1. Schematic diagram for preparation of purified natural zeolite (P) from natural zeolite tuff (S)

5.2. Preparation of Natural Zeolite Supported TiO_2 Composites

Natural zeolite supported TiO_2 composites were prepared by the thermal hydrolysis method as given detailed in literature (Yener, et. al., 2000). 5 g of natural zeolite and 0.5 M $TiCl_4$ solution (125 ml) was reacted at 95^oC for 3 hours. TiO_2/natural zeolite tuff ratio was 1:1 in $TiCl_4$ solution. After the reaction had completed, solution in reactor had been held until two phases were observed (for 1 day). 500 ml deionized water was added to bottom phase and it had been held until precipitation completed. This step had been repeated until pH of washing water was reached to deionized water. After washing steps, natural zeolite supported TiO_2 composites was dried at 60^oC and kept for characterization (Figure 5.2).

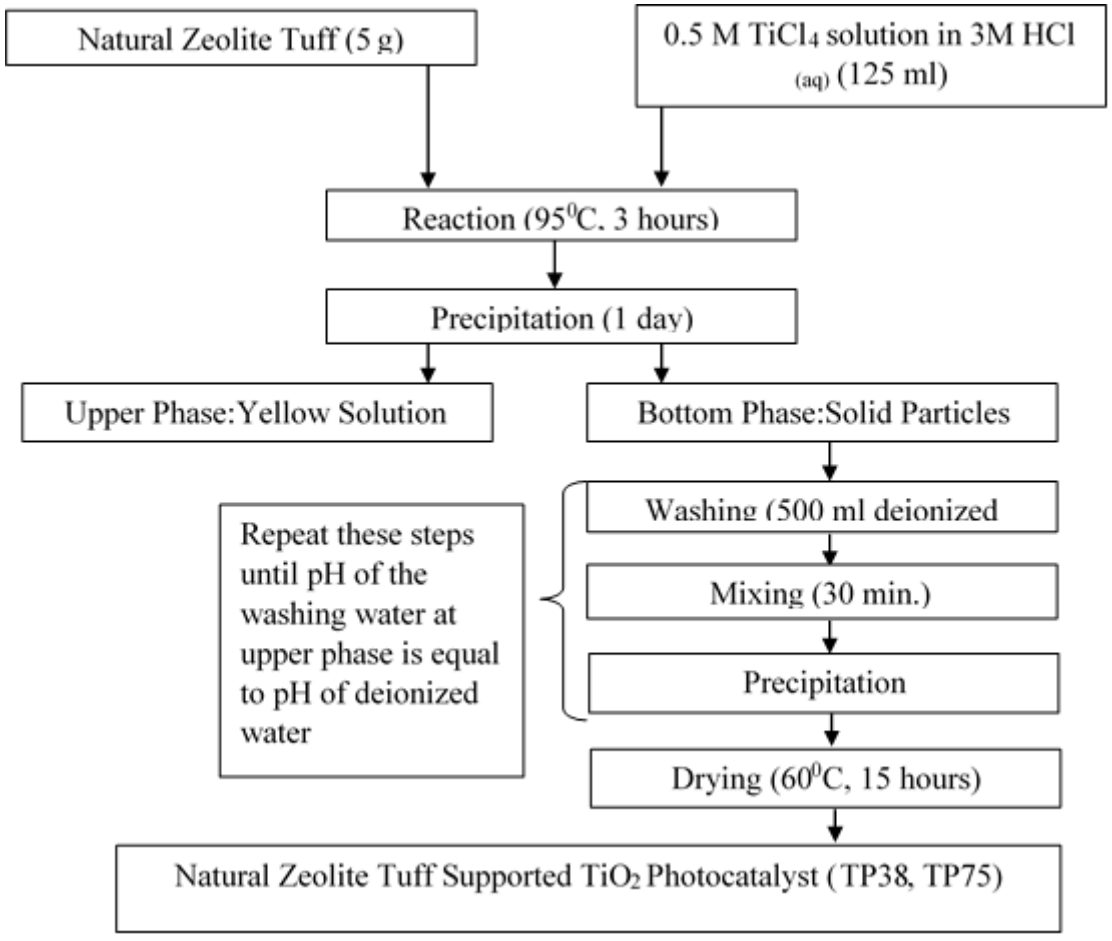

Figure 5.2. Schematic diagram for preparation natural zeolite supported TiO_2 composites

The morphologies of natural zeolite tuff and natural zeolite supported TiO_2 composites were determined via SEM-(FEI Quanta 250 FEG).

Crystalline structure were investigated using a Philips X'Pert Pro Diffractometer with Ni-filtered CuK_α (Wavelength λ=1.54056 Å) radiation in the range of 5 to 80°2θ values. Crystal size of the natural zeolite tuffs were calculated by using Scherrer equation.

$$\tau=\frac{K\,\lambda}{\beta\cos\theta} \tag{5.1}$$

where K is shape factor (0.9), β is broadening effect at Full-Width Half Maximum (FWHM) and corrected with β value for silicone, βins.

$$\beta=\sqrt{(\beta_{obs}{}^2-\beta_{ins}{}^2)} \tag{5.2}$$

Prior to particle size measurement at 25 ^oC by Malvern (Hydro 2000s), natural zeolite tuff was dispersed into water (0.01 w %) by ultrasonic bath (eia Cp102) for 10 min. 1 ml calgon (0.01 w %) can also be added into the solution if it is necessary.

The chemical analysis of natural zeolite tuff and natural zeolite tuff supported TiO_2 composites were performed via Induced Coupled Plasma Atomic Emission Spectroscopy, ICP-AES (Varian Liberty Series II). Natural zeolite tuff and natural zeolite tuff supported TiO_2 composites being as powder liquidized by using lithium tetra borate/meta borate. Fusion method was applied as shown in Figure 5.3.

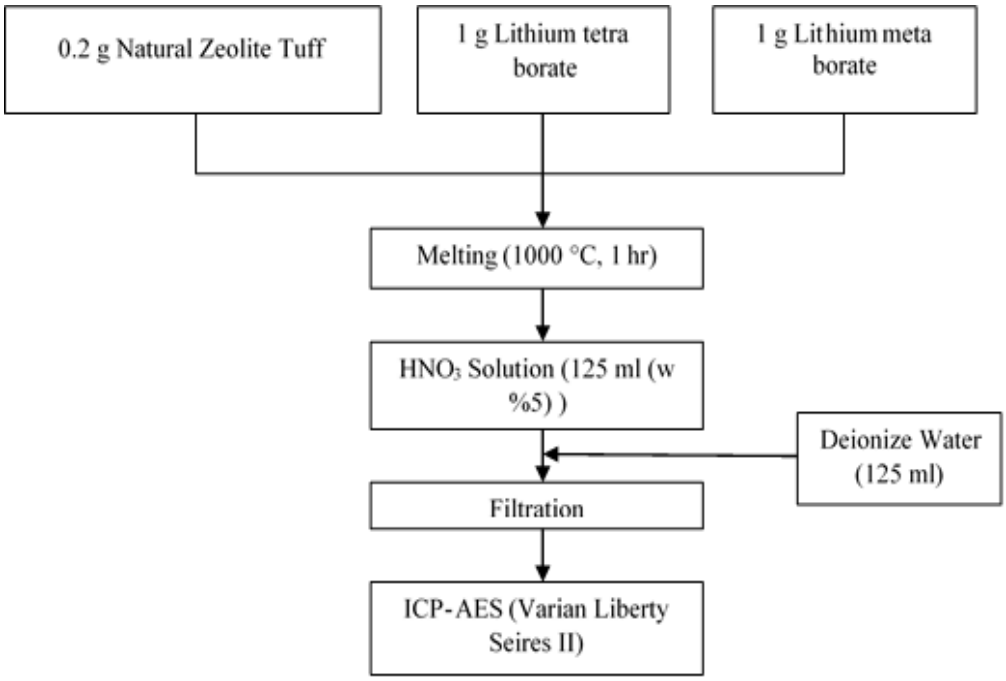

Figure 5.3. Schematic diagram for preparation of natural zeolite tuff and natural zeolite supported TiO_2 composites for ICP-AES analysis

Textural properties of natural zeolite tuff and natural zeolite supported TiO_2 composites were determined by evaluated N_2 adsorption isotherms at 77 K obtained from volumetric adsorption device (ASAP2010-Micromeritics). Prior to adsorption, the samples were degased under vacuum (10^{-6} Torr) for 24 hours at 300 ^oC.

Thermal behavior of samples were determined by using thermal gravimetric analysis (TGA 51, Shimadzu) conducted by measuring the weight loss of samples under dry N_2 stream with a heating rate of 10 ^oC/min.

5.3. Adsorption Studies

Adsorption of TPA for 10-100 ppm initial concentrations was conducted at stirring rate of 330 rpm in dark conditions. Besides to effect of initial concentration the influence of adsorbent concentration for the range of 0.2-1.5 g/l was studies.

Stock solution of TPA prepared by dissolving terephthalic acid in tetrahydrofuran (THF) was diluted with water (1/5) to obtain desired initial TPA concentration. UV spectrometer (Perkin Elmer, Lambda 45) was used to measure

absorbance at 241 nm wavelength (λ). Prior to the measurement of absorbance, pH of the solutions were adjusted to 2 with phosphoric acid buffer solution (Figure 5.4).

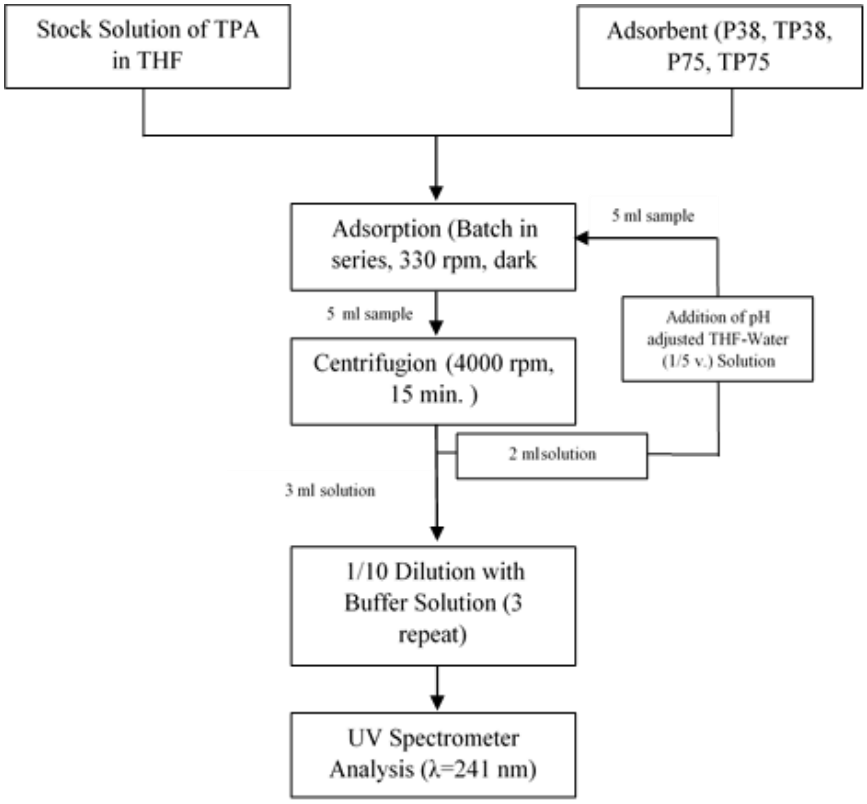

Figure 5.4. Schematic diagram of adsorption studies

CHAPTER 6

RESULTS AND DISCUSSION

In this chapter, kinetics of adsorption, an important step for photocatalytic degradation of terephthalic acid, on natural zeolite and natural zeolite supported TiO_2 composites will be presented.

6.1. Characterization of Natural Zeolite Tuff

As seen from SEM images (Figure 6.1) that as-received form of the grinded natural zeolite tuff (zeolite S) crystals was damaged owing to grinding.

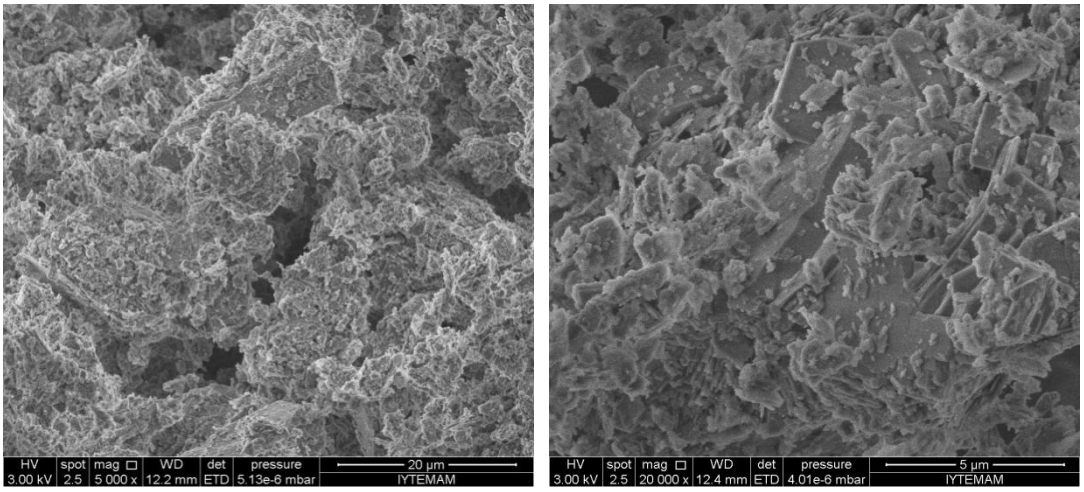

Figure 6.1. Scanning electron microscopy images of grinded natural zeolite tuff, particle size: ~20 µm (Magnification: 5000X, 20000X, FEI Quanta 250 FEG)

Figure 6.2-6.4 shows the SEM images of classified natural zeolite tuff depending on sieve size: <38 µm, 38-75 µm , >75 µm. Depending on the pre-purification steps applied, natural zeolites were coded as S, M or P for grinded, washed or purified natural zeolite tuff, respectively.

As seen from Figure 6.2-6.4 that washing steps made the crystalline structure of natural zeolite tuff more apparent for all sizes. On the other hand, crystalline structure of as-received form of zeolite (Code S) was damaged with water and weak acid treatment to obtain zeolite M and P, respectively.

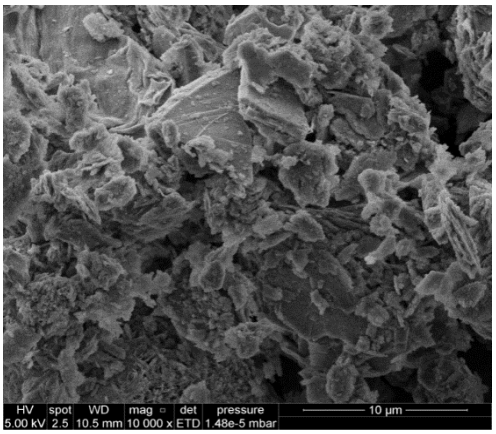

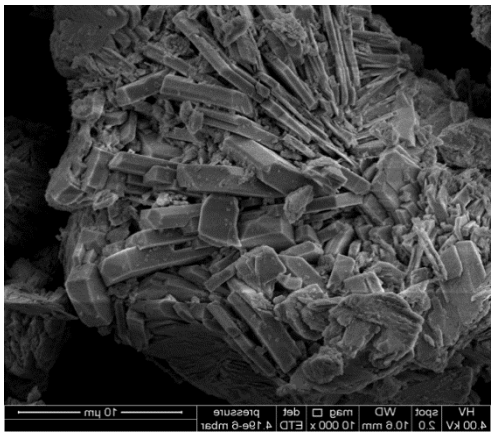

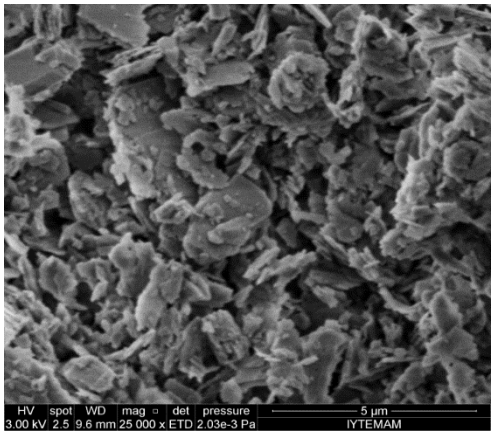

Figure 6.2. Scanning electron microscopy, SEM images of S: Grinded (upper), M: Washed (middle) and P: Purified (lower) natural zeolite tuff (sieve size: 38 µm) (Magnification: 10000X, 25000X, FEI Quanta 250 FEG)

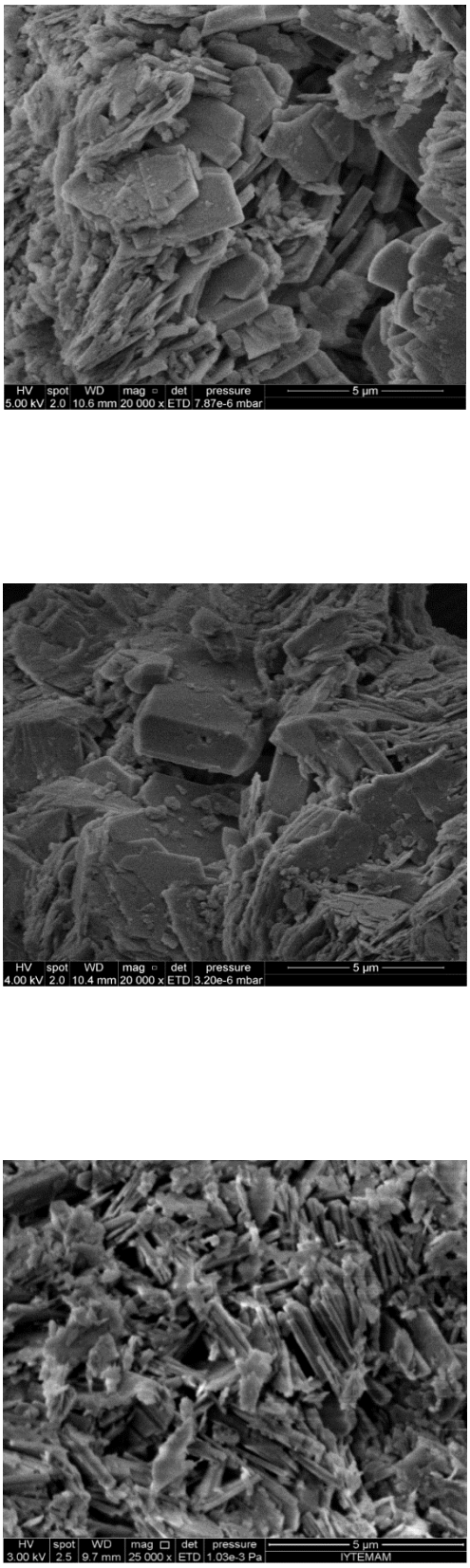

Figure 6.3. Scanning electron microscopy, SEM images of S: Grinded (upper), M: Washed (middle) and P: Purified (lower) natural zeolite tuff (sieve size: 38-75 µm) (Magnification: 20000X, 25000X, FEI Quanta 250 FEG)

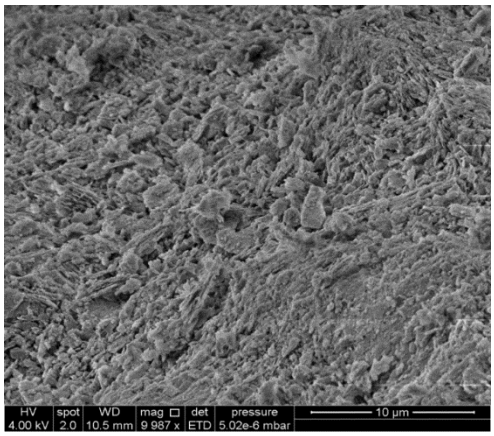

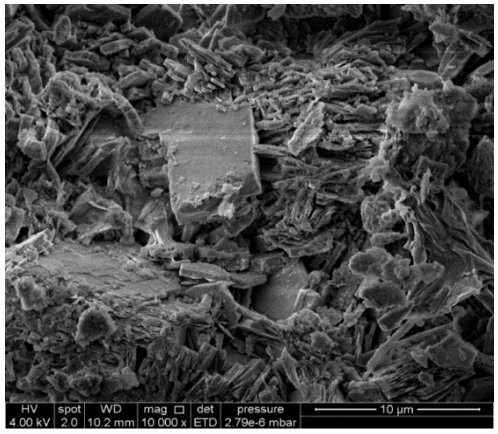

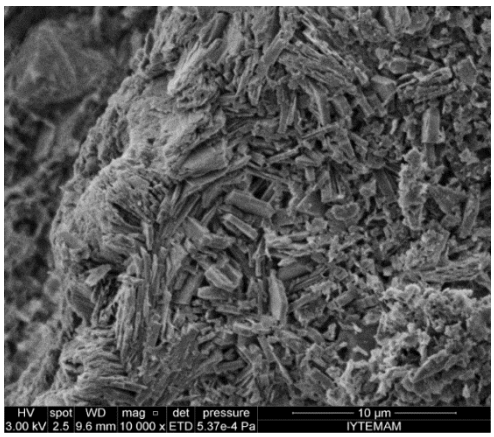

Figure 6.4. Scanning electron microscopy, SEM images of S: Grinded (upper), M: Washed (middle) and P: Purified (lower) natural zeolite tuff (sieve size: 75 µm) (Magnification: 10000X, FEI Quanta 250 FEG)

The X-Ray diffraction pattern of grinded natural zeolite tuff (zeolite S) given in Figure 6.5 has characteristic peaks of clinoptilolite (2Θ=9.827, 22.424 and 29.923) being the member of heulandite group of natural zeolite tuff. Additionally quartz (2Θ=26^{o}) is described as impurity in the natural zeolite tuff.

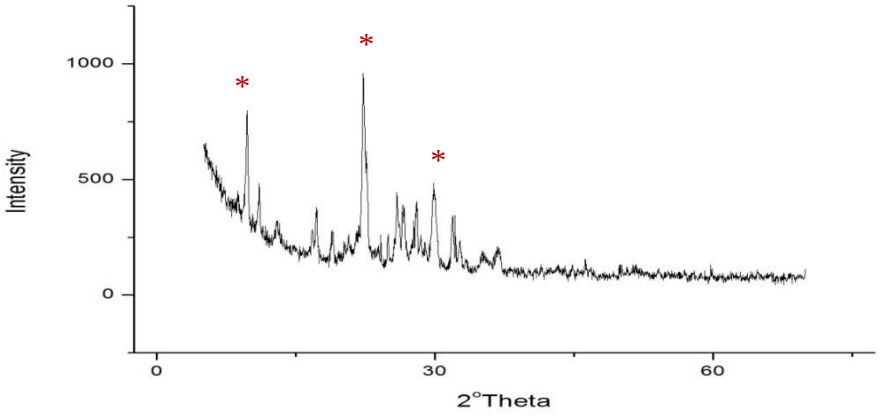

* indicates the characteristic peaks

Figure 6.5. X-Ray diffraction analysis of grinded natural zeolite tuff (zeolite S)

Comparison of X-Ray diffraction patterns of natural zeolite tuff S and M (Figure 6.6) shows that washing step applied was effective to purify the zeolite crystals.

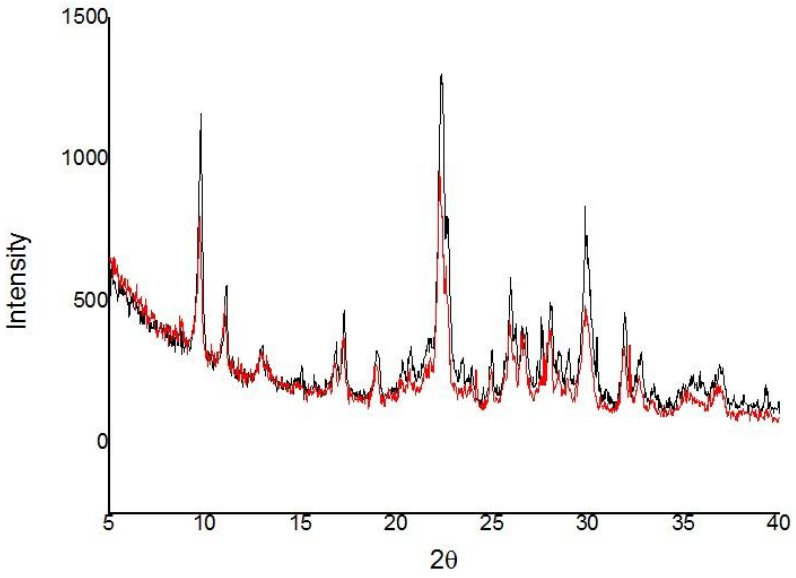

Figure 6.6. Comparison of S (red) and M (black) zeolites

Figure 6.7 demonstrates the particle size distribution of grinded natural zeolite tuff (zeolite S). As can be seen from the figure that particle size of natural zeolite tuff S has altered between 2-154 μm and its average size is 21 μm.

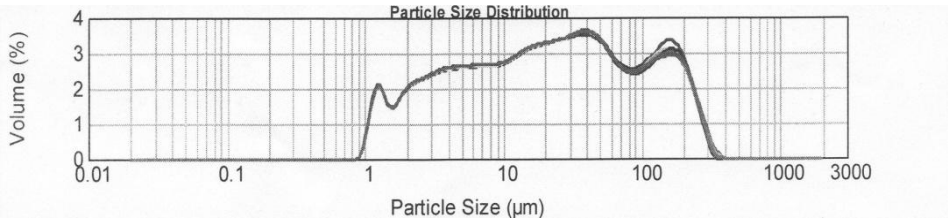

Figure 6.7. Particle size distribution of natural zeolite tuff S

The wet sieving based on discrete opening of mesh was used to classify natural zeolite tuff depending upon sieve opening of 38 µm and 75 µm.

The particle size distribution of purified zeolite (Zeolite P) is demonstrated at Figure 6.8. Average particle size of lower fraction of 38 µm sieve (Code: P38), middle fraction of 38-75 µm sieve (Code: P3875) and upper fraction of 75 µm sieve (Code: P75) were calculated as 25.3 µm. 54.2 µm and 154.4 µm, respectively.

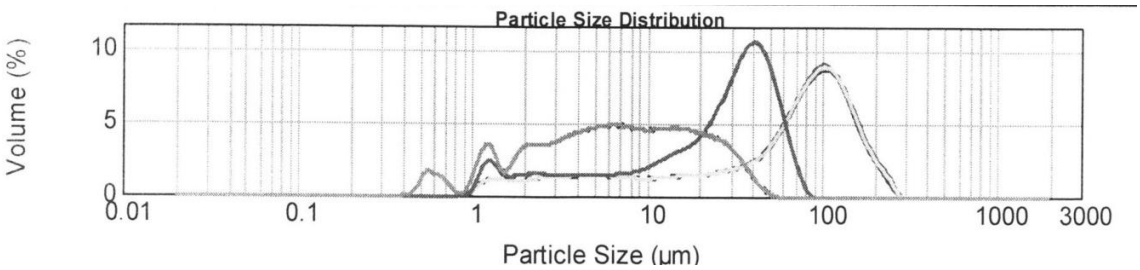

Figure 6.8. Particle size distribution of purified natural zeolite tuff (Zeolite P)

Table 6.1. The classification of zeolite P

Zeolite Code	Sieve Opening (µm)	Particle size constituting the %10 of volume (µm)	Particle size constituting the %50 of volume (µm)	Particle size constituting the %90 of volume (µm)
P38	<38	1.308	6.704	25.3
P3875	38 - 75	2.544	28.619	54.2
P75	>75	3.652	72.619	156.4

Figure 6.9 illustrates the XRD patterns of purified natural zeolite (Zeolite P). As seen from the figure that the characteristic peaks of clinoptilolite (2Θ=9.827, 22.424 and 29.923) are presented, even though unexpected peaks were observed for P75.

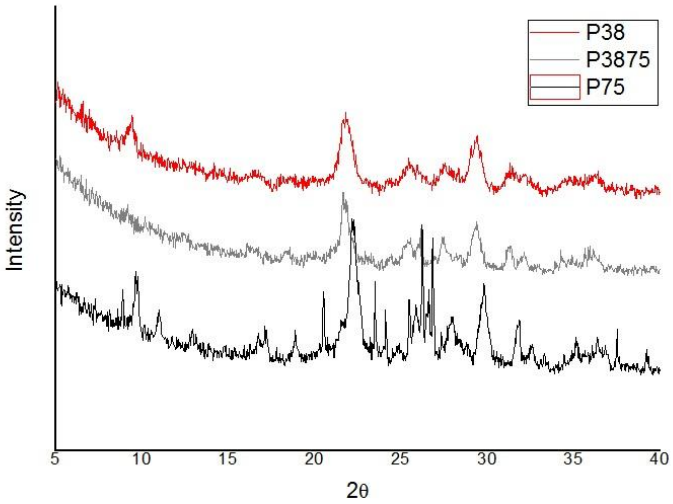

Figure 6.9. X-Ray diffraction diagrams of purified natural zeolite

XRD patterns of zeolites were evaluated to calculate crystal size by using Scherrer equation (Eq. 4.1). The crystal sizes of P38, P3875 and P75 were calculated as 12.5 nm, 17.48 nm and 20.8 nm, respectively. It is clear from the results that as particle size reduced so do crystal sizes. It confirmed the breakages seen from SEM analysis.

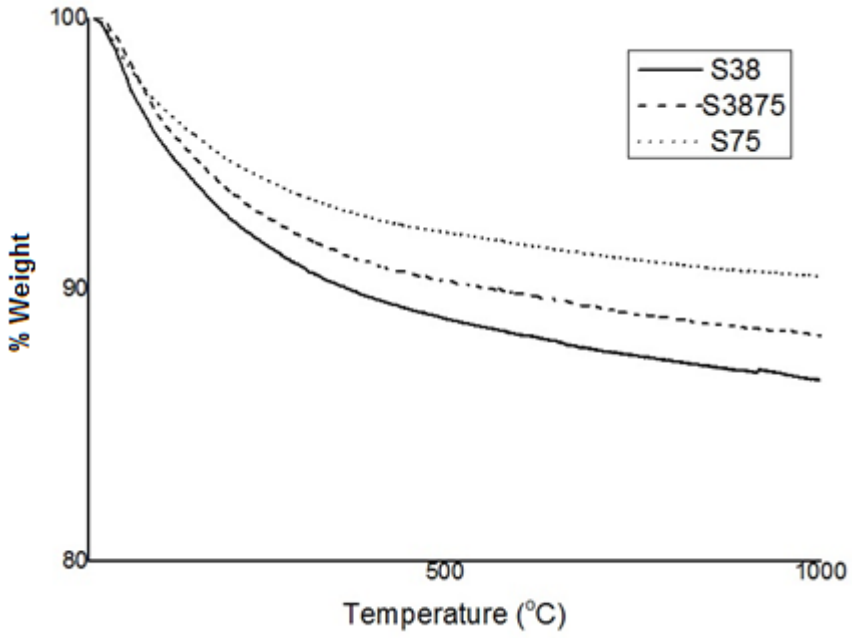

Figure 6.10. Thermogravimetric (TGA) curves of natural zeolite tuff as received form (zeolite S)

From the dehydration curves (Figure 6.10), zeolites were dehydrated with three steps: external water, loosely held and strongly held water for the range of 28-100 ^{o}C,

100-300^{o}C and 300-700^{o}C, respectively. The dehydrated amount was summarized in Table 6.2.

Table 6.2. Dehydrated amount during TGA of purified natural zeolite

Zeolite code	External Water,% (28-100^{o} C)	Loosely Held Water,% (100-300^{o} C)	Strongly Held Water,% (300-700^{o} C)	Total
P38	3.46	6.24	3.71	12.84
P3875	2.89	5.32	3.50	11.26
P75	2.52	4.68	2.54	9.94

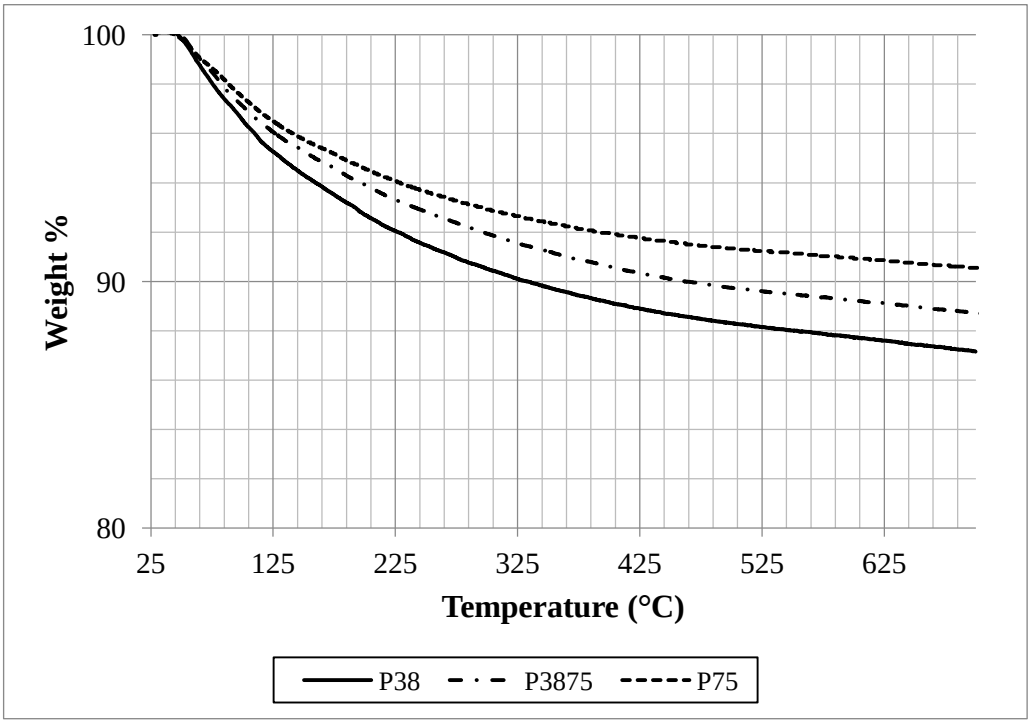

Figure 6.11. Thermogravimetric gravimetric analysis (TGA) curves of purified natural zeolite tuff (Zeolite P)

Table 6.3 shows the chemical analysis of purified zeolites.

Table 6.3. Chemical analysis of purified zeolites

Element (mg /g zeolite)	P38	P3875	P75
Al	1508.86	1591.45	1577
Ca	377.09	376.17	324

(cont. on next page)

Table 6.3. (cont.)

Element (mg /g zeolite)	P38	P3875	P75
Cu	1.10	1.27	1
Fe	197.47	234.01	204
K	1254.17	1297.85	1344
Mg	145.26	141.14	111
Mn	8.61	9.31	7
Na	159.51	249.55	361
Ni	0.76	4.30	5
Si	7265.80	8019.07	7450
Ti	12.63	14.27	17
Zn	5.34	2.20	2
Si/Al	4.82	5.04	4.72
ΣM+/ΣM2+	1.25	1.42	1.93
TEC ** (meq/ g zeolite)	2.93	3.13	3.18
% H_2O*	12.84	11.26	9.94

* Weight loss at 700^{o}C
** Total (Ca^{2+},Na^{+},K^{+}, Mg^{2+})

Si/Al ratio of purified natural zeolite (Si/Al:4.25-5.25) and the ratio of monovalent to bivalent cation ($\Sigma M^{+}/ \Sigma M^{++}$) was bigger than 1 ($Ca^{2+}<Na^{+}\cong K^{+}$) . Thus, it is determined that natural zeolite tuff is clinoptilolite rich low (Ca) silicate. It is thought that there is an interaction between clinoptilolite content and theoretical exchange capacity (TEC), and clinoptilolite content is also high in the natural zeolite tuff.

As can be seen from Table 6.4 that textural properties of clinoptilolite (zeolite S) with purification (zeolite P) was changed. The external area of the samples decreased; whereas the micropore area of the samples increased. Clinoptilolite had higher surface area in purified form than as-received form.

Table 6.4. Textural properties of S and P zeolites

Surface Area (m^2/g)*	S38	S75	P38	P75
External	13.22	6.16	6.41	6.71
Micropore	8.31	9.39	16.78	14.85
Total	21.53	15.56	23.19	21.56

*BET and t-plot methods are used to calculate the total and the external surface area, respectively

6.2. Characterization of Natural Zeolite Supported TiO_2 Composites

Scanning electron microscopy (SEM) images of clinoptilolite and clinoptilolite supported TiO_2 composites are given at Figure 6.12 and 6.13. Even the TiO_2 had widely covered the zeolite crystals, there were still uncoated crystals. Due to high titania to zeolite ratio used to prepare composites, agglomeration of TiO_2 on clinoptilolite crystals was also observed. The growth of TiO_2 particles in the pores of clinoptilolite was not expected since the molecular size of TPA (>6 Å) is bigger than the pore size of the clinoptilolite (3 Å).

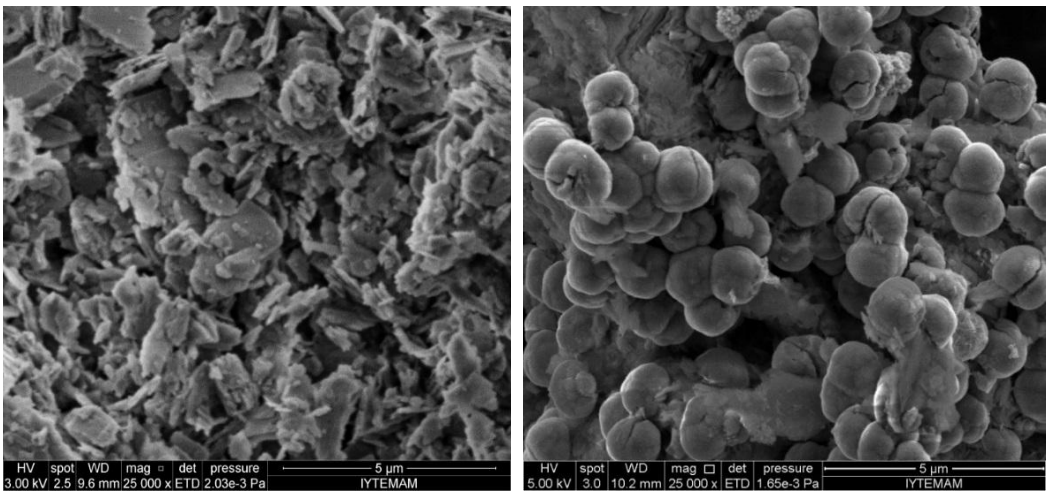

Figure 6.12. SEM images of clinoptilolite (P38) and clinoptilolite supported TiO_2 composites (TP38)

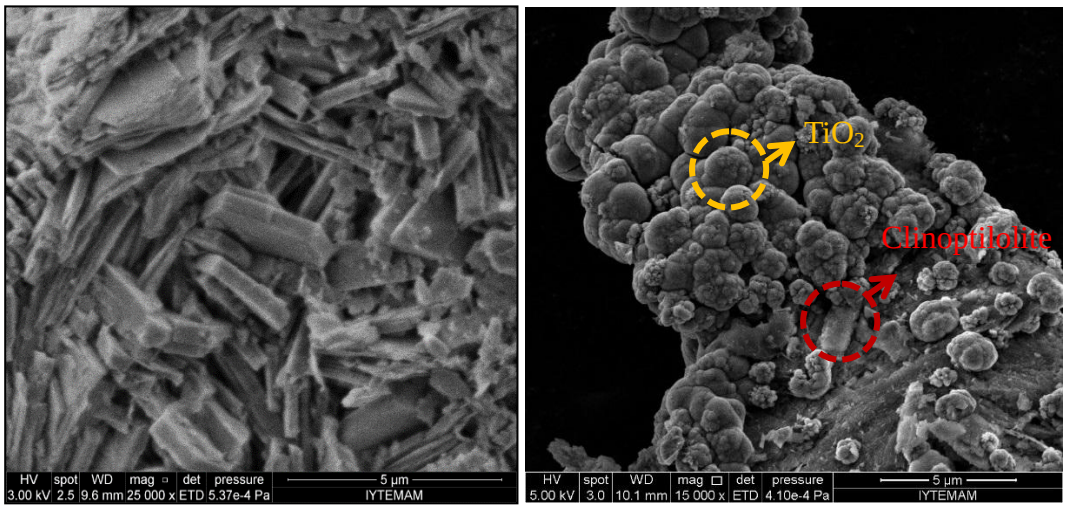

Figure 6.13. SEM images of clinoptilolite (P75) and clinoptilolite supported TiO_2 composites (TP75)

On the other hand (Figure 6.14-6.16) XRD patterns of clinoptilolite had vanished after coated its crystals with TiO_2 particles; the planes of [110], [101], [111], [211] rutile TiO_2 were established at 2 θ=27^o, 35.5 ^{o}, 42 ^{o}, and 53 ^{o}, respectively.

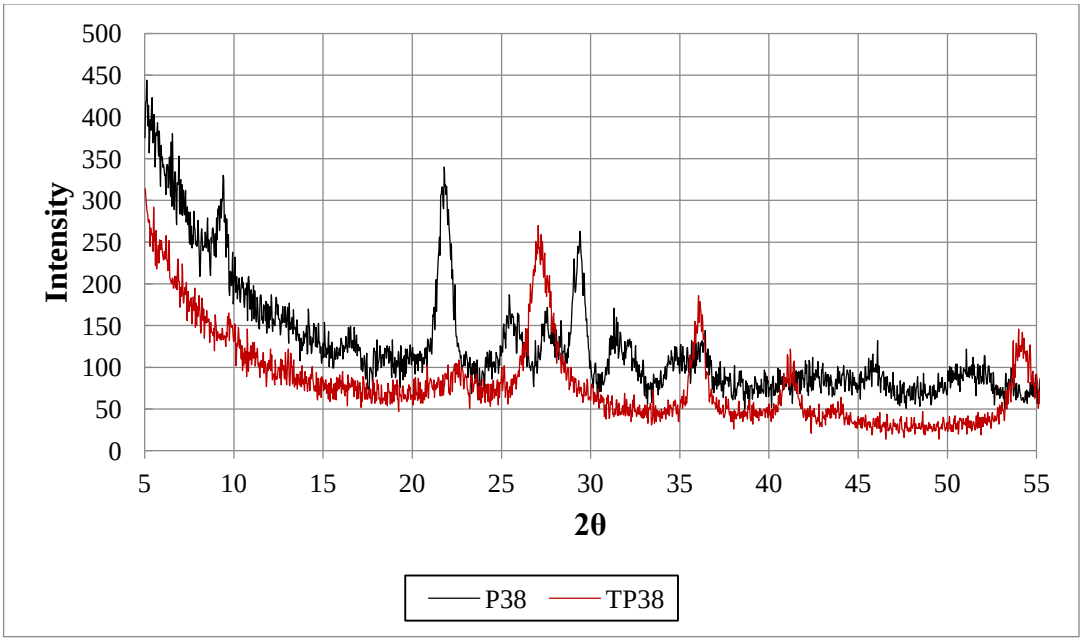

Figure 6.14. XRD results of clinoptilolite (P38) and clinoptilolite supported TiO_2 composites (TP38)

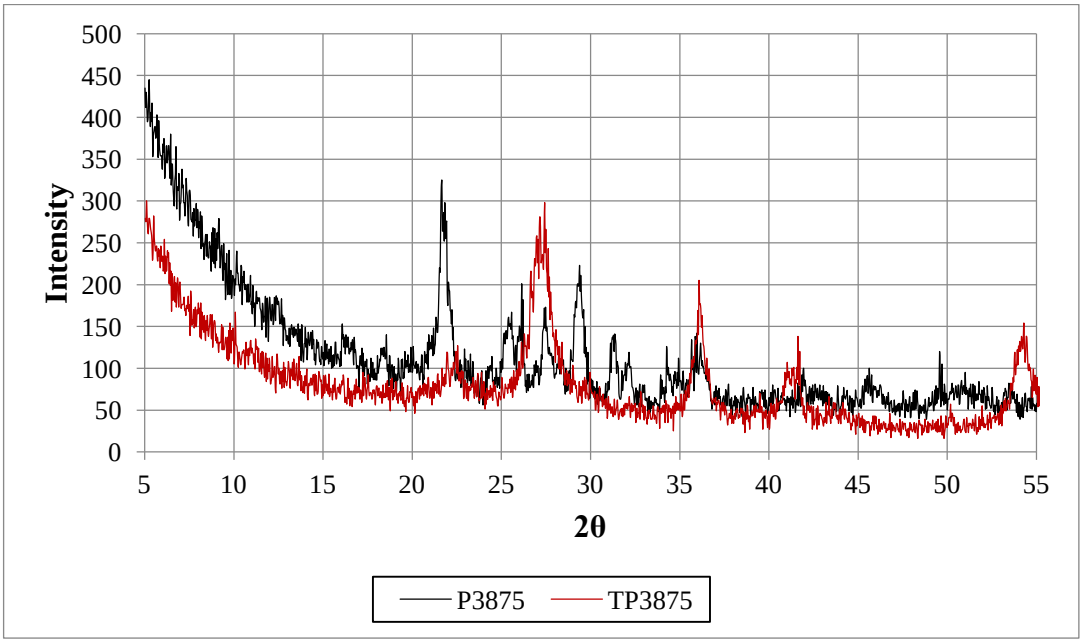

Figure 6.15. XRD results of clinoptilolite (P3875) and clinoptilolite supported TiO_2 composites (TP3875)

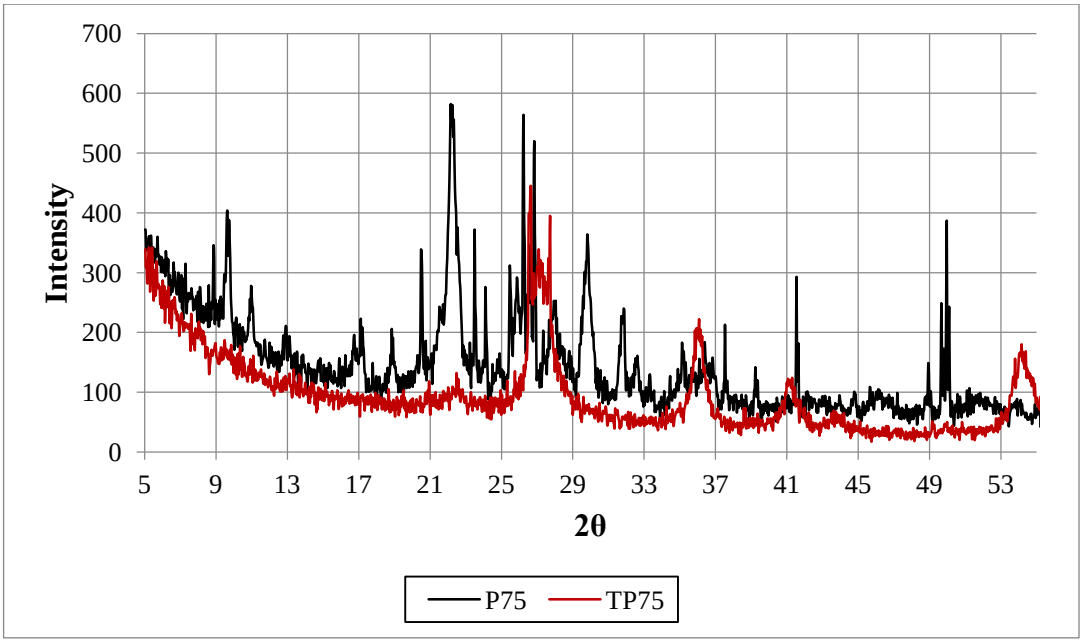

Figure 6.16. XRD results of clinoptilolite (P75) and clinoptilolite supported TiO_2 composites (TP75)

Chemical analysis of clinoptilolite supported TiO_2 composites is given in Table 6.5. The amount of titanium loaded (ΔTi) was notably higher than the amount of total cation (Σ Cation), aluminum (ΔAl) and iron (ΔFe). This is also the indication of agglomeration of TiO_2 on the surface.

Table 6.5. Chemical content of clinoptilolite supported TiO_2 composites

Element (mg /g zeolite)	**TP38**	**TP75**
Al	31.25	41.04
Ca	2.68	5.24
Cu	0.61	0.50
Fe	1.92	2.13
K	20.16	32.94
Mg	2.60	2.09
Mn	0.19	0.15
Na	5.88	15.21
Ni	0.27	0.21
Si	393.15	344.49
Ti	986.92	794.79
Zn	0.53	0.54
Si/Al	12.58	8.39

(cont. on next page)

Table 6.5. (cont.)

	TP38	**TP75**
Σ Cation (meq/g zeolit)**	1.80	1.22
ΔAl (meq/g zeolit)	3.51	2.74
ΔFe (meq/g zeolit)	0.23	0.23
ΔTi (meq/g zeolit)	82.20	66.17
% H_2O*	10.25	10.08

* Weight Loss at 700^oC
** Total (Ca^{2+},Na^+,K^+, Mg^{2+})

Not only cations but also aluminum and iron at framework was replaced with titanium. Zeolites having small particle size showed high replacement due to high available cation amount at the exterior surface after breakage of crystals.

During TiO_2 loading clinoptilolite was exposed to concentrated HCl (3M) in which dealumination can be observed as stated by Çakıcıoğlu and Ulku (2005). Figure 6.17 gives information about the effect of $TiCl_4$ precursor comparing the change in chemical composition when clinoptilolite was exposed to both 3 M HCl with $TiCl_4$ (THCl) and without $TiCl_4$ (HCl) for 3 hours. Figure 6.17 illustrates the ratios of elements after reaction of clinoptilolite with precursor and without precursor. The figure implies that $TiCl_4$ increased the removal of aluminum and calcium. On the other hand, $TiCl_4$ precursor hindered the removal of other elements.

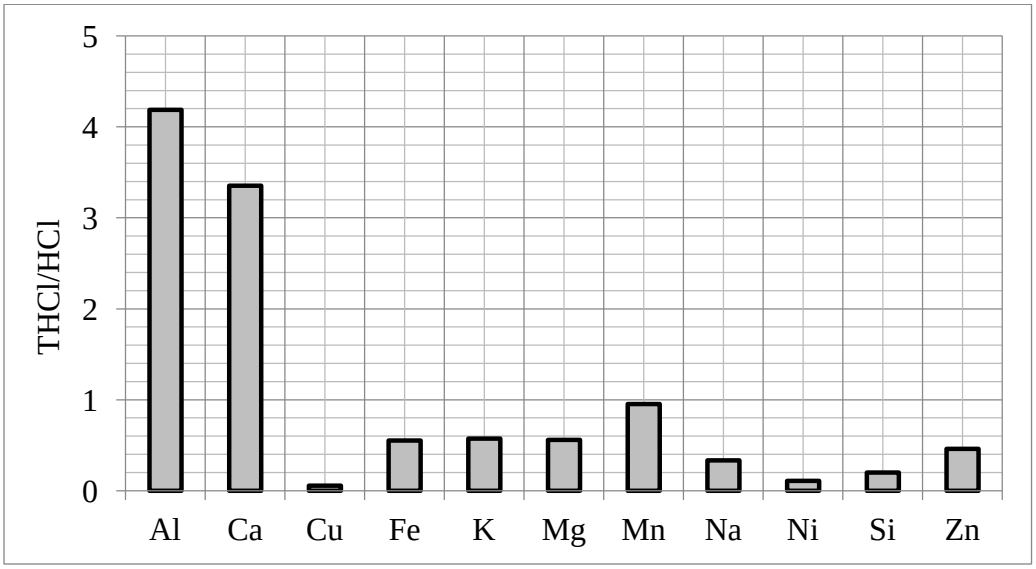

Figure 6.17. Comparison of the amount of elements in THCl and HCl solution after clinoptilolite interaction

During TiO_2 loading about 4 times aluminum was removed from the structure. Ca^{2+} is the highest replaced cation during the loading.

Weight loss of purified clinoptilolite supported TiO_2 composites up to 1000 ^oC for two particle sizes (TP38 and TP75) were measured as %10.25 and %10.08, respectively (Table 6.6).

Table 6.6. TGA results of clinoptilolite supported TiO_2 composites

Catalyst Name	**External Water,% (28-100^o C)**	**Loosely Held Water,% (100-300^o C)**	**Strongly Held Water,% (300-700^o C)**	**Total**
TP38	3.16	4.77	2.68	10.25
TP75	3.11	4.50	2.85	10.08

Figure 6.18 shows the weight (%) curves with temperature for clinoptilolite supported TiO_2 composites. Weight loss curves with increasing temperature were examined in three sections: 28-100 ^oC, 100-300^oC and 300-700^oC indicating that external, loosely held and strongly held waters, respectively. The weight loss % in this three sections were summarized in Table 6.6. Loosely bounded water in the composites (TPs) was much lower when compared to purified clinoptilolites (Ps), and total weight loss % are the same for TPs.

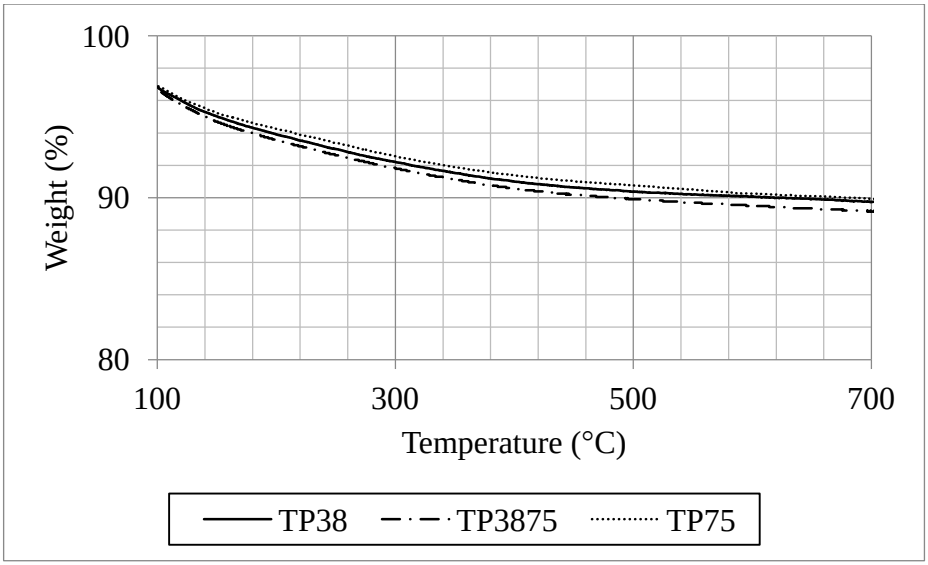

Figure 6.18. Weight loss of purified clinoptilolite supported TiO_2 composites with temperature

Figure 6.19 and 6.20 demonstrate nitrogen adsorption isotherms of clinoptilolite and clinoptilolite supported TiO_2 composites at 77 K. As can be seen from figures that nitrogen adsorption increased markedly after loading TiO_2 onto clinoptilolite. Adsorption and desorption isotherms were overlapped which means that there was not condensation.

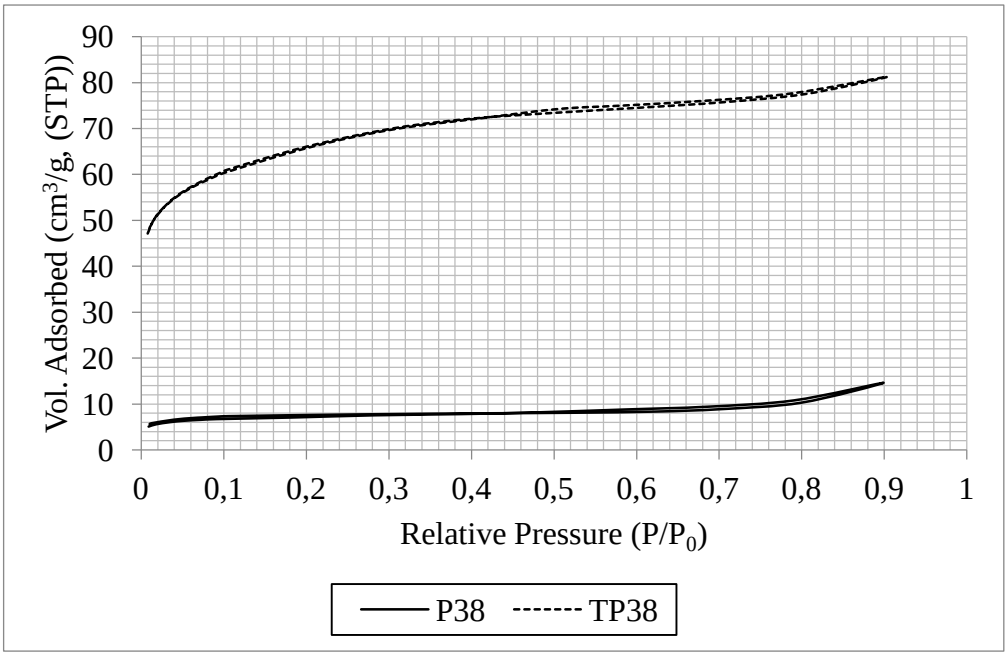

Figure 6.19. Nitrogen adsorption isotherms of clinoptilolite and clinoptilolite supported TiO_2 composites (P38, TP38 at 77 K)

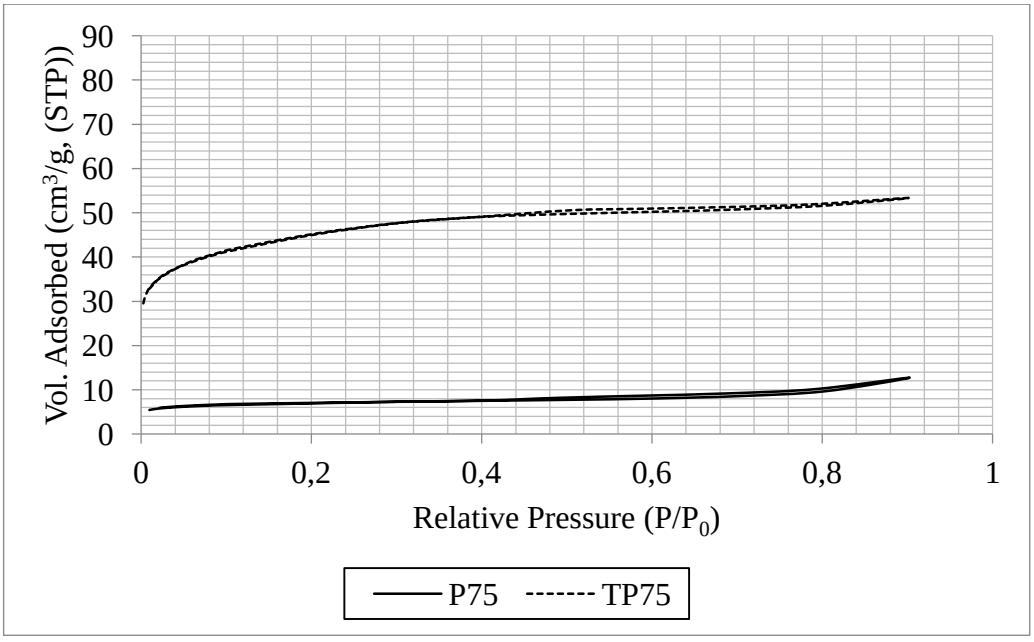

Figure 6.20. Nitrogen adsorption isotherms of clinoptilolite and clinoptilolite supported TiO_2 composites (P75, TP75 at 77 K)

Comparison of the textural properties of the natural zeolite supported TiO_2 composites with natural zeolites shows that surface areas were increased with loading (Table 6.8). The highest increase was observed for external surface area. This increase can be explained by the phenomenon of agglomeration of TiO_2 particles onto natural zeolite tuff.

Table 6.7. Change in the textural properties of clinoptilolite with TiO_2 loading

Surface Area (m^2/g)*	**P38**	**P75**	**TP38**	**TP75**
External	6.41	6.71	120.36	104.08
Micropore	16.78	14.85	89.97	38.24
Total	23.19	21.56	210.33	142.32

*BET and t-plot methods are used to calculate the total and external surface area, respectively.

Figure 6.21-6.22 illustrate the Fourier Transform Infrared Spectroscopy results of clinoptilolite and clinoptilolite supported TiO_2 composites. Bending vibrations at 580 cm^{-1} belonging to clinoptilolite had vanished after TiO_2 loading; whereas asymmetric stretching vibrations of framework observed in the range of 1200-1000 cm^{-1} did not affected. OH bending vibrations at 3622 cm^{-1} of clinoptilolite weakened after TiO_2 loading. This means that TiO_2 loading occurred substantially on –OH regions of clinoptilolite. Also, asymmetric Ti-O-Si bond vibrations formed after loading. The possible mechanism for formation of clinoptilolite supported TiO_2 composites might be that -H coming from the TiO_2 colloid particle reacts with the surface –OH combining with Al being in the zeolite so as to form water.

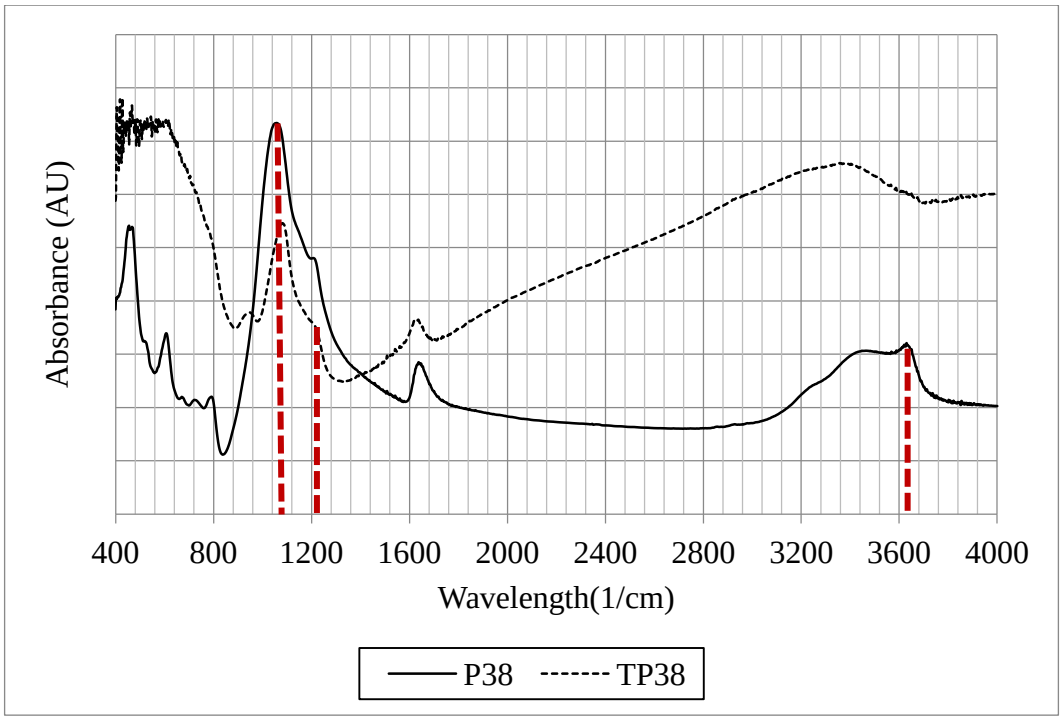

Figure 6.21. FTIR results of clinoptilolite and clinoptilolite supported TiO_2 composite (P38 and TP38)

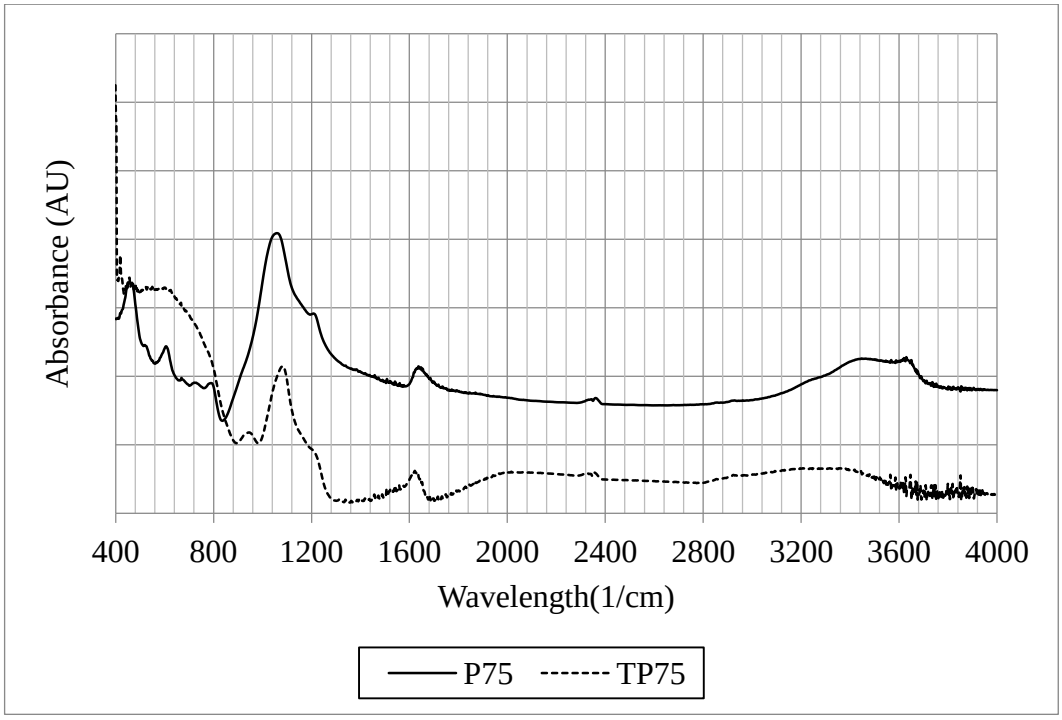

Figure 6.22. FTIR results of clinoptilolite and clinoptilolite supported TiO_2 composite (P75 and TP75)

6.3. The Adsorption of Terephthalic Acid (TPA)

In this study, it is focused on the kinetic studies and mass transfer mechanisms of adsorption of terephthalic acid on clinoptilolite and clinoptilolite supported TiO_2 composites. The kinetic studies of first order rate law and pseudo-second order reaction and diffusion models of intraparticle, Weber-Morris and external diffusion models are applied to identify the adsorption of terephthalic acid on the samples. These models were applied to clarify the mass transfer mechanism of the system to lead forth to photocatalytic degradation of the terephthalic acid. These models are fitted by linearizing experimental data and minimizing error.

$$\text{Error}= \sum [q_{exp}-q_{cal}]^2 \times \frac{1}{n} \qquad (6.1)$$

where, the subindex of (exp) and (cal) shows the experimental and calculated data, respectively, and n is the number of the observation.

6.3.1. The Effects of Adsorbent Amount

The effect of adsorbent amount on adsorption process was investigated for both zeolitic tuff and zeolitic tuff supported TiO_2 composites by changing adsorbent amount from 0.2 g/l to 1.5 g/l. Simultaneously, the adsorption percentage of terephthalic acid per unit mass of adsorbent was calculated to comprehend how the adsorbent amount affected the adsorption of terephthalic acid. Figure 6.23 illustrates the amount of adsorbed terephthalic acid per unit mass of adsorbent with respect to time for clinoptilolite of P38 with 20 ppm initial terephthalic acid concentration.

As can be seen from Figure 6.23 that the amount of adsorbed terephthalic acid decreased with increasing adsorbent amount. The molecular size of the terephthalic acid (>6 Å) is bigger than the pore size of the clinoptilolite (3 Å). However, terephthalic acid could not be transported through the pores of the clinoptilolite due to its bigger molecule size, terephthalic acid would be adsorbed on the external surface of the clinoptilolite or in the regions between clinoptilolite crystals. Moreover, it was known that the surface of the clinoptilolite was hydrophilic. This means that clinoptilolite favors water more than terephthalic acid due to its affinity properties.

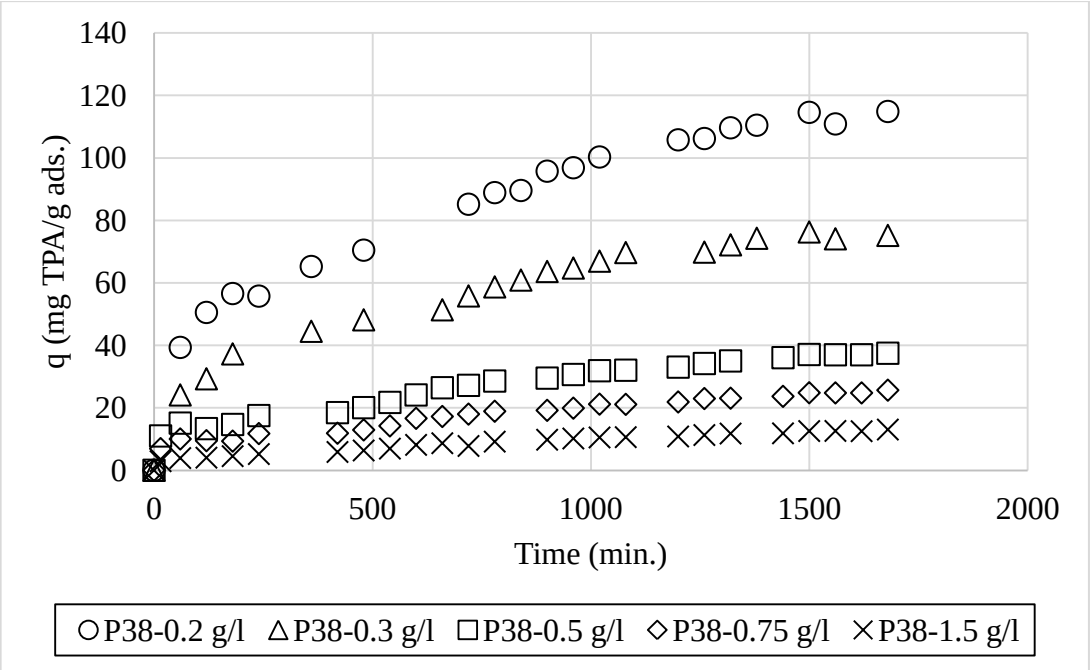

Figure 6.23. The effect of adsorbent amount on adsorption of terephthalic acid (Adsorbent: P38; initial terephthalic acid concentration: 20 ppm)

Even, the increasing adsorbent amount would provide more adsorption sites, there was adsorption of water instead of terephthalic acid. Thus, increasing adsorbent amount provided more adsorption sites for water molecules and the amount of adsorbed terephthalic acid per unit mass of adsorbent decreased with increasing adsorbent amount owing to attack of water molecules through external surface and regions constituted by the crystals of the clinoptilolite. Futhermore, adsorption percentage per unit mass of adsorbent showed no change with increasing adsorbent amount due to the adsorption of water molecules. Eventhough the amount of adsorbed terephthalic acid per unit mass of adsorbent altered with time, the adsorption percentages were obtained roughly similar for all adsorbent amounts due to adequate adsorption of terephthalic acid. Hence, it can be said that adsorbents were saturated with terephthalic acid. Figure 6.24 demonstrates the adsorption percentages for all adsorbent amounts of P38 clinoptilolite. At the end of the adsorption, maximum recovered terephthalic acid for increasing adsorbent amount were found as 81.32 %, 79.86 %, 76.19 %, 78.20 % and 79.55 %, respectively.

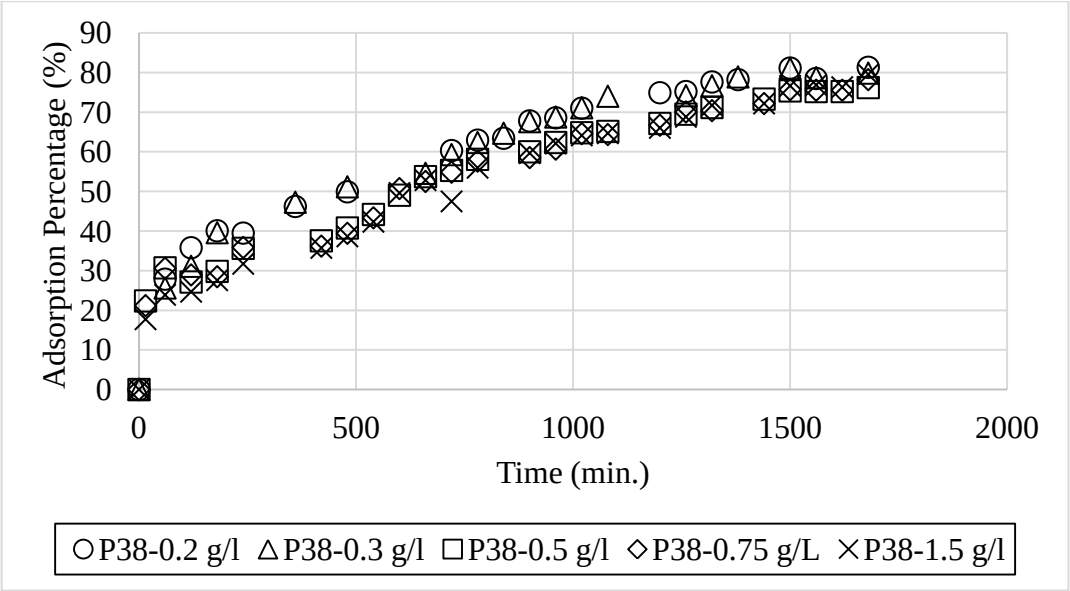

Figure 6.24. Terephthalic acid adsorption percentage (Adsorbent: P38; initial terephthalic acid concentration: 20 ppm; adsorbent amount: 0.2 g/l, 0.3 g/l, 0.5 g/l, 0.75 g/l and 1.5 g/l)

The same results were obtained for the adsorption of terephthalic acid onto P75 clinoptilolite. Figure 6.25 shows the amount of adsorbed terephthalic acid per unit mass of adsorbent for P75 clinoptilolite. At the end of the adsorption, maximum recovered terephthalic acid for increasing adsorbent amount were found as 72.45 %, 73.99 %, respectively.

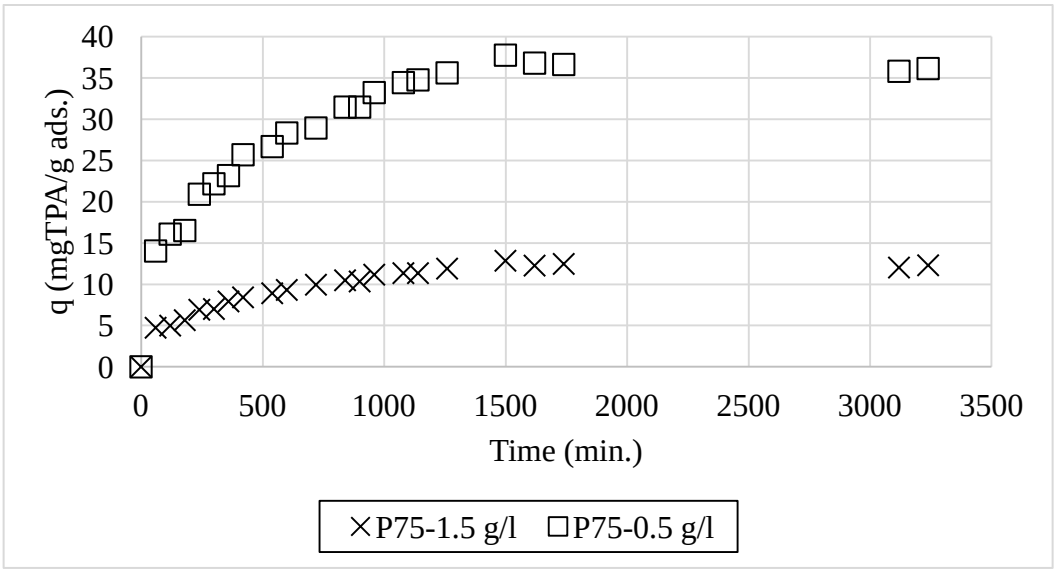

Figure 6.25. The effect of adsorbent amount on adsorption of terephthalic acid (Adsorbent: P75; initial terephthalic acid concentration: 20 ppm)

The effect of adsorbent amount was investigated for clinoptilolite supported TiO_2 composites at the same time. The same outcomes as obtained for clinoptilolite were achieved for the adsorption of terephthalic acid onto TP38 and TP75. Figure 6.26-6.27 demonstrates the adsorbent amount effect on terephthalic acid adsorption for TiO_2 composites. It can be deduced from the figure that TiO_2 were not totally covered onto clinoptilolite and this result was corroborated with the results obtained from scanning electron microscopy owing to existence of water adsorption.

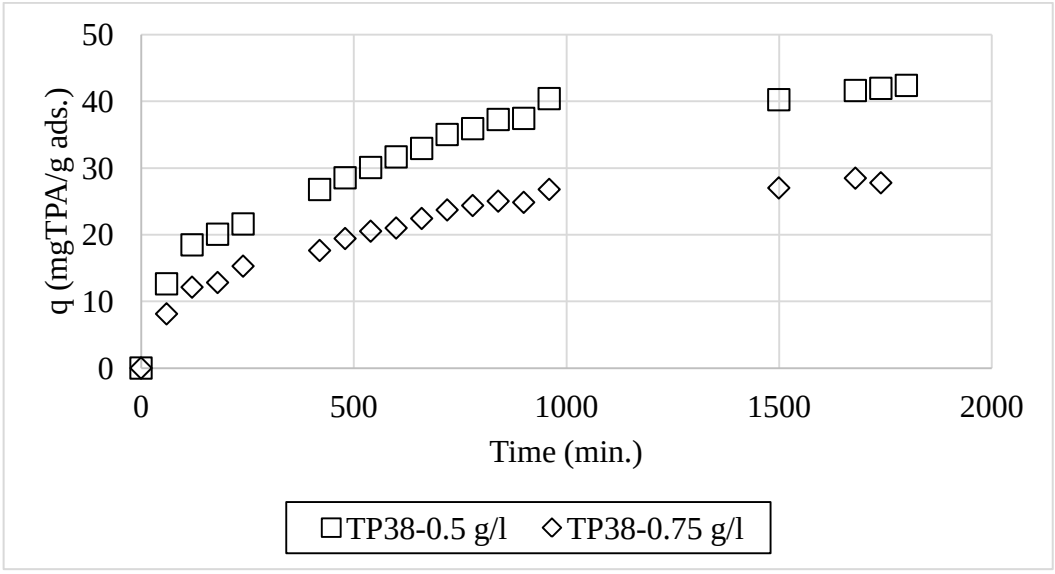

Figure 6.26. The effect of adsorbent amount on adsorption of terephthalic acid (Adsorbent: TP38; initial terephthalic acid concentration: 20 ppm)

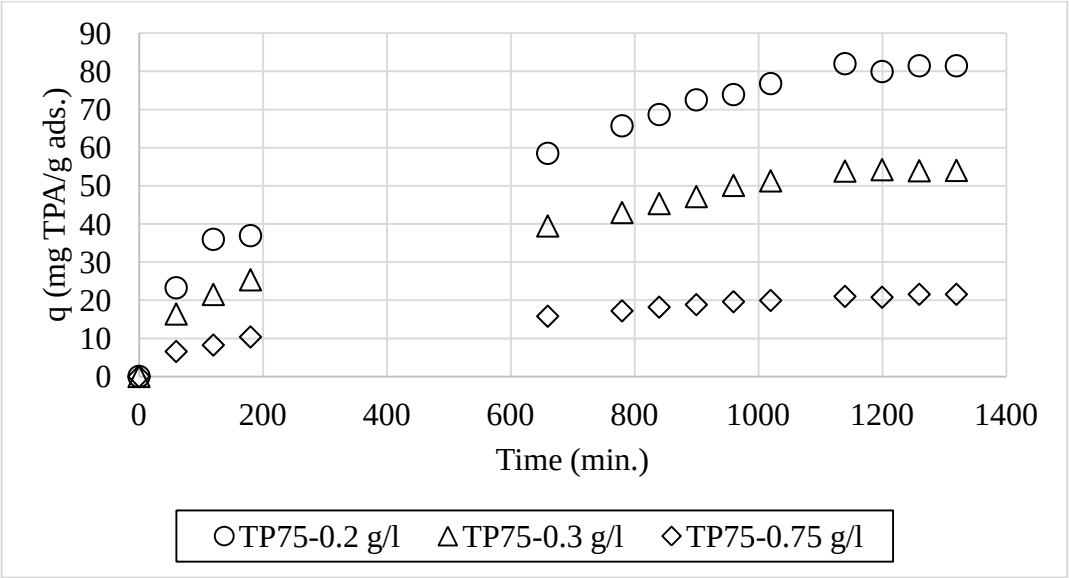

Figure 6.27. The effect of adsorbent amount on adsorption of terephthalic acid (Adsorbent: TP75; initial terephthalic acid concentration: 20 ppm)

Table 6.8 shows the maximum recovered terephthalic acid for TP38 and TP75. Terephthalic acid adsorption in percentage was obtained roughly same for TiO_2 composites as clinoptilolite.

Table 6.8. Adsorption percentage calculations for TP38 and TP75

Catalyst Amount (g/l)	*Adsorption Percentage (%)	
	TP38	TP75
0.2	-	70.33
0.3	-	69.97
0.5	75.15	-
0.75	73.88	69.73

*Initial terephthalic acid concentration: 20 ppm

6.3.2. The Effect of Initial Terephthalic Acid Concentration

Figure 6.28 shows the effect of initial terephthalic acid concentration for TP75 composites with 20 and 60 ppm initial TPA concentration. The figure indicates that the amount of adsorbed terephthalic acid per unit mass of adsorbent increased with increasing initial terephthalic acid concentration due to the excess amount of terephthalic acid molecules in the medium. This competitive adsorption increased the challenge between terephthalic acid molecules so did the amount of adsorbed terephthalic acid per unit mass of adsorbent.

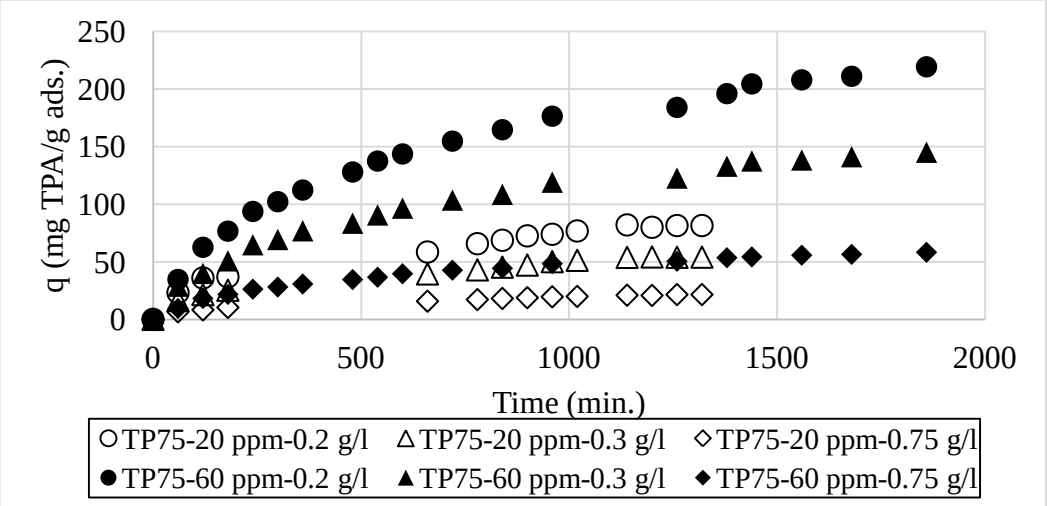

Figure 6.28. The effect of initial terephthalic acid concentration on adsorption of terephthalic acid (Adsorbent: TP75; adsorbent amount: 0.2 g/l, 0.3 g/l, and 0.75 g/l; initial terephthalic acid concentration: 20 and 60 ppm)

6.3.3. The Effect of Particle Size

Adsorption studies were applied for adsorbents having different particle size. It was though that there would be an effect of particle size on terephthalic acid adsorption. Figure 6.29 illustrates the effect of particle size on terephthalic acid adsorption for P38 clinoptilolite. Decrease in particle size would make the adsorption sites more accessible and the surface area higher. Even if there it was expected that P38 clinoptilolite would adsorb terephthalic acid more than P75 clinoptilolite, the amount of adsorbed terephthalic acid per unit mass of adsorbent was the same for clinoptilolite adsorbents due to the fact that the surface areas of the adsorbents were close to each other (P38:23.19 m^2/g; P75: 21.56 m^2/g).

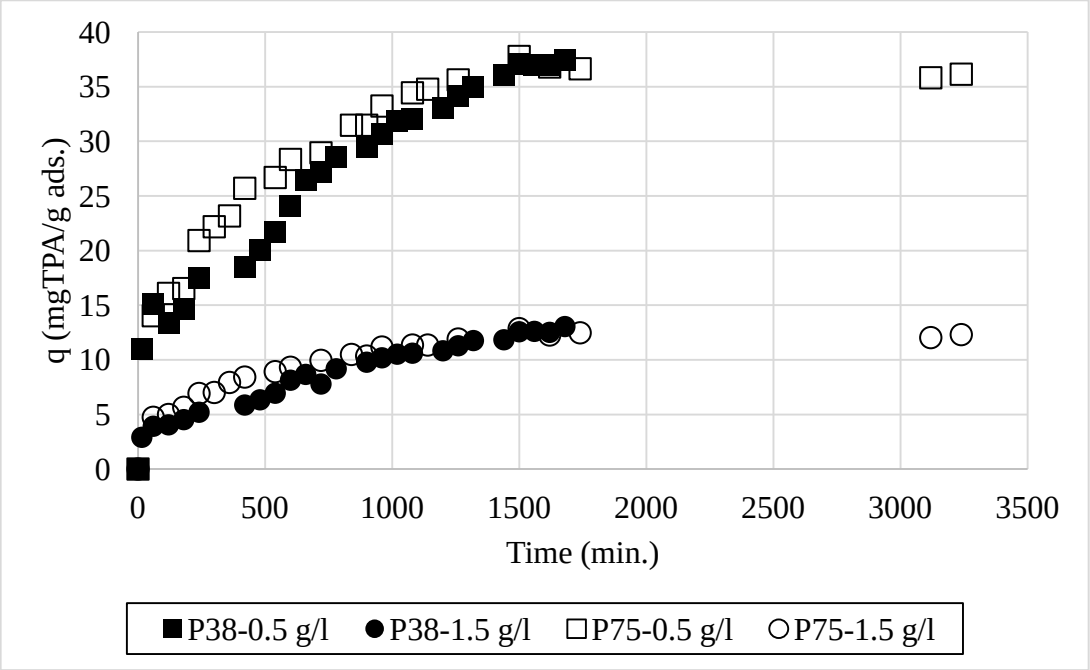

Figure 6.29. The effect of initial terephthalic acid concentration on adsorption of terephthalic acid (Adsorbent: P38 and P75; adsorbent amount: 0.5 g/l, 1.5 g/l,; initial terephthalic acid concentration: 20 ppm)

Moreover, the effect of particle size was observed for TP38 and TP75 composites (Figure 6.30) as expected. The amount of adsorbed terephthalic acid per unit mass of adsorbent increased with decreasing particle size. Decreasing particle size made the regions where terephthalic acid molecules adsorbed more accessible. Also, the surface area of the TP38 was higher than TP75 composite (TP38: 210.33 m^2/g, TP75:

142.32 m^2/g) and this difference in surface area made the more available adsorption sites for TP38 composite.

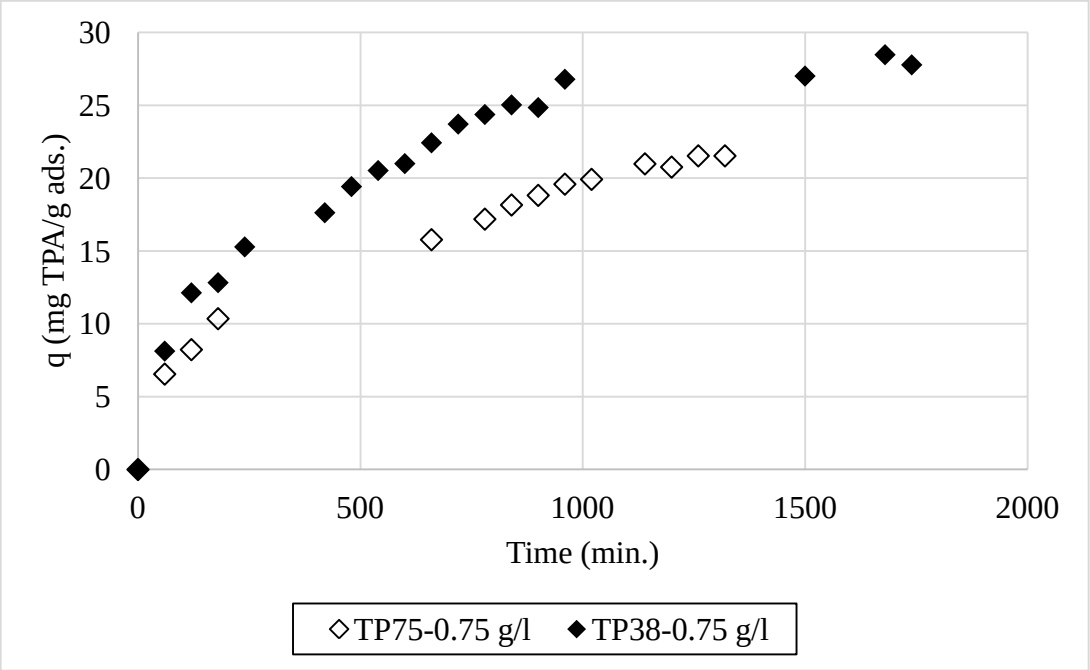

Figure 6.30. The effect of initial terephthalic acid concentration on adsorption of terephthalic acid (Adsorbent: TP38 and TP75; adsorbent amount: 0.75 g/l; initial terephthalic acid concentration: 20 ppm

6.3.4. The Effect of TiO_2 Loading

Figure 6.31 shows the effect of TiO_2 loading on the amount of adsorbed terephthalic acid per unit mass of adsorbent. It is known that clinoptilolite has high adsorption capacity; whereas it seemed that TiO_2 loading made the amount of adsorbed terephthalic acid increase at first blush. Figure 6.32 implies the amount of adsorbed terephthalic acid per area. However, TiO_2 loading seemed as affirmative for terephthalic acid adsorption due to high surface area and more available adsorption sites. Clinoptilolite provided more effective adsorption performance per 1 m^2 area of adsorbent.

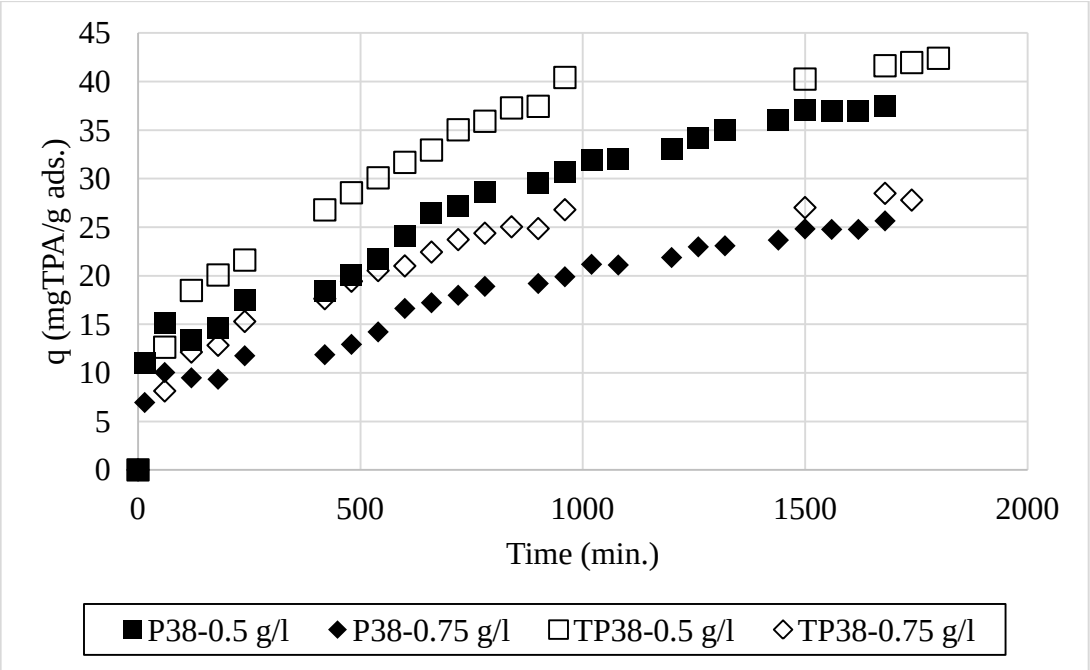

Figure 6.31. The effect of TiO_2 loading on adsorption of terephthalic acid (Adsorbent: P38 and TP38; adsorbent amount: 0.5 g/l, 0.75 g/l; initial terephthalic acid concentration: 20 ppm)

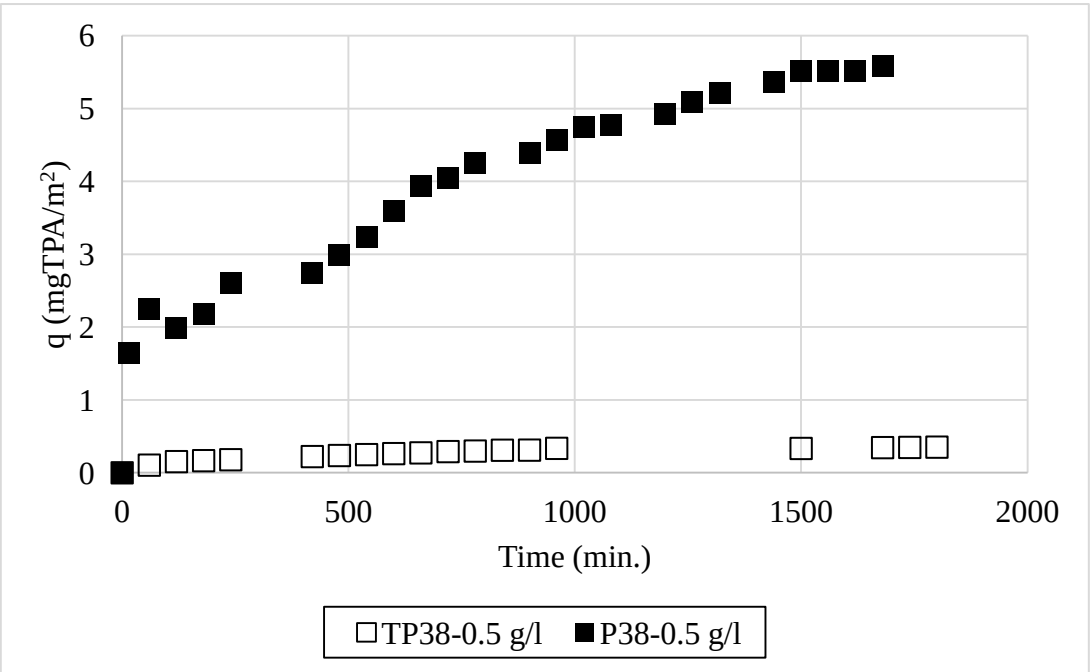

Figure 6.32. The effect of TiO_2 loading on terephthalic acid adsorption per area (Adsorbent: P38 and TP38; adsorbent amount: 0.5 g/l; initial terephthalic acid concentration: 20 ppm)

6.3.5. Diffusion Models: Intraparticle and/or External

6.3.5.1. Weber Morris Model

The kinetic experimental results were fitted to Weber Morris model to gain insight into the diffusion mechanisms and rate controlling step which is affecting the kinetics of adsorption. Figure 6.33 demonstrates the experimental data with respect to square root of time fitted to Weber-Morris model to comprehend which diffusion mechanism acted significant role in terephthalic acid adsorption of P38 clinoptilolite with 20 ppm initial terephthalic acid concentration.

$$q_t = k_{id} t^{0.5} + C \qquad (6.2)$$

where kid is the intraparticle diffusion rate constant, and C (mg/g) is the constant.

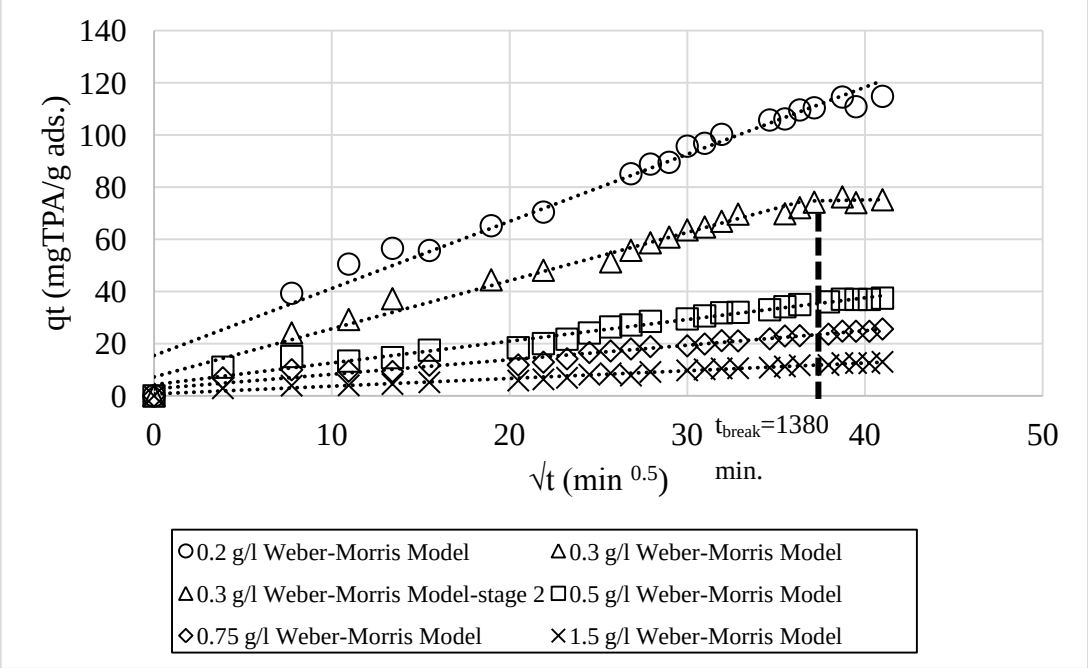

Figure 6.33. Kinetic curves of terephthalic acid adsorption on clinoptilolite (Adsorbent: P38; initial TPA conc.: 20 ppm; model: Weber-Morris model)

As mentioned previously that intraparticle diffusion rate constant, kid (mg g^{-1} $min^{0.5}$) was the slope of the plot of the amount of adsorbed terephthalic acid per unit mass of adsorbent with respect to square root of time. C is the intercept of the plot and

the values of C give an idea regarding the thickness of the boundary layer. If the intraparticle diffusion is the only rate limiting step, qt vs √t would be straight line and passes through the origin. Otherwise, other diffusion mechanisms as film diffusion and/or surface diffusion along with the intraparticle diffusion is also included. Hence, this model is very beneficial to comprehend whether the kinetics is controlled with only intraparticle diffusion or not. As can be seen from Figure 6.33 that there was one stage intraparticle diffusion model for distinct adsorbent amounts except for adsorbent amount of 0.3 g/l showing multi-linear plots of q vs √t curve. This means that experimental points were linear for whole range of time except for 0.3 g/l of adsorbent amount and more than one process was effective on adsorption process for 0.3 g/l adsorbent amount while intraparticle diffusion may be the only rate limiting step for other adsorbent amounts. This could be caused owing to the difference in mass transfer rate in initial and final stage of the adsorption. Table 6.9 shows the kinetic parameters (k_{id}, C, Error and R^2) evaluated by applying Weber Morris model to experimental data for the TPA adsorption on P38 clinoptilolite. Increasing adsorbent amount decreases the intraparticle diffusion rate constant. This means that intraparticle diffusion was slowing down with increasing adsorbent amount and intraparticle diffusion resistance increased with increasing adsorbent amount. For higher amounts, it can be said that rate limiting process was only owing to the intraparticle diffusion. The values of C corroborated the results of intraparticle diffusion rate constant, k_{id} due to the fact that the larger intercept means greater boundary layer effect. As it is seen from the table that the values of C decreasing with increasing adsorbent amount. Hence, the transfer was controlled by intraparticle diffusion with increasing adsorbent amount, thereby eliminating the boundary layer effect and external diffusion except for 0.3 g/l adsorbent amount.

Table 6.9. Kinetic parameters for the adsorption of terephthalic acid by Weber-Morris model (Adsorbent: P38; initial TPA conc: 20 ppm)

Adsorbent Amount (g/l)	kid (mg g^{-1} $min^{0.5}$)		C		Error	Correlation
	Stage 1	Stage 2	Stage 1	Stage 2		
0.2	2.57	-	15.41	-	259.89	0.97
0.3	1,85	0.12	7.19	70.18	50.47	0.97
0.5	0.79	-	4.28	-	32.60	0.97
0.75	0.53	-	2.68	-	12.99	0.97
1.5	0.29	-	0.68	-	0.99	0.97

The break point time obtained by the interception of two lines establishes if the transfer is controlled by intraparticle diffusion or film (external) diffusion. As can be seen from the figure that terephthalic acid adsorption on P38 clinoptilolite (0.3 g/l adsorbent amount) initially occurred thanks to intraparticle diffusion; whereas there was external diffusion after break point (1380 min.). It can be said that the active sites of clinoptiolite between the crystals were accessible due to intraparticle diffusion. High C value of second stage was calculated for the 0.3 g/l adsorbent amount and this shows that boundary layer affected the adsorption and the transfer was controlled by not only intraparticle diffusion but also external diffusion. Figure 6.34 illustrates the Weber Morris intraparticle plots for P75 clinoptilolite.

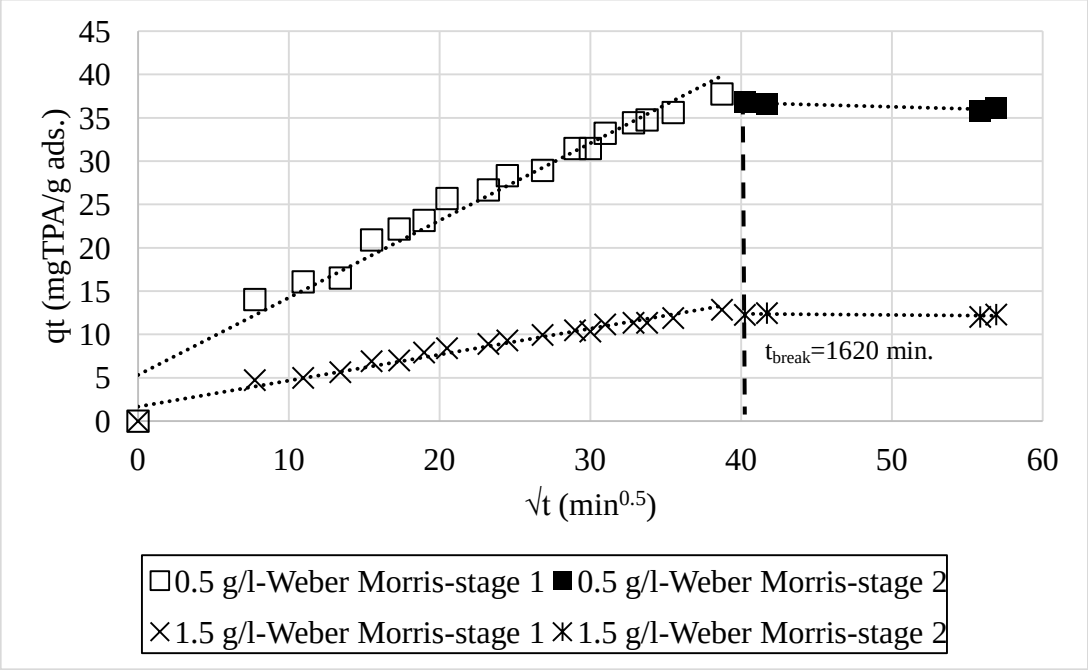

Figure 6.34. Kinetic curves of terephthalic acid adsorption on clinoptilolite (Adsorbent: P75; initial TPA conc.:20 ppm; model: Weber-Morris model)

As can be seen from the Figure 6.34 that experimental points were not linear for whole range of time for all adsorbent dosages and more than one process was effective on adsorption process. The transfer was controlled by both intraparticle diffusion and film diffusion. As mentioned previously that this result could be caused owing to the difference in mass transfer rate in initial and final stage of the adsorption. Initially, adsorption occurred due to intraparticle diffusion; whereas it occurred by external diffusion after break point time (1620 min.). Table 6.10 shows the kinetic parameters (k_{id}, C, Error and R^2) evaluated by applying Weber Morris model to experimental data

for the TPA adsorption on P75 clinoptilolite. As P38 clinoptilolite, intraparticle diffusion rate constant decreased with increasing adsorbent amount; whereas C values were higher when compared to C values belonging to P38 clinoptilolite for stages. However, errors were calculated very high especially for lower adsorbent amounts. This means that there was external diffusion resistance beside intraparticle diffusion resistance.

Table 6.10. Kinetic parameters for the adsorption of terephthalic acid by Weber-Morris model (Adsorbent: P75; initial TPA conc: 20 ppm)

Adsorbent Amount (g/l)	kid (mg g^{-1} $min^{0.5}$)		C		Error	Correlation
	Stage 1	Stage 2	Stage 1	Stage 2		
0.5	0.80	0.73	5.31	38.66	59.80	0.96
1.5	0.27	0.01	2.50	12.84	5.97	0.96

Same procedure was followed to comprehend the diffusion mechanism of terephthalic acid adsorption onto clinoptilolite supported TiO_2 composites (TP38 and TP75). Figure 6.35 and 6.36 illustrates the Weber Morris plots for TP38 and TP75 composites. Multi-linear curves of q vs √t were obtained for both composites. Hence, not only intraparticle diffusion but also film diffusion acted significant role in adsorption process. Dashed lines on the figures show the break time point for composites. Primarily, intraparticle diffusion controlled the adsorption process; whereas external diffusion was effective after break time point. It can be deduced from the figures that boundary layer exactly affected the adsorption process due to the formation of new TiO_2 layer on the exterior surface of the clinoptilolite. This means that there were resistances belonging to TiO_2 and clinoptilolite particles and external diffusion resistance increased with this combination and new layer formation. However, P38 had only one resistance due to clinoptilolite particles.

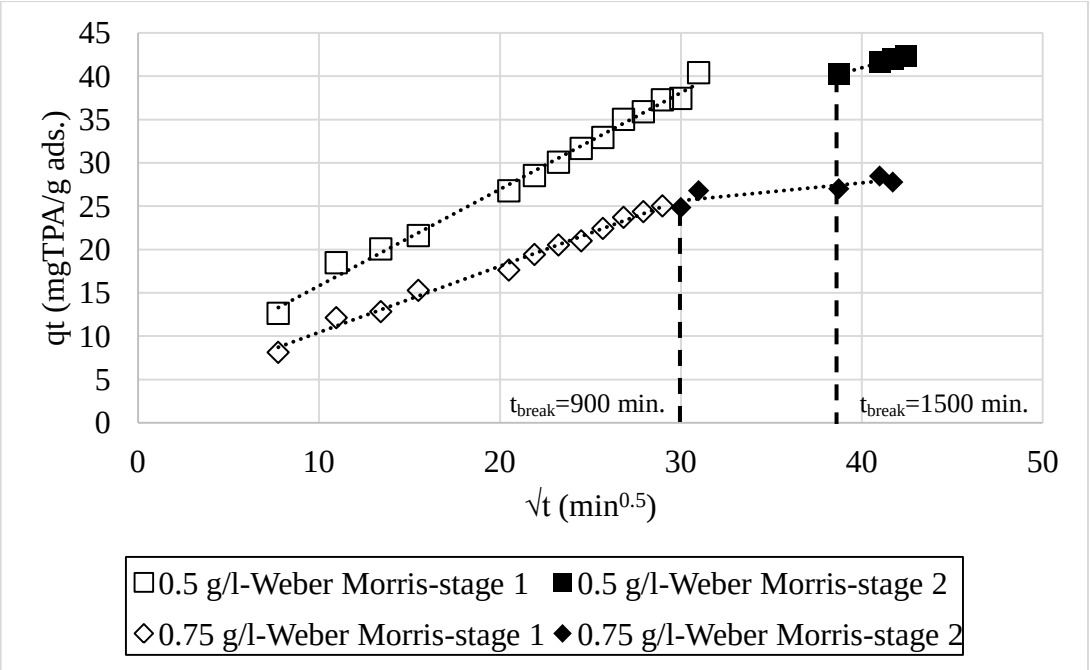

Figure 6.35. Kinetic curves of terephthalic acid adsorption on clinoptilolite (Adsorbent: TP38; initial TPA conc.:20 ppm; model: Weber-Morris model)

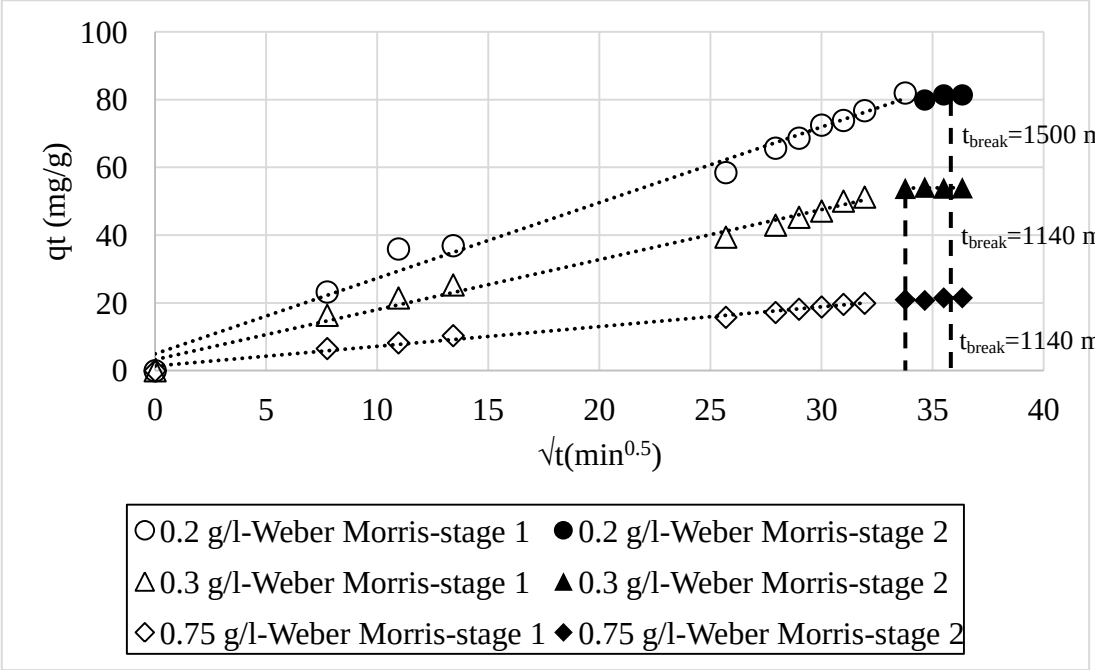

Figure 6.36. Kinetic curves of terephthalic acid adsorption on clinoptilolite (Adsorbent: TP75; initial TPA conc.: 20 ppm; model: Weber-Morris model)

Table 6.11 shows the kinetic parameters (k_{id}, C, Error and R^2) evaluated by applying Weber Morris model to experimental data for the TPA adsorption on TP38 and TP75 composites. When compared to P38 clinoptilolite, TP38 composite showed higher

intraparticle diffusion rate constants. Furthermore, changes in kinetic parameters were similar with one that obtained for clinoptilolite.

Table 6.11. Kinetic parameters for the adsorption of terephthalic acid by Weber-Morris model (Adsorbent: TP38 and TP75; initial TPA conc: 20 ppm)

TP38						
Adsorbent Amount (g/l)	kid (mg g^{-1} $min^{0.5}$)		C		Error	Correlation
	Stage 1	Stage 2	Stage 1	Stage 2		
0.5	1.11	0.58	4.70	17.89	16.61	0.97
0.75	0.76	0.21	2.82	19.43	5.48	0.97
TP75						
0.2	2.23	0.90	4.99	49.07	77.69	0.98
0.3	1.48	0.033	3.28	52.837	33.95	0.98
0.75	0.58	0.28	1.35	11.32	5.69	0.98

6.3.5.2. Intraparticle Diffusion Model

It is assumed that the transport of the terephthalic acid molecules from bulk liquid to the exterior surface of the adsorbent occurs rapidly. Hence, overall adsorption rate is established by the external or intraparticle diffusion due to the fact that external and intraparticle diffusion are successive processes in adsorption. Overall adsorption rate is determined by analyzing intraparticle and external diffusion to find the slower process. It is known that the mass transfer through the adsorbent particle occurs by pore diffusion and surface diffusion in parallel; whereas it is not easy to separate their portions and molecule size of the terephthalic acid is bigger than the pore size of the clinoptilolite and clinoptilolite supported composites. Therefore, there would not be terephthalic acid transport through the pores of the adsorbents. Adsorption of terephthalic acid occurs through the regions constituted by the crystals instead of pores of the clinoptilolite. In the literature, intraparticle diffusion mechanism seems as dominant in the kinetic model.

Hence, it is thought that there would be external and intraparticle diffusion from a well-stirred solution of limited volume owing to the applied adsorption procedure. Also, it is significant to calculate intraparticle diffusion coefficient to compare it to external mass transfer coefficient and to comprehend the slower process. Experimental

data were fitted to intraparticle diffusion equation (eqn 3.17) by minimizing the error. Table 6.12 shows the calculated intraparticle diffusion coefficients with respect to increasing adsorbent amount for P38 and P75 clinoptilolites. Also, the non-zero roots of the equation were calculated by using Matlab software. Six different roots were obtained to substitute them into intraparticle diffusion equation.

Table 6.12. Kinetic parameters for the adsorption of terephthalic acid by intraparticle diffusion equation (Adsorbent: P38 and P75; initial TPA conc: 20 ppm)

Adsorbent Amount (g/l)	D (m^2/s)×10^{17}		Error	
	P38	P75	P38	P75
0.2	4.43	-	0.0176	-
0.3	5.42	-	0.0168	-
0.5	4.42	387	0.0154	0.0098
0.75	3.80	-	0.4092	-
1.5	3.01	319	0.0213	0.0104

As can be seen from Table 6.12 that the values of intraparticle diffusion coefficients were calculated as very low and it oscillated with increasing adsorbent amount, even the calculated error values were very low. This means that there was slow diffusion inside the particles especially for the adsorbent having higher particle size. As it is known that particle size influences the intraparticle diffusion due to alteration of the surface area and diffusion paths. However, the surface area of the clinoptilolite samples were similar, nature of the P75 such as heterogeneity was different than the P38 and diffusion path had changed due to difference in particle size. Table 6.13 demonstrates the calculated kinetic parameters of intraparticle diffusion equation for clinoptilolite supported TiO_2 composites. Same results were observed for clioptilolite supported composites.

Table 6.13. Kinetic parameters for the adsorption of terephthalic acid by intraparticle diffusion equation (Adsorbent: TP38 and TP75; initial TPA conc: 20 ppm)

Adsorbent Amount (g/l)	D (m^2/s)×10^{16}		Error	
	TP38	TP75	TP38	TP75
0.2	-	200	-	0.0146
0.3	-	203	-	0.0146
0.5	1.26	-	0.0124	-
0.75	1.48	197	0.0129	0.0133

6.3.5.3. External Diffusion Model

As mentioned previously that intraparticle and external diffusion act predominant role in TPA adsorption. According to Weber Morris model, there was existence of external diffusion beside intraparticle diffusion. External diffusion model equation was obtained by neglecting c_s for the first short time period and using the initial condition $c=c_0$ at $t=0$.

$$\ln\frac{c}{c_0} = -\frac{m_A}{V_L} k_F a_m t \qquad (6.3)$$

where k_F is the external mass transfer coefficient (m/min), a_m (m^2/g) is the total surface area related to the adsorbent mass available ($a_m=A_s/m_A$).

External diffusion analyze was significant for all adsorbent type so as to comprehend the resistance from bulk liquid to exterior surface of the adsorbent and to decide which diffusion mechanism was more dominant in TPA adsorption process. External mass transfer coefficient was determined by plotting $\ln(c/c_0)$ with respect to time and kf was found thanks to the slope of this plot; whereas linear part of the plot was used to calculate external mass transfer coefficient. Table 6.14 and 6.15 demonstrates the calculated k_F values and error for P38, P75, TP38 and TP75.

Table 6.14. Kinetic parameters for the adsorption of terephthalic acid by external diffusion equation (Adsorbent: P38 and P75; initial TPA conc: 20 ppm)

Adsorbent Amount (g/l)	k_F (m/min)$\times 10^{11}$		Error	
	P38	P75	P38	P75
0.2	7,45	-	0.39	-
0.3	17.9	-	0.40	-
0.5	14.9	26.1	0.29	0.34
0.75	22.4	-	0.31	-
1.5	67.1	78.2	0.30	0.33

Table 6.15. Kinetic parameters for the adsorption of terephthalic acid by external diffusion equation (Adsorbent: TP38 and TP75; initial TPA conc: 20 ppm)

Adsorbent Amount (g/l)	k_F (m/min)×10^{12}		Error	
	TP38	TP75	TP38	TP75
0.2	-	4.32	-	0.17
0.3	-	6.49	-	0.31
0.5	24.9	-	0.33	-
0.75	31.2	16.2	0.32	0.30

External mass transfer coefficient increased with increasing adsorbent amount for all adsorbents. It was found that the amount of adsorbed terephthalic acid per unit mass of adsorbent increased with decreasing adsorbent amount. External mass transfer coefficients of clinoptilolite were higher than the one obtained for composites owing to addition of TiO_2 resistance. The driving force for external diffusion increased with increasing adsorbent amount. Thus, external mass transfer coefficient increased with increasing adsorbent amount due to increase in concentration gradient. When compared to intraparticle diffusion coefficients, external mass transfer coefficients for all adsorbents were high. Intraparticle diffusion was the slower process for overall adsorption process. The results indicate that the rate-controlling step of the terephthalic acid may vary throughout the adsorption process. In the first stage, external diffusion was dominant and it occurred faster. In the later stage, adsorption process slowed down by intraparticle diffusion which was dominant. However, there was boundary layer effect for all adsorbents. Moreover, all error values were calculated as lower than 0.40. Biot calculations for all adsorbents were given as Table 6.16. It can be seen from Table 6.16 that external diffusion and intraparticle diffusion were comparable. Intraparticle diffusion was not sole rate-limiting step and there were some degree of boundary layer control in terephthalic acid adsorption as mentioned previously.

Table 6.16. Biot number calculations for adsorption of terephthalic acid (Adsorbent: P38, P75, TP38, and TP75; initial TPA conc.:20 ppm)

Adsorbent Amount (g/l)	Bi×10^5			
	P38	P75	TP38	TP75
0.2	11800	-	-	10

(cont. on next page)

Table 6.16. (cont.)

Adsorbent Amount (g/l)	Bi×10^5			
	P38	P75	TP38	TP75
0.3	23100	-	-	14
0.5	23700	3000	1830	-
0.75	41261	-	1950	38
1.5	15600	11000	-	-

6.3.6. Adsorption Kinetics: First Order Rate Law/ Pseudo-Second Order Model

Reaction kinetic models were beneficial so as to provide insights to the reaction pathways and to the mechanism of adsorption reactions. The solute uptake rate controlling the residence time of sorbate uptake at the solid-solution interface can easily be described by these models. Hence, these models are very significant to estimate the removal rate of terephthalic acid from the aqueous tetrahydrofuran solution. Thus, first order rate law and pseudo-second order model were investigated as reaction kinetic models for terephthalic acid adsorption. Reaction kinetics models were carried out to describe the interaction between adsorbate and adsorbent. Moreover, it is important to find the order of reaction to establish the overall reaction rate, effectiveness and Damköhler which is important for comparison of film diffusion and reaction. Hence, it was determined the reaction order to make sense of mass transfer mechanism.

Primarily, first order rate law (eqn 3.21) was applied by linearizing experimental data. The slope of the plot of ln (c/c_0) with respect to time yielded the first-order rate constant. Even if the first order rate equation can seem as identical to film diffusion equation, the driving forces of film diffusion and first order rate law are distinct. In the first order rate law; the driving force is the difference between the final equilibrium loading that is constant for a given initial concentration and adsorbent dosage and the time, t.

Secondly, pseudo-second order reaction model (eqn 3.23) is carried out to define the aqueous terephthalic acid-clinoptilolite and clinoptilolite supported TiO_2 composite systems. In the model, the adsorption is second-order, and the chemical adsorption

including valent forces through exchanging or sharing molecules between clinoptilolite and/or clinoptilolite supported TiO_2 composites is the rate limiting step. Linear regression was carried out to calculate the pseudo second-order rate constant and t/qt vs t was plotted to calculate pseudo-second order rate constant, initial adsorption rate and the amount of adsorbed terephthalic acid per unit mass of adsorbent at equilibrium.

Table 6.17 and 6.18 show the first order rate constants, pseudo-second order rate constants, initial adsorption rates, equilibrium, and error values for P38 and P75. As can be seen from the error values, first order rate law was well fitted to experimental data and it did not change with the adsorbent amount. The amount of adsorbed terephthalic acid per unit mass of adsorbent at equilibrium decreased with increasing adsorbent amount due to affinity to water molecules instead of carboxylic acid molecules. This result was corroborated with results in the figure given as Figure 6.23. Also, initial adsorption occurred rapidly for low adsorbent amounts and pseudo second order rate constant increasing with increasing adsorbent amount.

Table 6.17. Kinetic parameters for the adsorption of terephthalic acid by first order rate law and pseudo-second order (Adsorbent: P38; initial TPA conc: 20 ppm)

Adsorbent Amount (g/l)	First Order		Pseudo Second Order				
	$k\times10^3$ (1/min)	Error	qe (mg/g)	$k\times10^5$ (g/mg min)	V_0 (mg/g min)	Error	Correlation
0.2	1.29	0.0088	131.58	2.53	0.44	45.17	0.90
0.3	1.26	0.0068	88.50	3.53	0.28	16.99	0.89
0.5	1.04	0.0074	43.86	6.23	0.12	10.93	0.90
0.75	1.03	0.0073	29.50	8.82	0.08	5.11	0.90
1.5	1.01	0.0045	15.43	14.1	0.03	0.96	0.92

Table 6.18. Kinetic parameters for the adsorption of terephthalic acid by first order rate law and pseudo-second order (Adsorbent: P75; initial TPA conc: 20 ppm)

Adsorbent Amount (g/l)	First Order		Pseudo Second Order				
	$k\times10^3$ (1/min)	Error	qe (mg/g)	$k\times10^4$ (g/mg min)	V_0 (mg/g min)	Error	Correlation
0.5	1.23	0.02	38.91	1.40	0.21	3.45	0.70
1.5	1.23	0.02	13.23	3.70	0.07	0.39	0.72

Table 6.19 and 6.20 illustrate the kinetic parameters of first order rate law and pseudo-second order reaction model for TP38 and TP75 TiO_2 composites. The same interpretations were valid for TiO_2 composites. For clinoptilolite and clinoptilolite supported TiO_2 composites, increasing particle size made the amount of adsorbed terepththalic acid per unit mass of adsorbent decrease. Intraparticle diffusion resistance increased with increasing particle size and diffusion path changed. Also, the available adsorption sites for P75 and TP75 were less than P38 and TP38 due to low surface area. Hence, the amount of adsorbed TPA at equilibrium was lower for high particle size.

Table 6.19. Kinetic parameters for the adsorption of terephthalic acid by first order rate law and pseudo-second order (Adsorbent: TP38; initial TPA conc: 20 ppm)

Adsorbent Amount (g/l)	First Order		Pseudo Second Order				
	$k\times10^3$ (1/min)	Error	qe (mg/g)	$k\times10^5$ (g/mg min)	V_0 (mg/g min)	Error	Correlation
0.5	1.29	0.0001	48.08	7.86	0.18	3.15	0.83
0.75	1.34	0.009	32.15	12.00	0.12	1.23	0.83

Table 6.20. Kinetic parameters for the adsorption of terephthalic acid by first order rate law and pseudo-second order (Adsorbent: TP75; initial TPA conc: 20 ppm)

Adsorbent Amount (g/l)	First Order		Pseudo Second Order				
	$k\times10^3$ (1/min)	Error	qe (mg/g)	$k\times10^5$ (g/mg min)	V_0 (mg/g min)	Error	Correlation
0.2	1.08	0.006	96.15	3.84	0.36	18.02	0.94
0.3	1.07	0.005	64.10	5.68	0.23	7.59	0.94
0.75	1.05	0.006	25.06	15.1	0.09	0.95	0.94

Figure 6.37 demonstrates the kinetic curves obtained by fitting experimental data to the models for P38. The points, dashed line and line on the curve represents the experimental data, The figure implies that Weber-Morris model was not well correlated to experimental data; whereas the correlation of the curve was high for pseudo second order reaction model. Moreover, error values calculated for pseudo second order reaction model were lower than the values for Weber Morris model.

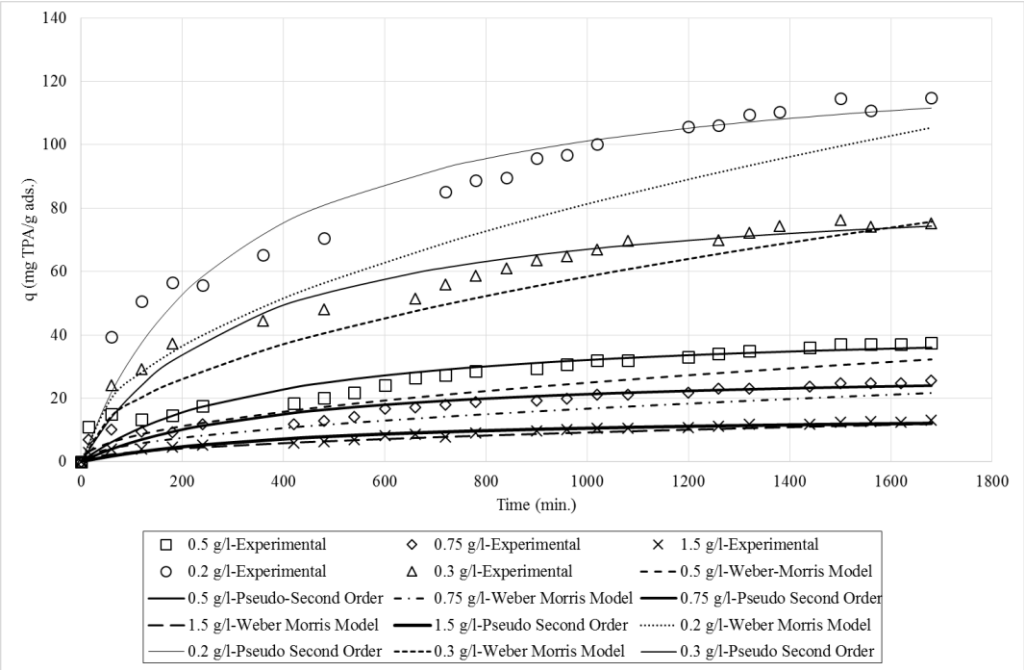

Figure 6.37. Kinetic curves of terephthalic acid adsorption on clinoptilolite (Adsorbent: P38; adsorbent amount: 0.2 g/l, 0.3 g/l, 0.5 g/l, 0.75 g/l, 1.5 g/l; initial TPA conc.: 20 ppm; model: Pseudo-second order (line), Weber-Morris model (dashed line), experiments: points.

It was assumed that the reaction was first order due to the low error and high correlation values of first order rate law. Hence, Damköhler calculations were applied by assuming the reaction as first order to comprehend whether the adsorption was controlled by diffusion or reaction. Film diffusion effectiveness, reaction rate constant and overall reaction rate constant were calculated beside the Damköhler calculations. Table 6.21 demonstrates the Damköhler calculations for terephthalic acid adsorption. Diffusion mechanism controls the global rate provided that Damköhler number is calculated as bigger than 0.1. Table 6.21 indicates that calculated Damköhler numbers for all adsorbents obeyed this phenomenon that diffusion mechanism controlled the terephthalic acid adsorption. Moreover, reaction rate constants (km) were calculated bigger than the external mass transfer coefficient. This means that film diffusion was the slower process than the reaction and diffusion mechanism was the rate-limiting step for terephthalic acid adsorption.

Table 6.21. Damköhler calculations for adsorption of terephthalic acid (Adsorbent: P38, P75, TP38 and TP75; initial TPA conc: 20 ppm)

Catalyst Amount (g/l)	km×10^{10}				Da			
	P38	P75	TP38	TP75	P38	P75	TP38	TP75
0.2	1.15	-	-	1.90	0.23	-	-	0.42
0.3	3.03	-	-	2.90	0.25	-	-	0.43
0.5	3.12	6.65	10.3	-	0.31	0.38	0.34	-
0.75	4.18	-	13.3	7.32	0.28	-	0.35	0.43
1.5	11.6	18.5	-	-	0.26	0.35	-	-
	Effectiveness				kov×10^{11}			
0.2	0.81	-	-	0.70	9.34	-	-	13.4
0.3	0.80	-	-	0.70	24.2	-	-	20.3
0.5	0.76	0.72	0.74	-	23.8	48.2	76.9	-
0.75	0.78	-	0.74	0.70	32.7	-	97.9	51.1
1.5	0.80	0.74	-	-	92.00	137	-	-

Blank studies were applied in order to remove the blank solution effect on terepththalic acid adsorption. Same procedure was followed without any adsorbent in the medium. Figure 6.38 demonstrates the concentration changes of blank solution with addition of aqueous tetrahydrofuran solution and without addition of aqueous tetrahydrofuran solution.

6.3.7. Blank Studies

Blank studies were applied in order to remove the blank solution effect on terepththalic acid adsorption. Same procedure was followed without any adsorbent in the medium. Figure 6.38 demonstrates the concentration changes of blank solution with addition of aqueous tetrahydrofuran solution and without addition of aqueous tetrahydrofuran solution.

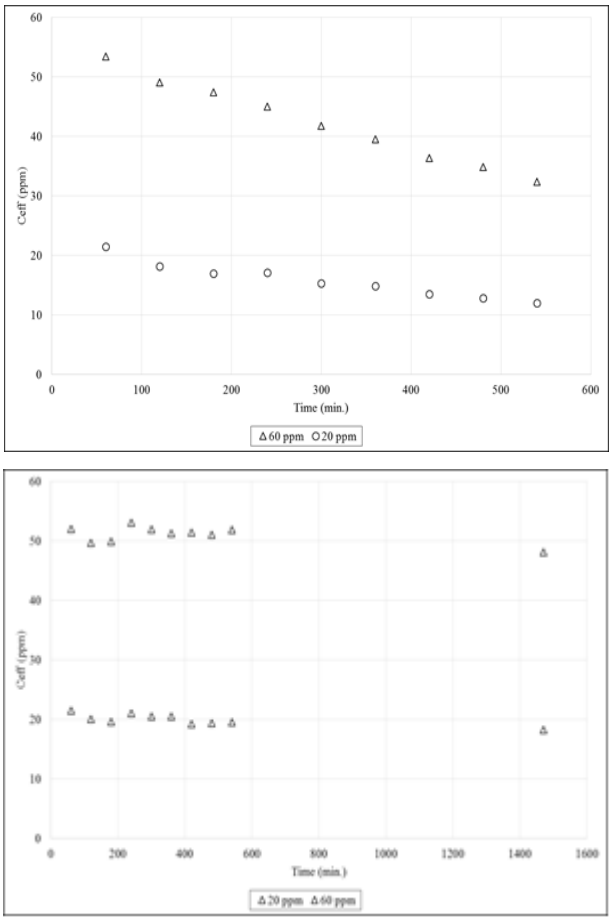

Figure 6.38. Concentration change of blank solution with addition of THF solution (upper); without THF addition (lower) (initial TPA conc.:20 and 60 ppm)

After 9 hours, the concentration changes for 20 ppm and 60 ppm were calculated as 55% and 49%, respectively. Hence, the calculations were modified in the adsorption studies by the leading of blank study. Also, pH values were measured during the blank studies and it was given as Figure 6.39. The pH of the solution dropped from 4.28 to 3.91 for 20 ppm and from 3.98 to 3.8 for 60 ppm initial terephthalic acid concentration. This pH change occurred due to the addition of tetrahydrofuran-water (20%v.) solution (its pH value changed between 3-4) into beaker for an every hour.

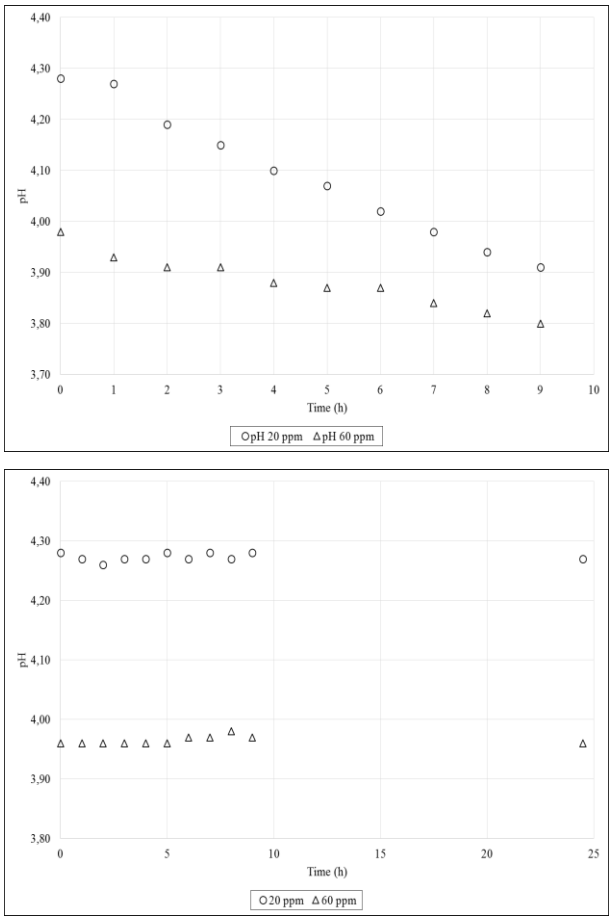

Figure 6.39. pH change of blank solution with addition of THF solution (upper); without THF addition (lower) (initial TPA conc.:20 and 60 ppm)

6.3.8. pH Change During Terephthalic Acid Adsoprtion

As mentioned previously that the influence of pH on adsorption process is complex and the effect of pH depends on the surface chemistry of the terephthalic acid and the adsorbents; clinoptilolite and clinoptilolite supported TiO_2 composites. Especially, the point of zero charge (pH_{zpc}) of the adsorbent affects the adsorption process and the pH of the aqueous tetrahydrofuran solution has strong effect on the surface charge properties of the adsorbents. Hence, it influences the electrostatic interaction between the adsorbent surface and terephthalic acid molecules. The point of zero charge of TP38 and TP75 are 5.55 and 4.91, respectively. Thus, the surface charges of TP38 and TP75 were positive at pH being lower than pH_{zpc}. Moreover, the pK_a value of terephthalic acid is roughly 3.52 and terephthalic acid is ionized to terephthalic acid anion above this value. Hence, the optimum pH should be in the range of these two pH values ($pK_a<pH<pH_{zpc}$) due to the enrichment in the electrostatic interaction among the

terephthalic acid anions and the surface of the adsorbent. The number of negatively charged regions on the adsorbent surface increase at pH being above the pH_{zpc}. A negatively charged surface site is not affirmative for TPA adsorption owing to the electrostatic repulsion. Table 6.22 demonstrates the pH change during terephthalic acid adsorption.

Table 6.22. pH change during terephthalic acid adsorption (Adsorbent: P38, P75, TP38, TP75; adsorbent amount: 1.5 g/l; initial TPA conc.: 20 ppm)

Time (hour)	P38	P75	TP38	TP75
1	5.66	4.44	4.80	4.28
2	5.53	4.34	4.71	4.21
3	5.38	4.29	4.63	4.15
4	5.24	4.24	4.55	4.12
5	5.16	4.18	4.48	4.06
6	5.01	4.14	4.42	4.03
8	4.89	4.04	4.23	3.90

The results explains that pH of medium decreased with respect to time. This means that TPA anions had been formed during the adsorption process due to being above its pKa value. Even if the surface of the adsorbents were negatively charged (Table 6.23), these pH values were suitable in order not to increase negatively charged sites of the adsorbent surface. Hence, the electrostatic interaction between TPA anions and surface of the adsorbent enriched. Moreover, it is known that the adsorption of anions increases with decreasing pH. Therefore, the pH of the adsorption medium decreased to pH value in the range of pKa of terephthalic acid and pH_{zpc} of the adsorbents and the pH values during the adsorption remained between these ranges.

Table 6.23. Zeta potential measurements of adsorbents

Adsorbent	Zeta Potential [mV]	pH
P38	-32.4± .27	8.06
P75	-38.8± .78	4.91
TP38	-27.33± .57	5.55
TP75	-19.23± 0.60	4.91

CHAPTER 7

CONCLUSION

In this study, preparation of natural zeolite supported TiO_2 composites was targeted to remove model pollutant of terephthalic acid (TPA). Natural zeolite tuff was purified and identified as clinoptilolite rich (Ca) silicate. Clinoptilolite and clinoptilolite supported TiO_2 composites were characterized via Scanning Electron Microscopy, Volumetric adsorption instrument, X-ray diffractometer, Fourier Transformer Infrared, Induced Coupled Plasma Atomic Emmision Spectroscopy, and Thermal Gravimetric Analyzer. In the preparation of TiO_2 composites Ti-O-Al and Ti-O-Si bonds are formed.

The sorption of terephthalic acid which is the preliminary step for photocatalytic degradation was performed in dark conditions at room temperature by altering adsorbent amount from 0.2 to 1.5 g/l for the initial TPA concentration of 20-60 ppm. The effects of adsorbent particle size, and TiO_2 loading were also investigated. The amount of adsorbed TPA per unit mass of adsorbent decreased with increasing adsorbent amount due to the affinity of adsorbents to water molecules more than TPA molecules.

Sorption mechanism was described by fitting the kinetic sorption data to diffusion models (Weber-Morris model, intraparticle diffusion model, and external diffusion) and reaction kinetic models (first order rate law and pseudo second order rate law). First order rate law was well correlated to experimental data for clinoptilolite and clinoptilolite supported TiO_2 composites. Weber-Morris Model was applied to comprehend whether only intraparticle diffusion was the rate controlling step or not. More than one intraparticle resistance for P75, TP38, TP75, and one intraparticle resistance for P38 was observed. On the other hand, there was boundary layer effect for all adsorbents. According to Biot number calculations, intraparticle diffusion was not the sole rate-limiting step for TPA adsorption. Moreover, Damköhler calculations were applied by assuming the reaction as first order to comprehend whether the adsorption was controlled by diffusion or reaction. Damköhler numbers were calculated greater than 0.1, indicating that diffusion controlled the mass transfer rate.

REFERENCES

Abate, G. and J. C. Masini. 2003. Influence of pH and ionic strength on removal processes of a sedimentary humic acid in a suspension of vermiculite. Colloids and Surfaces A: Physicochemical and Engineering Aspects 226:25-34.

Ackley, M. W. and R. T. Yang. 1991. Diffusion in ion-exchanged clinoptilolites. Aiche Journal 37:1645-1656.

Akizuki, M., Y. Kudoh, and S. Nakamura. 1999. Growth texture and symmetry of heulandite-Ca from Poona, India. The Canadian Mineralogist 37:1307-1312.

Alberti, A. 1972. On the crystal structure of the zeolite heulandite. Tschermaks mineralogische und petrographische Mitteilungen 18:129-146.

Alberti, A. 1975. The crystal structure of two clinoptilolites. Tschermaks mineralogische und petrographische Mitteilungen 22:25-37.

Alberti, A. and G. Vezzalini. 1983. The thermal behaviour of heulandites: A structural study of the dehydration of Nadap heulandite. Tschermaks mineralogische und petrographische Mitteilungen 31:259-270.

Armağan, B., M. Turan, and M. S. ęlik. 2004. Equilibrium studies on the adsorption of reactive azo dyes into zeolite. Desalination 170:33-39.

Armbruster, T. 1993. Dehydration mechanism of clinoptilolite and heulandite; single-crystal X-ray study of Na-poor, Ca-, K-, Mg-rich clinoptilolite at 100 K. American Mineralogist 78:260-264.

Armbruster, T. and M. E. Gunter. 1991. Stepwise dehydration of heulandite-clinoptilolite from Succor Creek, Oregon, U.S.A.; a single-crystal X-ray study at 100 K. American Mineralogist 76:1872-1883.

Auerbach, S. M., K. A. Carrado, and P. K. Dutta. 2003. Handbook of Zeolite Science and Technology. Taylor & Francis.

Bosso, S. T. and J. Enzweiler. 2002. Evaluation of heavy metal removal from aqueous solution onto scolecite. Water Research 36:4795-4800.

Breck, D. W. 1973. Zeolite molecular sieves: structure, chemistry, and use. Wiley.

Breck, D. W. 1974. Zeolite Molecular Sieves: Structure, Chemistry and Use. John Wiley and Sons, New York.

Bresciani-Pahor, N., M. Calligaris, G. Nardin, L. Randaccio, E. Russo, and P. Comin-Chiaramonti. 1980. Crystal structure of a natural and a partially silver-exchanged heulandite. Journal of the Chemical Society, Dalton Transactions:1511-1514.

Burriesci, N., S. Valente, R. Ottanà, G. Cimino, and C. Zipelli. 1984. Utilization of zeolites in spinach growing. Zeolites 4:5-8.

Capasso, S., C. Colella, E. Coppola, P. Iovino, and S. Salvestrini. 2007. Removal of humic substances from water by means of calcium-ion-enriched natural zeolites. Water Environment Research 79:305-309.

Capasso, S., S. Salvestrini, E. Coppola, A. Buondonno, and C. Colella. 2005. Sorption of humic acid on zeolitic tuff: a preliminary investigation. Applied Clay Science 28:159-165.

Dyer, A. 2002. Bish D. L. & Ming D. W. (Editors) Natural Zeolites: Occurrences, Properties, Applications.: Reviews in Mineralogy and Geochemistry, 45. 2001, 662 pp. Price US$32. ISBN 1529-6466. Clay Minerals 37:733.

Englert, A. H. and J. Rubio. 2005. Characterization and environmental application of a Chilean natural zeolite. International Journal of Mineral Processing 75:21-29.

Enriquez, R. and P. Pichat. 2001. Interactions of Humic Acid, Quinoline, and TiO2 in Water in Relation to Quinoline Photocatalytic Removal. Langmuir 17:6132-6137.

Erdem, E., N. Karapinar, and R. Donat. 2004. The removal of heavy metal cations by natural zeolites. Journal of Colloid and Interface Science 280:309-314.

Ersoy, B. and M. S. Celik. 2004. Uptake of aniline and nitrobenzene from aqueous solution by organo-zeolite. Environmental Technology 25:341-348.

Gerasimova, V. N. 2003. Natural Zeolites as Petroleum Product Adsorbents. Chemistry for Sustainable Development 11:471-478.

Green, M., A. Mels, O. Lahav, and S. Tarre. 1996. Biological-ion exchange process for ammonium removal from secondary effluent. Water Science and Technology 34:449-458.

Gregg, S. J. and K. S. W. Sing. 1967. Adsorption, surface area, and porosity. Academic Press.

Gunay, A. 2007. Application of nonlinear regression analysis for ammonium exchange by natural (Bigadiç) clinoptilolite. Journal of Hazardous Materials 148:708-713.

Gunter, M. E., T. Armbruster, T. Kohler, and C. R. Knowles. 1994. Crystal structure and optical properties of Na- and Pb-exchanged heulandite-group zeolites. American Mineralogist 79:675-682.

Hambley, T. W. and J. C. Taylor. 1984. Neutron diffraction studies on natural heulandite and partially dehydrated heulandite. Journal of Solid State Chemistry 54:1-9.

Ichikawa, S.-i., L. Mahardiani, and Y. Kamiya. 2014. Catalytic oxidation of ammonium ion in water with ozone over metal oxide catalysts. Catalysis Today 232:192-197.

Inglezakis, V. and S. Poulopoulos. 2006. Adsorption, Ion Exchange and Catalysis: Design of Operations and Environmental Applications. Elsevier Science.

Kithome, M., J. W. Paul, L. M. Lavkulich, and A. A. Bomke. 1998. Kinetics of ammonium adsorption and desorption by the natural zeolite clinoptilolite. Soil Science Society of America Journal 62:622-629.

Koyama, K. and Y. Takéuchi. 1977. Clinoptilolite: the distribution of potassium atoms and its role in thermal stability. Page 216 Zeitschrift für Kristallographie.

Kuleyin, A. 2007. Removal of phenol and 4-chlorophenol by surfactant-modified natural zeolite. Journal of Hazardous Materials 144:307-315.

Leone, V., P. Iovino, S. Canzano, S. Salvestrini, and S. Capasso. 2013. Water Purification From Humic Acids By Clinoptilolite-Rich Tuff Extended abstract. Environmental Engineering and Management Journal 12:3-6.

Li, F. F., Y. S. Jiang, L. X. Yu, Z. W. Yang, T. Y. Hou, and S. M. Sun. 2005. Surface effect of natural zeolite (clinoptilolite) on the photocatalytic activity of TiO2. Applied Surface Science 252:1410-1416.

Malkoç, E. 2012. Natural Materials as Low Cost Adsorbents for Water Treatment. Application of Adsorbents for Water Pollution Control:347-362.

McCabe, W. L., J. Smith, and P. Harriott. 2005. Unit Operations of Chemical Engineering. McGraw-Hill Education.

McKay, G., M. S. Otterburn, and A. G. Sweeney. 1980. The removal of colour from effluent using various adsorbents—III. Silica: Rate processes. Water Research 14:15-20.

Mondale, K. D., R. M. Carland, and F. F. Aplan. 1995. The comparative ion-exchange capacities of natural sedimentary and synthetic zeolites. Minerals Engineering 8:535-548.

Mumpton, F. A. 1981. Utilization of natural zeolites. Mineralogy and geology of natural zeolites. Mineralogical Society of America.

Nikazar, M., K. Gholivand, and K. Mahanpoor. 2008. Photocatalytic degradation of azo dye Acid Red 114 in water with TiO2 supported on clinoptilolite as a catalyst. Desalination 219:293-300.

Oter, O. and H. Akcay. 2007. Use of natural clinoptilolite to improve, water quality: Sorption and selectivity studies of lead(II), copper(II), zinc(II), and nickel(II). Water Environment Research 79:329-335.

Polat, E., M. Karaca, H. Demir, and N. A. Onus. 2004. Use Of Natural Zeolite (Clinoptilolite) In Agriculture. Journal of Fruit and Ornamental Plant Research 12.

Robert, D. and J. Weber. 2000. Study of the Adsorption of Dicarboxylic Acids on Titanium Dioxide in Aqueous Solution. Adsorption 6:175-178.

Sani, A., G. Vezzalini, P. Ciambelli, and M. T. Rapacciuolo. 1999. Crystal structure of hydrated and partially NH4-exchanged heulandite. Microporous and Mesoporous Materials 31:263-270.

Shafaei, A., M. Nikazar, and M. Arami. 2010. Photocatalytic degradation of terephthalic acid using titania and zinc oxide photocatalysts: Comparative study. Desalination 252:8-16.

Shoumkova, A. 2011. Zeolites for water and wastewater treatment: An overview. Australian Institute of High Energetic Materials.

Skoulikides, T. N. 1989. Physical Chemistry I 1.2. Symetria Editions, Athens, Greece

Smyth, J. R., A. T. Spaid, and D. L. Bish. 1990. Crystal structures of a natural and a Cs-exchanged clinoptilolite. American Mineralogist 75:522-528.

Stolz, J., P. Yang, and T. Armbruster. 2000. Cd-exchanged heulandite: symmetry lowering and site preference. Microporous and Mesoporous Materials 37:233-242.

Taborda, A. V., M. A. Brusa, and M. A. Grela. 2001. Photocatalytic degradation of phthalic acid on TiO2 nanoparticles. Applied Catalysis A: General 208:419-426.

Thiruvenkatachari, R., T. O. Kwon, J. C. Jun, S. Balaji, M. Matheswaran, and I. S. Moon. 2007. Application of several advanced oxidation processes for the destruction of terephthalic acid (TPA). Journal of Hazardous Materials 142:308-314.

Townsend, R. P. 1986. Ion-exchange in zeolites - some recent developments in theory and practice. Pure and Applied Chemistry 58:1359-1366.

Tsitsishvili, G. V., T. G. Andronikashvili, G. N. Kirov, and L. D. Filizova. 1992. Natural Zeolites. Ellis Horwood, England.

Wang, S. and Z. H. Zhu. 2006. Characterisation and environmental application of an Australian natural zeolite for basic dye removal from aqueous solution. J Hazard Mater 136:946-952.

Wiszniowski, J., D. Robert, J. Surmacz-Gorska, K. Miksch, and J. V. Weber. 2002. Photocatalytic decomposition of humic acids on TiO2 Part I: Discussion of adsorption and mechanism. Journal of Photochemistry and Photobiology a-Chemistry 152:267-273.

Worch, E. 2012. Adsorption Technology in Water Treatment: Fundamentals, Processes, and Modeling. De Gruyter.

Xu, R., W. Pang, J. Yu, Q. Huo, and J. Chen. 2009. Chemistry of Zeolites and Related Porous Materials: Synthesis and Structure. Wiley.

Yang, P. and T. Armbruster. 1996. Na, K, Rb, and Cs Exchange in Heulandite Single-Crystals: X-Ray Structure Refinements at 100 K. Journal of Solid State Chemistry 123:140-149.

APPENDIX A

PARTICLE SIZE DISTRIBUTION

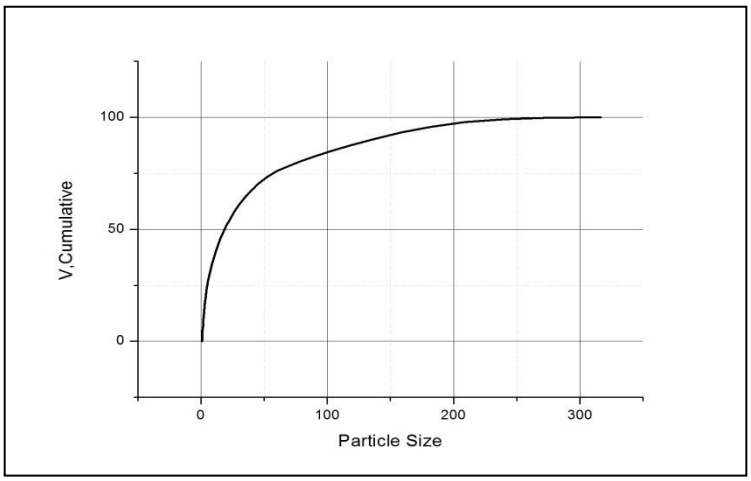

Figure A 1. Particle Size Distribution of Tuff S

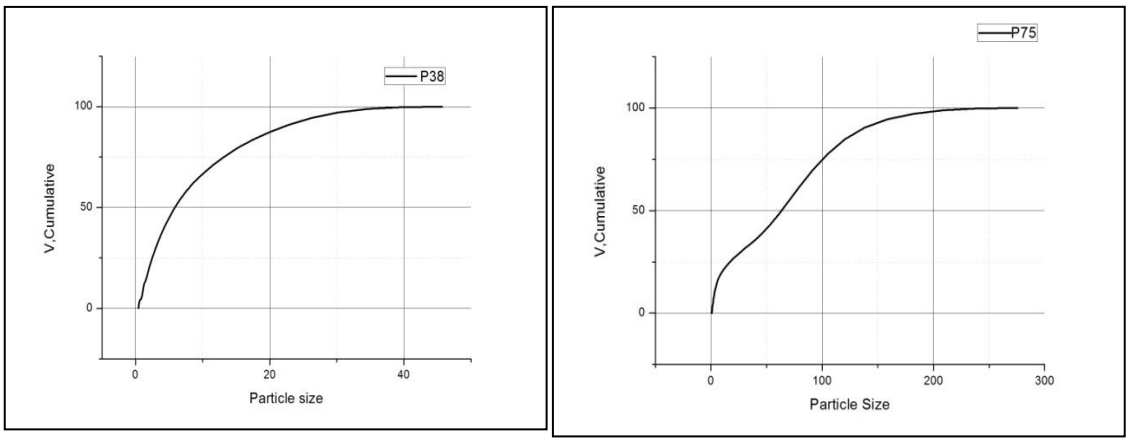

Figure A 2. Particle Size Distribution of Purified Natural Zeolite Tuff at sieve <38 μm (left) and >75 μm (right)

APPENDIX B

SOLUBILITY OF TEREPHTHALIC ACID (TPA) IN TETRAHYDROFURAN (THF) AND WATER

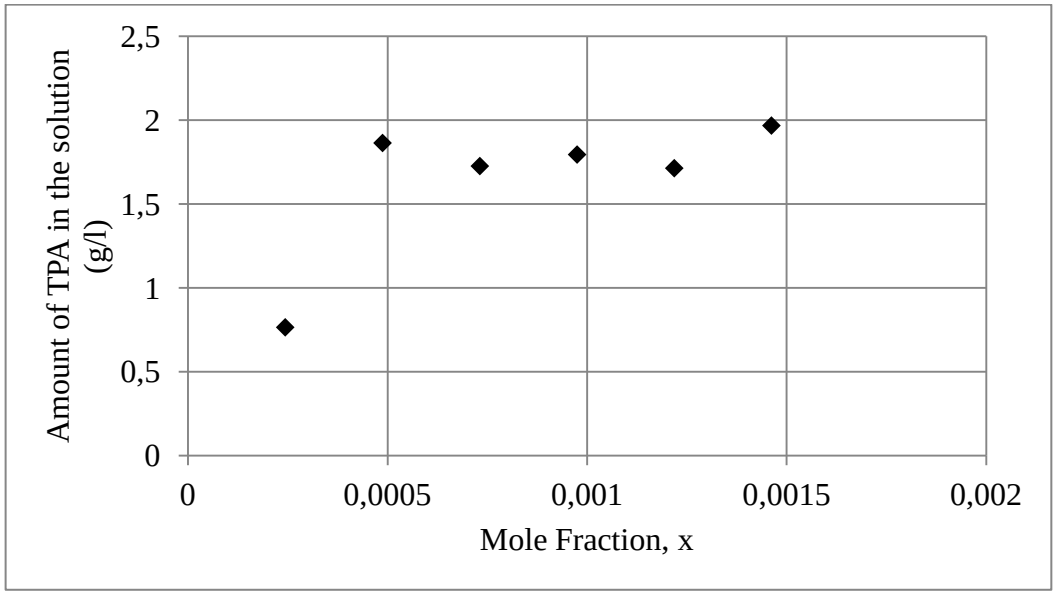

Figure B 1. Solubility of terephthalic acid (tpa) in tetrahydrofuran (THF)

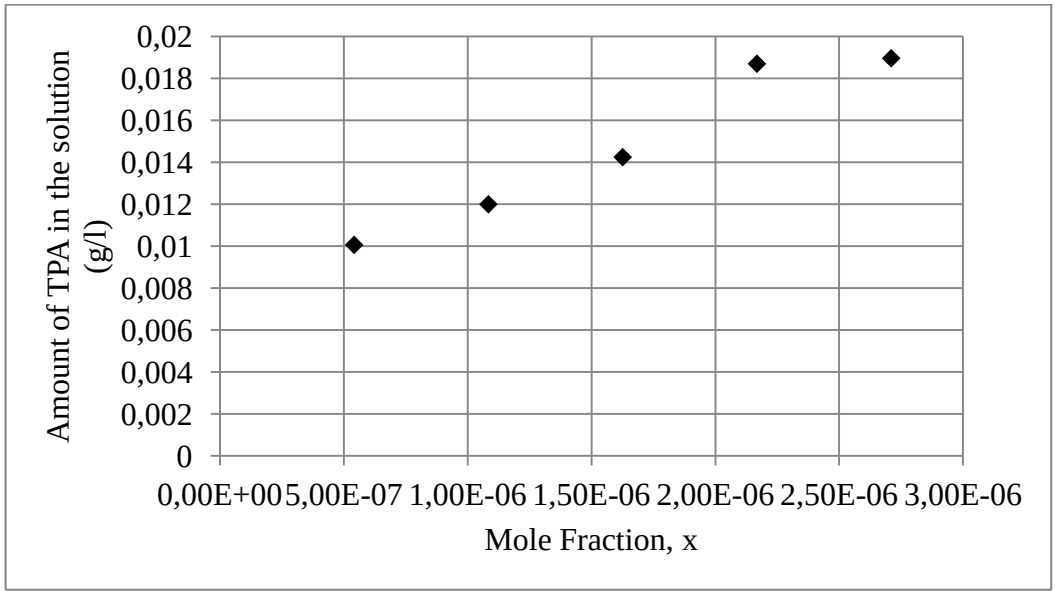

Figure B 2. Solubility of terephthalic acid (TPA) in water